Consumers Power
POWERING MICHIGAN'S PROGRESS
Palisades Nuclear Plant: 27780 Blue Star Memorial Highway, Covert, MI 49043

Kurt M. Haas
Plant Safety and Licensing Director

April 24, 1995

Nuclear Regulatory Commission
ATTN: Document Control Desk
Washington, DC 20555

DOCKET 50-255 LICENSE DPR-20 PALISADES PLANT -
RESPONSE TO REQUEST FOR ADDITIONAL INFORMATION TO SUPPORT NRC REVIEW OF THE PROJECT PLAN FOR ADDRESSING ALLOY 600 ISSUES

In a letter dated February 27, 1995, we submitted our Project Plan for Addressing Alloy 600 Issues. The NRC's April 13, 1995 letter described the additional information needed to complete review of the Project Plan. A conference call with the NRC was held on Tuesday April 18, 1995, to review our interpretation of the questions and discuss our preliminary response to the information request.

Our response to the NRC's April 13, 1995 request for additional information is provided in Attachment 1. Note that we have responded to the revised third question discussed during the April 18, 1995 conference call and not the question stated in the NRC's April 13, 1995 letter.

SUMMARY OF COMMITMENTS

This letter contains no new commitments.

Kurt M Haas
Plant Safety and Licensing Director

CC Administrator, Region III, USNRC
NRR Project Manager, USNRC
NRC Resident Inspector - Palisades

Attachment

9505030326 950424
PDR ADOCK 05000255
P PDR

A023
1/1

ATTACHMENT 1

Consumers Power Company
Palisades Plant
Docket 50-255

RESPONSE TO REQUEST FOR ADDITIONAL INFORMATION TO SUPPORT NRC REVIEW OF THE PROJECT PLAN FOR ADDRESSING ALLOY 600 ISSUES

April 24, 1995

RESPONSE TO NRC APRIL 13, 1995
REQUEST FOR ADDITIONAL INFORMATION

NRC Question:

*(1) **Spray Nozzle Safe End** and **Surge Nozzle Safe End** sections both postulate corrosion rates and times to failure. Where did this data come from? (page 22)*

CPCo Response:

The data for the corrosion rates and times to failure were obtained from engineering analyses performed by B&W Nuclear Technologies (BWNT) specifically for Palisades. They are:

1. BWNT Calculation No: 32-1235177-00, "FM Assessment of Palisades Alloy 600 Components." (Reference 3.10.10 in Alloy 600 Project Plan, proprietary version). The BWNT calculation uses corrosion rates developed by BWNT and Peter Scott's model ("An Analysis of Primary Water Stress Corrosion Cracking in PWR Steam Generators," in proceedings, Specialists Meeting On Operating Experience With Steam Generators, Brussels, Belgium, September 16-20, 1991) to calculate times to failure.

2. BWNT Calculation No: 51-1235130-00, "Service Life Assessment of Pressurizer Spray and Surge Nozzle Safe Ends."

The results of these Palisades specific calculations agree with the previous generic evaluations performed by ABB-CE for CE plants. The plant specific calculations have been reviewed and accepted by Palisades engineering staff. They are currently being documented as Palisades engineering analyses per the requirements of our Administrative Procedures. A copy of a non-proprietary version of these calculations are attached. BWNT calculation 51-1235130-01, Attachment 2, is the non-proprietary version of the service life assessment and BWNT calculation 32-1238965-00, Attachment 3, is the non-proprietary version of the FM assessment.

NRC Question:

*(2) **Safety Valve Flanges** states that the nozzle girth butt welds were post-weld stress relieved making them less susceptible to PWSCC [primary water stress corrosion cracking] then Alloy 600 safe ends. What heat treatment was performed? At what temperature and soak times? (page 22)*

CPCo Response:

The shop weld joining the pressurizer safety relief valve nozzle to the safety relief valve flange was stress relieved along with the Pressurizer vessel in a furnace at 1150°F. The soak time for this stress relief is not currently available. If necessary this information should be available from ABB-CE records but additional time would be

required to obtain this information. More discussion on the PWSCC susceptibility of the three safety valve line safe-ends and flanges was provided in the CPCo response to NRC request No. 12 in our letter to the NRC dated October 20, 1993.

The Alloy 600 Project identified 251 Alloy 600 locations in the PCS (not including steam generator tubes) which were ranked with respect to their PWSCC susceptibility using a prioritization scheme. The safety valve flanges were also re-visited as a part of this process and it was confirmed that they are generally less susceptible to PWSCC.

NRC Question:

*(3) **Control Rod Drive Mechanism (CRDM) Nozzle**. Are the generic evaluations performed by the industry valid for Palisades? If so, please provide details. If not, provide a safety assessment for Palisades including likelihood of ejection, crack susceptibility, crack growth rate and leak detection capabilities and system evaluations. (page 24)*

CPCo Response:

ABB-CE performed the following Safety Evaluations for the Combustion Engineering Owner's Group (CEOG) plants:

1. CEN-607, "Safety Evaluation of the Potential for and Consequence of Reactor Vessel Head Penetration Alloy 600 ID Initiated Nozzle Cracking."

2. CEN-614, "Safety Evaluation of the Potential for and Consequence of Reactor Vessel Head Penetration Alloy 600 OD Initiated Nozzle Cracking."

Palisades participated in this CEOG Task for developing these Safety Evaluations for the CEOG plants. The analysis inputs used for these safety evaluations bound the nozzle geometry and operating parameters for Palisades. Hence, both these safety evaluations are applicable to Palisades. These safety evaluations can be made available to the NRC, if necessary.

Moreover, NUREG/CR-6245, "Assessment of Pressurized Water Reactor Control Rod Drive Mechanism Nozzle Cracking", states that CRDM nozzle cracking is not a short term safety issue. Due to the J-groove weld geometry, all detected cracks in the industry found on the inside surface have been axially oriented. As stated in the NUREG, it is highly unlikely that growth of an axial crack will lead to nozzle rupture. Leak from the axial crack would be detected long before the crack reaches the critical flaw size. An OD initiated circumferential crack is possible but it may take well beyond the licensed life of the plant to result in a rupture of the nozzle. Per the NUREG, plausible scenarios following a postulated rupture of a CRDM are covered within the design basis of the plant. For Palisades these scenarios have been addressed in the FSAR Chapter 14 accident analysis for control rod drop (FSAR section 14.4), control rod ejection (FSAR section 14.16) and small break LOCA (FSAR section 14.17).

NRC Question:

(4) ***Safe End and Full Penetration Welded Nozzle****. How are the crack growth rates established? (page 25)*

CPCo Response:

The crack growth rates for Palisades Alloy 600 components are established by BWNT Calculation 32-1235177-00, "FM Assessment of Palisades Alloy 600 Components" (Reference 3.10.10 on Project Plan). The fatigue crack growth due to design cycle loading was calculated using Paris' Law, similar to that given in Article A-4000 of Section XI of the ASME Boiler and Pressure Vessel Code. The stress corrosion crack growth was calculated using Peter Scott's model ("An Analysis of Primary Water Stress Corrosion Cracking in PWR Steam Generators," in proceedings, Specialists Meeting On Operating Experience With Steam Generators, Brussels, Belgium, September 16-20, 1991). Appropriate temperature correction for the difference in operating temperature between the different Alloy 600 components and the SG tubes was employed in Peter Scott's Model. A copy of a non-proprietary version of the fracture mechanics assessment calculation (BWNT Calculation No. 32-1238965-00, "Fracture Mechanics Assessment of Palisades Alloy 600 Components") is attached.

NRC Question:

(5) ***Identify PWSCC inspection methods and procedures****. Do any of the mockups have implanted SCC crack or are they machined notches only (EDM [electro discharge machined])? (page 29)*

CPCo Response:

The mockups contain thermal fatigue cracks. Thermal fatigue cracks are implanted because the flaw dimensions can be controlled during the implant process. The use of these cracks of known sizes allows the mockups to contain flaws which fully test the capabilities of the examination techniques for flaw detection and sizing. The mockups therefore contain no implanted SCC cracks or EDM machined notches.

A working Meeting with the NRC Region III staff was held on April 3, 1995, where details of the Palisades Alloy 600 inspection program were presented. Mr. John Jacobson (Chief, Materials and Processes Section, III), Mr. Jerome Shapkar, Mr. Melvin Holmberg, Mr. Tom O'Leary, Mr. Wayne Kropp and Mr. J. W. McCormick-Barger were present at this working meeting. The proposed inspection plan and techniques were presented to those NRC staff present and no concerns were raised.

NRC Question:

*(6) **Safety vs Non-safety Components**. What unique contributing factors for PWSCC were evaluated for Palisades? (page 44)*

CPCo Response:

There are no specific or unique contributing factors identified for PWSCC in Alloy 600 components at Palisades. The most commonly identified parameters contributing to PWSCC are high tensile stress, high temperature, and primary water environment, which are not unique to Palisades.

NRC Question:

(7) What are "enhanced" ultrasonic examinations? (page 51, 7.2.1)

CPCo Response:

Enhanced ultrasonic examinations refers to examination techniques which exceed the standard ASME Section XI examination methods which increase the examination reliability of components. In this case, "enhanced" ultrasonic examination refers to the use of various examination parameters such as; automated data collection and analysis, longitudinal waves, focused search units, increased scanning sensitivity and tip diffraction sizing. "Enhanced" also refers to the application of the ultrasonic techniques optimized for the examinations to be performed using mockups of similar geometry with the implanted thermal fatigue cracks.

NRC Question:

(8) What is the time frame for these evaluations? (page 52, 7.2.2)

CPCo Response:

The Analysis described in Section 7.2.2 outlines the approach to work considered by the Alloy 600 Project Team in the early phases of the Project. Later this list was refined into the scope of work for the 1995 Refueling outage as described in Section 3.1.2 of the Project Plan. Detailed analysis of identified highly susceptible Alloy 600 components was performed by BWNT and CPCo. All planned detailed evaluations will be completed prior to the 1995 refueling outage.

ATTACHMENT 2

Consumers Power Company
Palisades Plant
Docket 50-255

SERVICE LIFE ASSESSMENT OF PALISADES SPRAY AND SURGE NOZZLE SAFE ENDS BWNT CALC No. 51-1235130-01

April 24, 1995

9505030328 950424
PDR ADOCK 05000255
P PDR

B&W NUCLEAR TECHNOLOGIES

ENGINEERING INFORMATION RECORD

Document Identifier 51-1235130-01

Title Service Life Assessment of Pressurizer Spray and Surge Nozzle Safe Ends

PREPARED BY:	REVIEWED BY:
Name CA Campbell/DE Killian	Name S Fyfitch
Signature CA Campbell/DE Killian Date 4/20/95	Signature S Fyfitch Date 4/20/95

Technical Manager Statement: Initials KE Ill.

Reviewer is Independent.

Remarks:

This document presents service life assessments of the pressurizer spray nozzle safe end and surge nozzle safe end at Palisades. Both safe ends were fabricated from Alloy 600 and are a concern with regard to PWSCC. The relative susceptibilities of these safe ends to PWSCC are evaluated in comparison to the PORV safe end (also fabricated from Alloy 600), which will be replaced during the 1995 refueling outage.

This document is a deliverable for Task III.1, "Service Life Extension for the Existing Spray Nozzle," and Task V.1, "Service Life Extension for the Existing Surge Nozzle Safe End."

Revision 01 is the non-proprietary version of Revision 00.

*** NON-PROPRIETARY ***

1.0 Purpose

The purpose of this document is to present the service life assessments for the Palisades pressurizer spray nozzle safe end and surge nozzle safe end.

2.0 Background

Alloy 600 is used extensively in the primary coolant system (PCS) of pressurized water reactors (PWRs). For example, pressurizer nozzles and safe ends, control element drive mechanism nozzles, and steam generator tubing have all been fabricated from Alloy 600. In recent years, however, numerous failures of Alloy 600 components have occurred due to primary water stress corrosion cracking (PWSCC). Steam generator tubing is known for numerous failures, but pressurizer, control rod drive mechanism, and hot leg nozzles have also been affected. The pressurizer power operated relief valve (PORV) safe end at Palisades was repaired in September/October 1993 following detection of PWSCC cracks in the vicinity of the safe end weld. This safe end will be replaced during the 1995 refueling outage.

Following the detection of PWSCC in the PORV safe end at Palisades and its repair in 1993, Consumers Power Company (CPCo) is currently reviewing the Alloy 600 locations throughout the pressurizer and primary coolant piping to determine appropriate actions to be taken. In the pressurizer, the spray nozzle safe end and surge nozzle safe end are of concern. The spray nozzle safe end was fabricated from the same heat of material as the PORV safe end (which has already failed) and the surge nozzle safe end, which operates at approximately 640°F, was fabricated from material also believed to be relatively susceptible to PWSCC. [Note: The temperature element nozzles in the pressurizer at Palisades, also fabricated from Alloy 600, have been addressed separately.]

The following sections describe the requirements for PWSCC of Alloy 600 components to occur, and the assessed service life for both the spray nozzle safe end and surge nozzle safe end relative to the PORV safe end, which has already failed due to PWSCC.

3.0 Primary Water Stress Corrosion Cracking

Primary water stress corrosion cracking is a degradation mechanism of Alloy 600 that occurs as a result of

- a susceptible material,
- a tensile stress (including both operating and residual stress), and
- a pressurized water reactor (PWR) primary water environment.

All of these factors must be present in order for PWSCC to occur.

The susceptibility of Alloy 600 material depends on several factors including the chemical composition, heat treatment during manufacture of the material, heat treatment during fabrication of the component, and operating parameters of the component. Chemical composition and heat treatment are interrelated in several ways. For example, one reason for annealing Alloy 600 is to solutionize the carbon in the alloy. (Figure 1 illustrates the solubility of carbon in Alloy 600 as a function of annealing temperature.) As the material cools, chromium carbides precipitate from solution at both intragranular and intergranular locations. If the cooldown from the anneal is sufficiently slow, a greater number of carbides will precipitate at the grain boundaries (i.e., intergranularly), and the resistance to PWSCC will be improved. Well decorated grain boundaries are an indication that an Alloy 600 material has received a proper heat treatment and that sufficient carbon was available in solution to combine with chromium. If adequate amounts of carbon and chromium exist but the anneal was not at a high enough temperature or sufficient time was not allowed to solutionize the carbon, an adequate amount of carbon will not be available to precipitate intergranularly as chromium carbides, leading to minimal grain boundary decoration. Most precipitation occurs during cooldown following annealing; however, stress relief treatments can lead to additional precipitation. The primary goal of stress relief, however, is to allow a local realignment of highly strained regions to reduce internal stresses. Carbon and chromium concentration gradients are also reduced given extended time at temperature. Thus, if the anneal has not adequately solutionized carbon for chromium carbide precipitation at the grain boundaries, stress relief treatment will not affect intergranular carbide precipitation and will not reduce susceptibility to PWSCC.

Tensile stresses, resulting from both residual and operating stresses, can be significant for some Alloy 600 components. Operating stresses are produced from mechanical and thermal loading, while residual stresses are generated as a result of fabrication, installation, and welding processes. Residual stresses are more difficult to quantify than operating stresses and, in many instances, are of a higher magnitude than operating stresses.

PWSCC is a thermally activated degradation mechanism; that is, as the temperature increases, the rate of PWSCC increases. Thus, the hot leg

temperature of the RCS creates a more aggressive environment in which the Alloy 600 components must operate.

The cracking observed in PWRs to date is typically axially-oriented (although circumferentially-oriented cracks have been observed) and occurs in an area, such as a weld heat affected zone (HAZ), that has high residual tensile stresses. In partial penetration welded components such as nozzles, the residual stresses are inherently higher in the circumferential direction than in the axial direction. In this case, therefore, cracking in a homogeneous material with no initial flaws would be expected to occur axially due to the higher circumferential residual stresses. However, axially-oriented residual stresses on the inside surface of nozzle-to-safe-end welds (i.e., butt welds) have been shown to be greater than circumferentially-oriented residual stresses at this location.[1]

4.0 Assessment of Palisades Pressurizer Safe Ends

CPCo has provided BWNT with available information regarding the spray nozzle safe end, surge nozzle safe end, and PORV safe end. This information has been reviewed and the material characteristics and operating conditions for each of these safe ends is tabulated below.

	Spray Nozzle Safe End	Surge Nozzle Safe End	PORV Safe End
Heat Number	NX5222	26190	NX5222
Carbon Content (%)	0.090	0.065	0.090
Yield Strength (ksi)	77.5	51.2	77.5
Ultimate Tensile Strength (ksi)	114.0	100.3	114.0
Anneal Temp. (°F)*	1650	1650	1650
Operating Temp. (°F)	540**	640	640
Environment	liquid	liquid	steam
Flow Rate (gpm)	50-70**	stagnant#	stagnant
Outside Diameter (in.)	4.500	12.750	6.000
Inside Diameter (in.)	3.692	10.740	3.000
Nominal Wall Thickness (in.)	0.404	1.005	1.500+
Attachment Weld	Full	Full	Full
Stress Relief [Vessel side/Piping side]	Yes/No##	Yes/No##	Yes/No##

* Annealing temperature is assumed to be approximately 1650°F based on standard industry practice for Alloy 600 material.

** Flow rate through the spray nozzle and safe end is believed to be approximately 50-70 gpm. This continuous high flow rate (from the cold leg piping) leads to an operating temperature of approximately 540°F, that of the cold leg piping.

\# Flow through the surge nozzle safe end during normal operation is minimal, thus the environment is essentially stagnant.

\## It is believed that all three safe ends were shop-installed; therefore, it is assumed that the pressurizer-to-safe-end weld was stress relieved with the pressurizer. The safe-end-to-piping weld, on the other hand, would not have received any stress relief treatment.

\+ The nominal wall thickness of the PORV safe end is 1.5"; however, the thickness of this safe end at the location of failure (at the safe-end-to-piping weld) is approximately 0.5".

Figures 2 through 4 illustrate the spray nozzle safe end, surge nozzle safe end, and PORV safe end, respectively.

The spray nozzle safe end and PORV safe end were fabricated from the same heat of material (NX5222), while the surge nozzle safe end was fabricated from a separate heat (26190). However, the carbon contents of heats NX5222 and 26190 are relatively high at 0.090% and 0.065%, respectively, as shown above. Since the actual annealing temperatures for these heats are not available, a temperature of 1650°F is assumed (as identified in the above table) for both material heats. A 1650°F anneal temperature is insufficient to solutionize 0.065% carbon as shown in Figure 1 -- the solubility curve for carbon in Alloy 600, which follows the following equations:[2]

$$^{\circ}C = 1449 + 130.3[\ln(\%C)] \quad \textbf{(1)}$$

or,

$$^{\circ}F = 2640 + 234.5[\ln(\%C)] \quad \textbf{(2)}$$

where %C is the weight percent carbon in the material. At 1650°F, only 0.015% carbon will go into solution. Thus, since very little of the carbon is able to go into solution during a 1650°F anneal, neither of the two material heats is expected to have extensive grain boundary carbide decoration. Also, extensive intragranular carbides (within each grain) are expected for these materials due to the high carbon contents of the two heats. Based on composition and expected microstructural

features following heat treatment, both material heats are relatively susceptible to PWSCC.

The operating temperature of the spray nozzle safe end is 540°F, which is essentially the temperature of the cold leg; this temperature is due to the continuous flow of primary coolant within the spray nozzle safe end (except at shutdown conditions). The operating temperature of both the surge nozzle safe end and PORV safe end is significantly higher at 640°F. The environments within the PORV safe end and surge nozzle safe end are considered to be essentially stagnant. Based on temperature alone, PWSCC susceptibility of the spray nozzle safe end is lower than that of the other two safe ends.

The total stress states of the three safe ends are not known. Compared to residual stresses, the operating stresses are considered to be low. Residual stresses within the safe ends resulting from fabrication and installation (including welding) have not been determined to date but peak tensile stresses can be conservatively estimated to be approximately the yield strength of the material. Thus, residual tensile stresses in the spray nozzle safe end and PORV safe end could be somewhat higher than the residual tensile stresses within the surge nozzle safe end (yet similar relative to the different yield strengths of the two materials). It should also be noted that poor welding (e.g., poor reworking) of the PORV and surge nozzle safe ends has been identified,[3,4] and it is believed that the spray nozzle safe end weld was reworked in a similar manner. This rework increases the residual stresses at these locations.

It is assumed (as noted in the above table) that the three safe ends were installed in the shop and, thus, were stress relieved with the pressurizer. However, the safe-end-to-piping welds did not receive any stress relief treatment since these welds were completed in the field. Stress relief may have slightly reduced PWSCC susceptibility of the safe end materials at the pressurizer-to-safe-end welds. At the safe-end-to-piping weld, the safe end materials are expected to be somewhat more susceptible to PWSCC. It should be noted, however, that the safe ends are still believed to be susceptible to PWSCC based on previous heat treatments and composition of the safe end materials.

One other difference to note is that the three safe ends vary significantly in size. The surge nozzle safe end has the largest nominal diameter of the three safe ends, followed by the PORV safe end, with the spray nozzle safe end having the smallest diameter. [Note: As mentioned earlier, the PORV safe end is significantly thinner at the safe-end-to-piping weld (~0.5") than its nominal thickness of 1.5".] All safe end welds are full penetration welds, and (based on diameter) the surge nozzle safe end is expected to have the largest welds, by volume, of the three safe ends.

Based on a materials standpoint, both the surge nozzle and spray nozzle safe ends are relatively susceptible to PWSCC due to composition (i.e.,

high carbon content), insufficient heat treatment, and poor welding of the safe ends leading to significant residual stresses.

5.0 PWSCC Crack Growth Assessment

A crack growth assessment has been performed for the spray nozzle safe end and the surge nozzle safe end.[5] In this assessment, both PWSCC and fatigue crack growth were evaluated to determine the remaining service life of these two safe ends. Three aspect ratios (i.e., crack length/crack depth) were considered for various initial flaw depths in this assessment.

Postulated semi-elliptical axial and circumferential internal surface flaws were evaluated in accordance with the fracture toughness requirements set by the ASME Boiler and Pressure Vessel Code, Section XI, IWB-3612,[6] considering the potential for crack growth and failure by net section collapse (limit load). Critical flaw sizes were determined considering both fatigue crack growth due to design cyclic loading and stress corrosion crack growth due to steady state stresses. Two approaches were used to assess the remaining service life of the pressurizer surge and spray nozzle safe ends for postulated surface flaws. The first approach uses a conservative, constant through-wall stress to account for residual and applied loading mechanisms, while the second approach utilizes a residual stress distribution from NUREG-0313[1] and actual applied stresses.

It is recognized that circumferential PWSCC could be the primary mode of failure for full penetration type nozzles with girth butt welded (i.e., full penetration welded) safe ends for two reasons: (1) high residual axial stresses may be present at the location of the girth butt weld; and (2) additional operational loads are produced by the attached piping. At the same time, compressive circumferential stress at the root of the weld, typical of butt welded piping components, tends to decrease the likelihood of axially-oriented PWSCC. Although the probability of finding axial flaws may be low, both axial and circumferential failure modes are addressed in the constant through-wall stress approach.

The use of a constant through-wall stress distribution was meant to be a conservative approach that precludes the need to determine actual loading conditions. The combination of weld shrinkage, pressure loads, material discontinuity, and external piping loads produces a complicated stress pattern that can best be predicted using a detailed analytical technique, such as elastic-plastic finite element analysis. Alternatively, a constant through-wall stress equal to the material yield strength at room temperature can be used to bound the total stress at operating temperature. Based on tabulated yield strengths from Section III of ASME Code, room temperature yield strengths are approximately 125% of yield strengths at operating temperatures greater than 500°F. Room temperature yield strength was applied as a constant

through-wall operating stress level for the evaluation of both axial and circumferential flaws. Consistent with this conservative approach for treating residual plus operational loads, the axial load used to assess the potential for net section collapse was derived considering a constant through-wall axial stress equal to the material yield strength at operating temperature.

Based on research conducted on large diameter boiling water reactor (BWR) stainless steel piping, it may be particularly conservative to assume a constant value of through-wall axial stress for evaluating circumferential flaws in girth butt welded safe ends. NUREG-0313 presents a nonlinear through-wall stress distribution (described by a fourth order polynomial) for axial residual stresses in 12" diameter piping joined by girth butt welds.

In the second approach, the inner surface residual stress was set equal to the material yield strength at operating temperature, and the remaining through-wall distribution followed the fourth-order polynomial described in NUREG-0313.[1] A constant through-wall primary plus secondary operating stress was derived from Section NB-3653, Equation (10), of the ASME Boiler and Pressure Vessel Code,[7] considering contributions from internal pressure, external piping moments, and thermal discontinuity between the Alloy 600 safe end and stainless steel piping. The resultant external piping moment is due to deadweight and thermal loads. Although operating stresses add directly to residual stresses in a purely linear analysis, the total is limited by elastic-plastic material behavior. To account for some strain hardening, but still control the magnitude of the total stress, the total stress at operation was limited to 125% of the operating temperature yield strength in this analysis.

Since an upper bound, constant through-wall stress condition used in the first approach is not used with the NUREG-based approach, the normal condition fracture toughness acceptance criterion no longer inherently bounds the faulted condition criterion. This required that the faulted condition fracture toughness acceptance criterion be checked at each crack depth, along with the normal condition criterion. A constant through-wall axial stress was calculated for faulted conditions using Equation (10) of the ASME Code[7] considering design pressure, deadweight plus thermal plus safe shutdown earthquake (SSE) seismic loads, and thermal discontinuity. In addition, the equivalent axial load used to check for net section collapse (limit load) was based on this same faulted condition stress.

The Palisades plant has 500 heatup and cooldown design cycles. In calculating fatigue crack growth, the maximum stress (i.e., yield strength) is combined with the minimum stress (i.e., zero at shutdown) to determine a cyclic stress range. The amount of fatigue crack growth was found to contribute only about 1% of the total crack growth as compared to PWSCC. For this reason, and based on experience, it was determined that accounting for smaller transients in the fatigue crack

growth analysis was not required. For stress corrosion crack growth at a given location, the maximum stress state is used to evaluate the corrosion crack growth within a given time span.

The leading industry thoughts on initial flaw size is that machining or fabrication processes leave a thin layer of high residual stress at the surface. Some quantitative measurements have been made using the X-ray diffraction technique; measured depths range from 0.002" in some cases to 0.010", which was measured at approximately 50 ksi. These values are dependent upon surface finishes and reaming following extrusion or machining. It is conservative, therefore, to assume an initial crack size of 0.010" for subcritical crack growth analysis for PWSCC. Thus, an initial flaw depth of 0.010" was implemented.[5]

5.1 Results from Initial Analysis - Constant Through-Wall Stress

For an initial flaw depth of 0.010", the remaining service life (i.e., time-to-failure) of the safe ends was calculated based on a constant through-wall stress for both axial and circumferential flaws. This data is tabulated below:

Component	Time-to-Failure (years) Based on Constant Through-Wall Stress					
	Axial Flaw			Circumferential Flaw		
	l/a#=2	l/a=4	l/a=6	l/a=2	l/a=4	l/a=6
Surge Nozzle Safe End	40.00	40.00	40.00	40.00	40.00	40.00
Spray Nozzle Safe End*	40.00 37.12	40.00 6.32	35.12 2.64	40.00 38.64	40.00 8.00	40.00 3.60

\# l/a is aspect ratio (length/depth);
* Top number in each cell is for the spray nozzle safe end at 540°F; bottom number is at 640°F.

Since a flaw depth of 0.010" is below minimum detection limits by ultrasonic (UT) inspection, plots of remaining life vs. crack depth were also developed.[5] Remaining life is shown as a function of crack depth for the spray nozzle safe end at 540°F and 640°F and the surge nozzle safe end in Figures 5 through 7 for axial flaws and in Figures 8 through 10 for circumferential flaws. These plots can be used to determine the remaining life based on an existing (and detectable) PWSCC crack. The allowable flaw sizes for the surge and spray nozzle safe ends are identified below for one operating cycle (18 months).

Component	Maximum Allowable Flaw Size (Inches) Based on Constant Through-Wall Stress					
	Axial Flaw			Circumferential Flaw		
	l/a#=2	l/a=4	l/a=6	l/a=2	l/a=4	l/a=6
Surge Nozzle Safe End	0.270	0.135	0.075	0.270	0.145	0.085
Spray Nozzle Safe End*	0.285 0.035	0.215 0.015	0.155 0.010	0.320 0.035	0.270 0.020	0.205 0.015

\# l/a is aspect ratio (length/depth);
* Top number in each cell is for the spray nozzle safe end at 540°F; bottom number is at 640°F.

Flaws that exceed the maximum allowable sizes identified above are not acceptable for one cycle of operation.

Since the spray nozzle safe end is much smaller (nominally) than both the surge nozzle and PORV safe ends, failure of the spray nozzle safe end is more dependent upon the temperature at which this safe end operates when compared to the surge nozzle safe end. At an operating temperature of 540°F, PWSCC failure of the spray nozzle safe end is of less concern; however, at an operating temperature of 640°F, time-to-failure of the spray nozzle safe end is calculated to be 2.64 years for an axial flaw and 3.60 years for a circumferential flaw, each having a 6/1 aspect ratio. [Note: Time-to-failure was calculated at both 540 and 640°F for the spray nozzle safe end since the operating temperature of this safe end depends on the flow rate of coolant through the safe end. It is assumed that the flow rate is high (50-70 gpm), leading to an operating temperature approaching that of the cold leg piping (540°F).] Also, the maximum allowable flaw sizes calculated for an operating temperature of 640°F are not detectable by UT inspection.

It should be noted that lower flow rates (including fluctuation of flow rate during operation) and the resulting higher operating temperatures of the spray nozzle safe end would lead to increased crack growth rates.

5.2 Results from Alternate Analysis - NUREG-0313 Approach

For an initial circumferential flaw depth of 0.010", the remaining service life (i.e., time-to-failure) of the safe ends was calculated based on NUREG-0313 and is identified below:

Component	Time-to-Failure (years) Based on NUREG-0313					
	Axial Flaw			Circumferential Flaw		
	l/a#=2	l/a=4	l/a=6	l/a=2	l/a=4	l/a=6
Surge Nozzle Safe End	N/A	N/A	N/A	40.00	40.00	40.00
Spray Nozzle Safe End*	N/A N/A	N/A N/A	N/A N/A	40.00 40.00	40.00 10.64	40.00 5.36

\# l/a is aspect ratio (length/depth);
* Top number in each cell is for the spray nozzle safe end at 540°F; bottom number is at 640°F.
N/A Not applicable

Similarly, the maximum allowable flaw sizes were calculated for the surge and spray nozzle safe ends using the NUREG-0313 approach; this data is tabulated below:

Component	Maximum Allowable Flaw Size (Inches) Based on NUREG-0313					
	Axial Flaw			Circumferential Flaw		
	l/a#=2	l/a=4	l/a=6	l/a=2	l/a=4	l/a=6
Surge Nozzle Safe End	N/A	N/A	N/A	0.550	0.415	0.320
Spray Nozzle Safe End*	N/A N/A	N/A N/A	N/A N/A	0.360 0.240	0.360 0.180	0.360 0.130

\# l/a is aspect ratio (length/depth);
* Top number in each cell is for the spray nozzle safe end at 540°F; bottom number is at 640°F.
N/A Not applicable

Again, flaws that exceed the maximum allowable sizes as shown above are not acceptable for one cycle of operation, based on the NUREG-0313 approach. Figures 11 through 13 illustrate remaining life vs. flaw size for the three cases tabulated above.

The maximum allowable flaw sizes shown above, unlike those calculated for constant through-wall stress (per Section 5.1), are all greater than

the UT detection limit of 2 mm (0.079"). However, the maximum allowable flaw size calculated for the spray nozzle safe end at an operating temperature of 640°F is significantly less than that corresponding to a 540°F operating temperature.

6.0 Summary

From a materials standpoint, all three safe ends are considered highly susceptible to PWSCC based on the chemical compositions, fabrication information, operational parameters, and details of installation known at this time. Thus, both the surge nozzle and spray nozzle safe ends are considered to be of concern with regard to PWSCC crack growth. The surge nozzle safe end operates at the same operating temperature (640°F) as the PORV nozzle safe end, although the surge nozzle safe end has a constant wall thickness of 1.005" whereas the wall thickness of the PORV safe end decreases from 1.5" (nominal) to approximately 0.5" at the safe end-to-piping weld where the failure occurred. It should be noted that the carbon content of the surge nozzle safe end is somewhat lower than that of the PORV and spray nozzle safe end material, but this difference is insignificant relative to the insufficient annealing treatments that both material heats received. Again, the stress relief treatment given to the three safe ends and safe-end-to-pressurizer welds is not believed to have significantly improved resistance to PWSCC at these locations.

The PORV safe end, which leaked and was repaired in 1993, failed after 23 years of service (~9 EFPY). It is known that poor fabrication and welding were performed on this safe end, as mentioned previously. It is expected that the spray nozzle safe end would be somewhat less susceptible to PWSCC at a normal operating temperature of 540°F, although some rework is believed to have been done on the spray nozzle safe end weld as well. Since the heat of material is the same for both of these safe ends, however, extensive additional life (i.e., resistance to PWSCC cracking) of the spray nozzle safe end is not expected, even at a low operating temperature. The surge nozzle safe end, since it was fabricated from a different heat of material, may be slightly less susceptible than the other two safe ends, although the rework completed on this safe end weld would increase susceptibility to PWSCC due to the induced residual stresses.

With regard to the PWSCC crack growth calculations described in Section 5.1, the remaining life of the spray nozzle safe end is calculated to be relatively short at an operating temperature of 640°F once a PWSCC crack initiates. At 540°F, the time-to-failure of this safe end is calculated to be 35.12 years for an axial flaw or 40 years for a circumferential flaw, each with an initial flaw size of 0.010" and a 6/1 aspect ratio. The results of the alternate analysis, reported in Section 5.2, identify the time-to-failure of the spray nozzle safe end to be 40 years and 5.36 years, respectively, for operating temperatures of 540°F and 640°F. This data is based on a circumferential flaw with an initial flaw size of 0.010" and a 6/1 aspect ratio. The surge nozzle safe end was

determined to have a remaining life of 40 years for an axial or circumferential flaw (based on both analyses), also for an initial flaw size of 0.010" and a 6/1 aspect ratio.

There are other items to consider as well. For example, if the spray nozzle safe end fails due to PWSCC and the plant operates for some time before the leak is detected, there is a concern regarding boric acid corrosion of carbon and low alloy steel components in the vicinity. Much of the coolant is expected to flash to steam, but low flowing leaks of liquid coolant can cause severe degradation of these susceptible materials to occur.[8] Also, failure of the surge nozzle could lead to significant leakage below the pressurizer in an area that is difficult to access.

7.0 Recommendations

Based on the above information, failure of both the surge nozzle safe end and spray nozzle safe end due to PWSCC is of concern. The spray nozzle safe end is believed to be somewhat more susceptible to PWSCC and would be expected to fail sooner due to its smaller size. As a minimum, therefore, it is recommended that Alloy 690 material be procured and stored for fabrication of a replacement spray nozzle safe end in the event that failure of this safe end occurs. As mentioned above, if the operating temperature of the existing spray nozzle safe end remains approximately 540°F, PWSCC of the safe end will be delayed. If 640°F is the more appropriate operating temperature, PWSCC of the spray nozzle safe end will occur sooner, and fabrication of the procured material into a replacement safe end should be considered.

Since remaining life is calculated based upon the size of an existing flaw, it is also recommended that regular non-destructive examinations be performed on the spray nozzle safe end, at a minimum, so that any flaws within this safe end can be detected as early as possible. [Note: If no flaws are detected during the 1995 inspection based on an approximate minimum detection limit of 2 mm (0.079"), the next inspection should be performed after two operating cycles.] Once a crack is detected, however, repair of the spray nozzle safe end needs to be performed since a detectable crack is expected to grow through-wall within 1-2 operating cycles, depending on the operating temperature.

NDE inspection of the surge nozzle safe end is not as critical due to its large size. However, due to the consequences of a leak at this location -- a possible loss of coolant accident (LOCA) -- an initial inspection of this safe end is recommended to identify if any cracks do exist. Follow-up inspections can be performed at the utility's discretion (based on the results of previous inspections) to identify the initiation of new cracks or to monitor the growth of existing cracks. In order to avoid a "special order" and a long lead time in the event of a failure, it is recommended that Alloy 690 material be procured and stored for fabrication of a replacement surge nozzle safe end.

8.0 References

1. Hazelton, W.S., and W.H. Koo, "Technical Report on Material Selection and Processing Guidelines for BWR Coolant Pressure Boundary Piping," NUREG-0313, Rev. 2, U.S. Nuclear Regulatory Commission, Washington, D.C., January 1988.

2. Sarver, J.M., Crum, J.R., and Mankins, W.L., "Effect of Carbide Precipitation on the Corrosion Behavior of Inconel Alloy 690," Presented at Corrosion 87, San Francisco, California, 1987.

3. Czajkowski, C.J., "Palisades Nuclear Plant Safe-End to Pipe Cracking," MCE-E2089-02, Brookhaven National Laboratory, Upton, NY, January 1994.

4. Consumers Power Company Document Control Center Cartridge No. 67, Frame 2220.

5. Killian, D.E., "Fracture Mechanics Assessment of Palisades Alloy 600 Components," BWNT Document No. 32-1238965-00, B&W Nuclear Technologies, Lynchburg, Virginia, April 1995.

6. ASME Boiler and Pressure Vessel Code, Section XI, 1986 Edition.

7. ASME Boiler and Pressure Vessel Code, Section III, Subsection NB, 1986 Edition.

8. Ouellette, C.A., "B&W Boric Acid Corrosion Research and the Wastage and Inspection Procedures for RCS Leakage," BAW-2126, B&W Nuclear Technologies, Lynchburg, Virginia, December 1990.

FIGURE 1

SOLUBILITY DIAGRAM FOR ALLOY 600

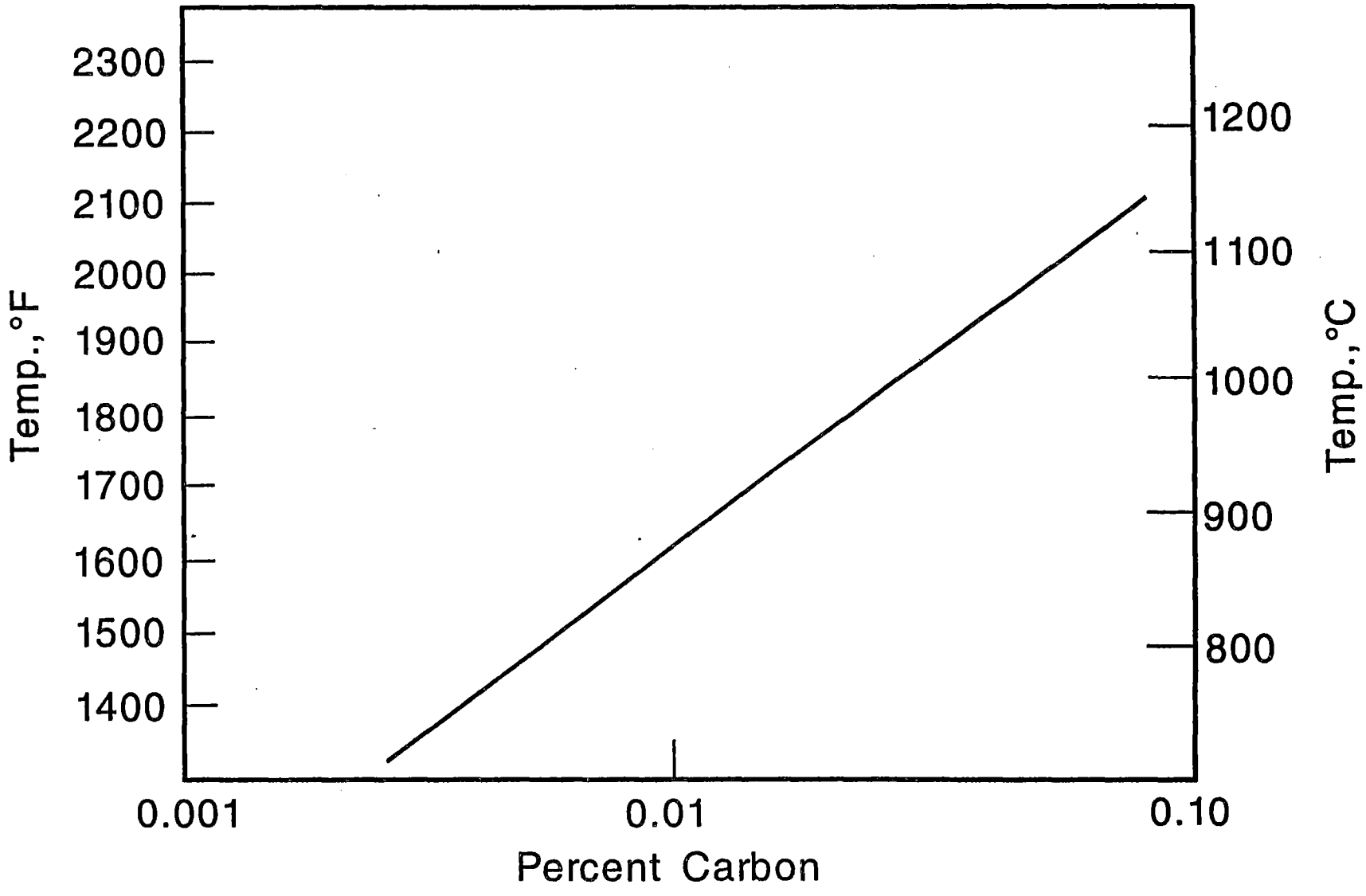

FIGURE 2

SPRAY NOZZLE SAFE END

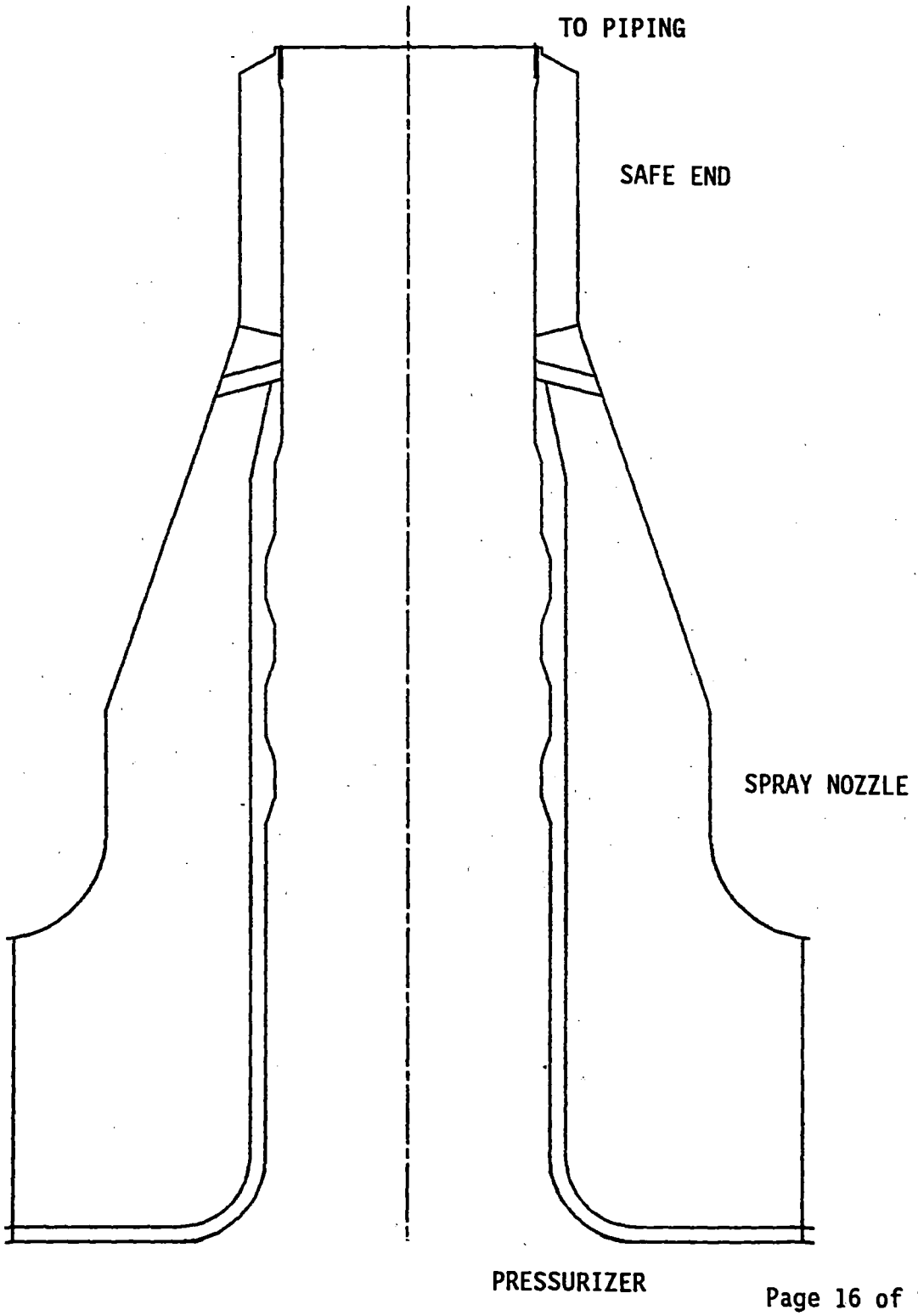

FIGURE 3

SURGE NOZZLE SAFE END

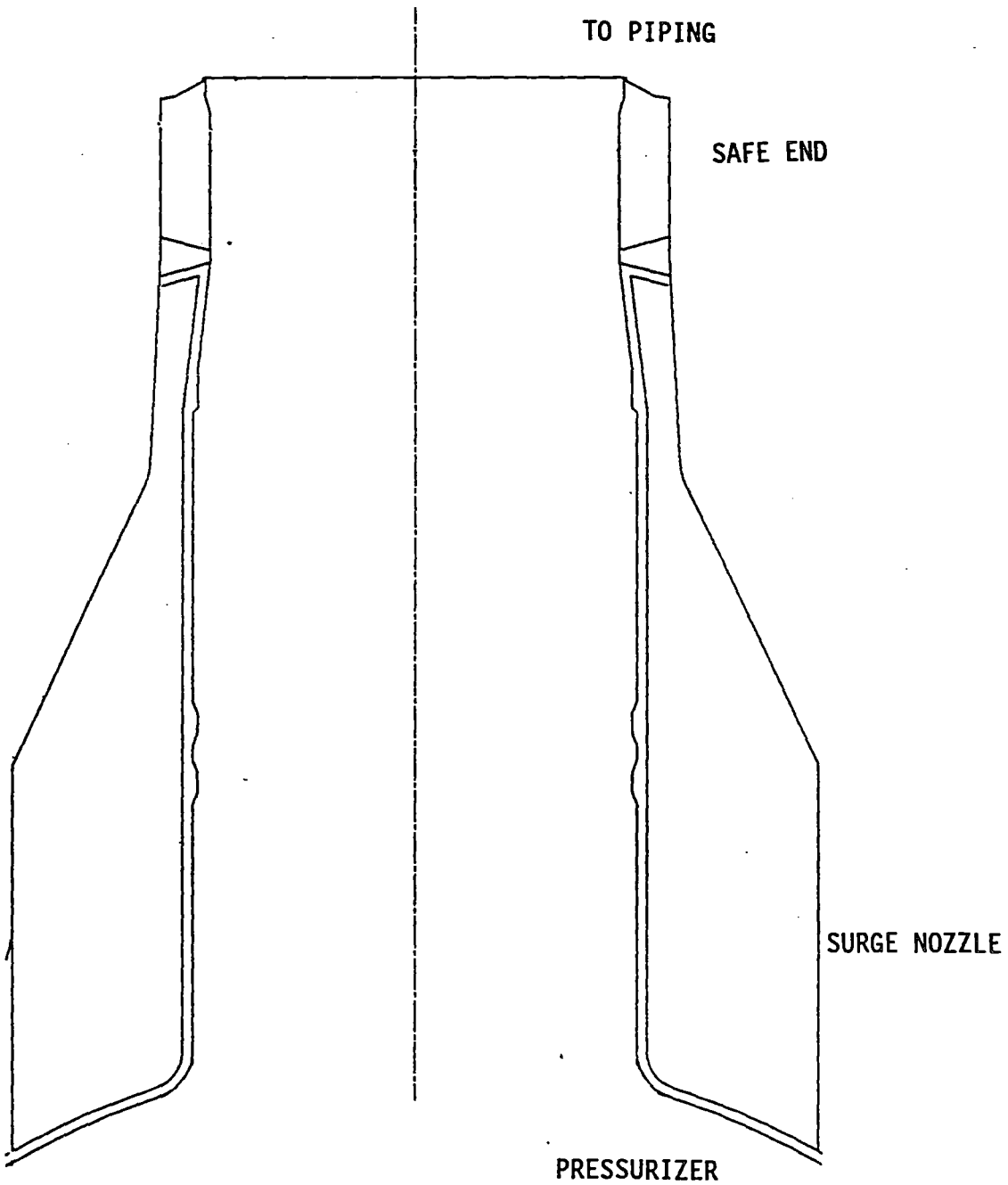

FIGURE 4

PORV SAFE END

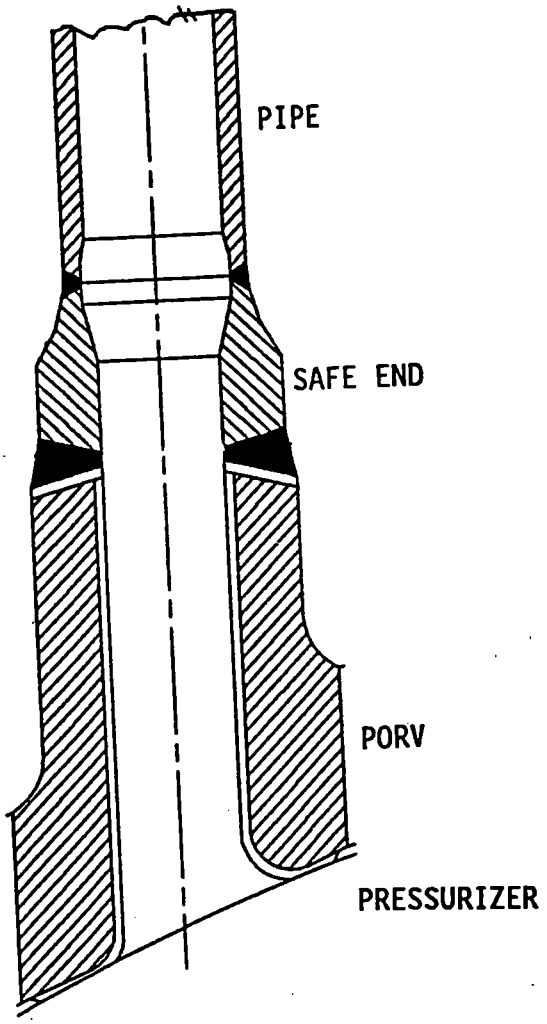

FIGURE 5

REMAINING LIFE VS. INITIAL CRACK DEPTH
FOR THE PRESSURIZER SPRAY NOZZLE SAFE END
AXIAL FLAW AT T_{op}=540°F
(Ref. 5)

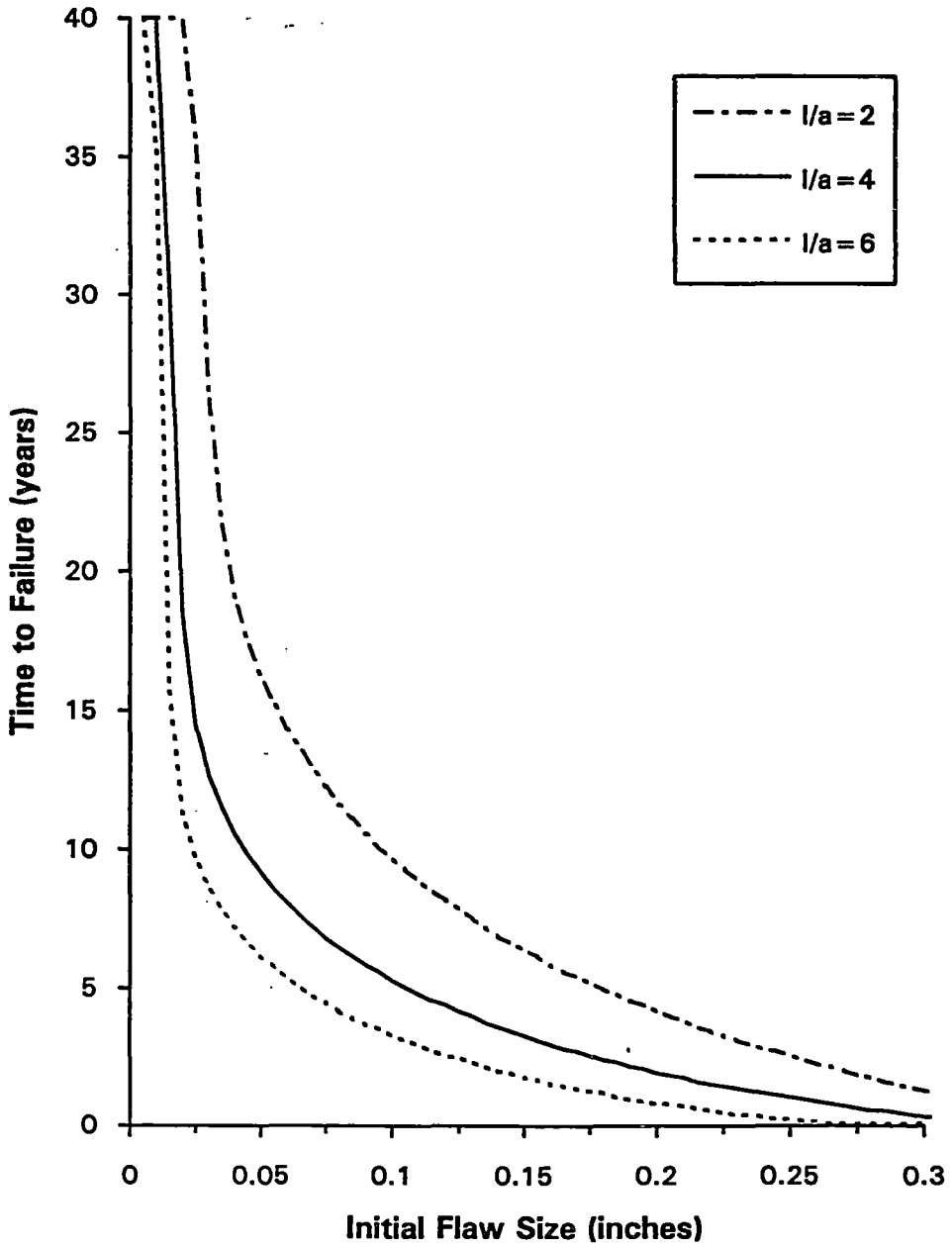

FIGURE 6

REMAINING LIFE VS. INITIAL CRACK DEPTH
FOR THE PRESSURIZER SPRAY NOZZLE SAFE END
AXIAL FLAW AT T_{op}=640°F
(Ref. 5)

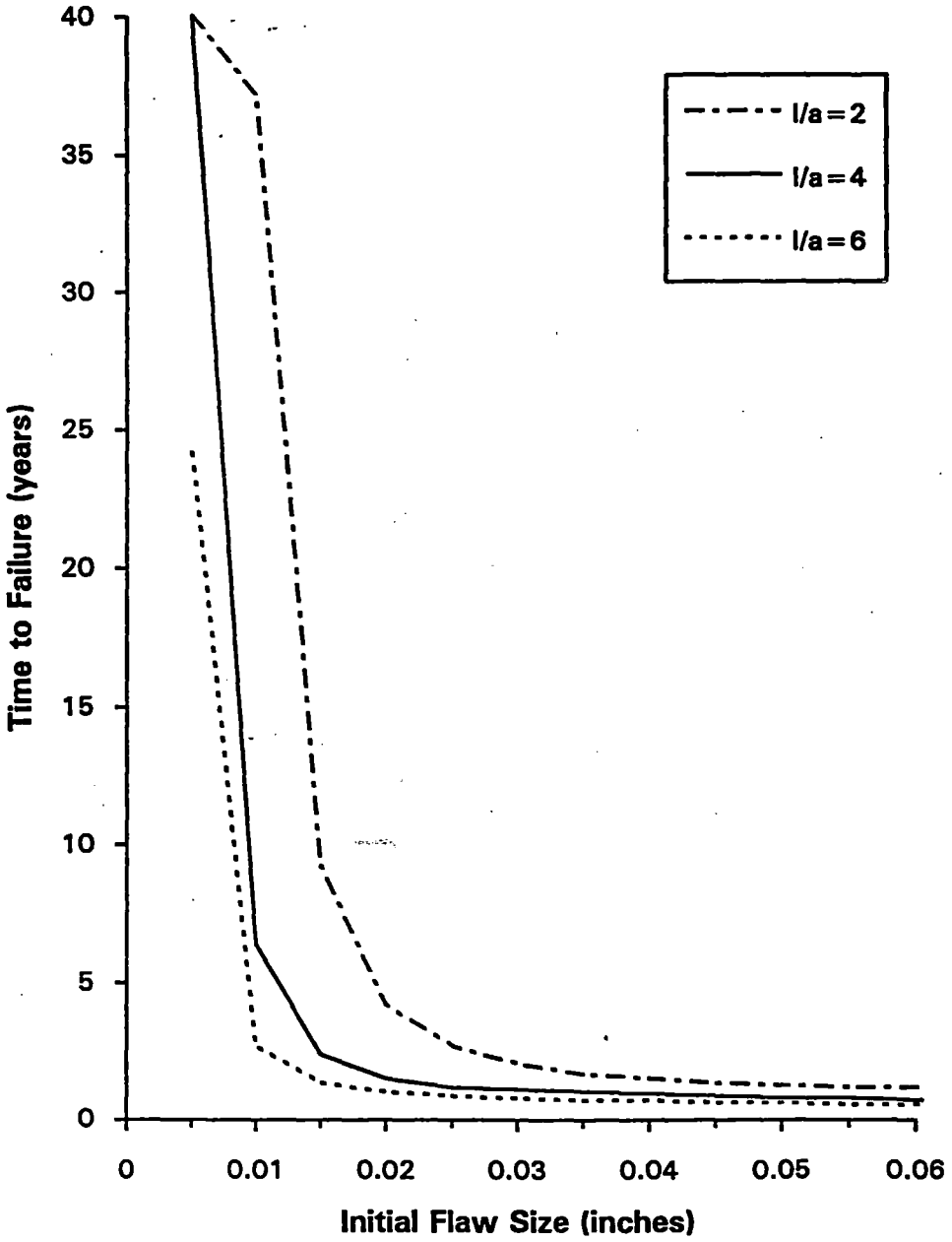

FIGURE 7

REMAINING LIFE VS. INITIAL CRACK DEPTH
FOR THE PRESSURIZER SURGE NOZZLE SAFE END
AXIAL FLAW
(Ref. 5)

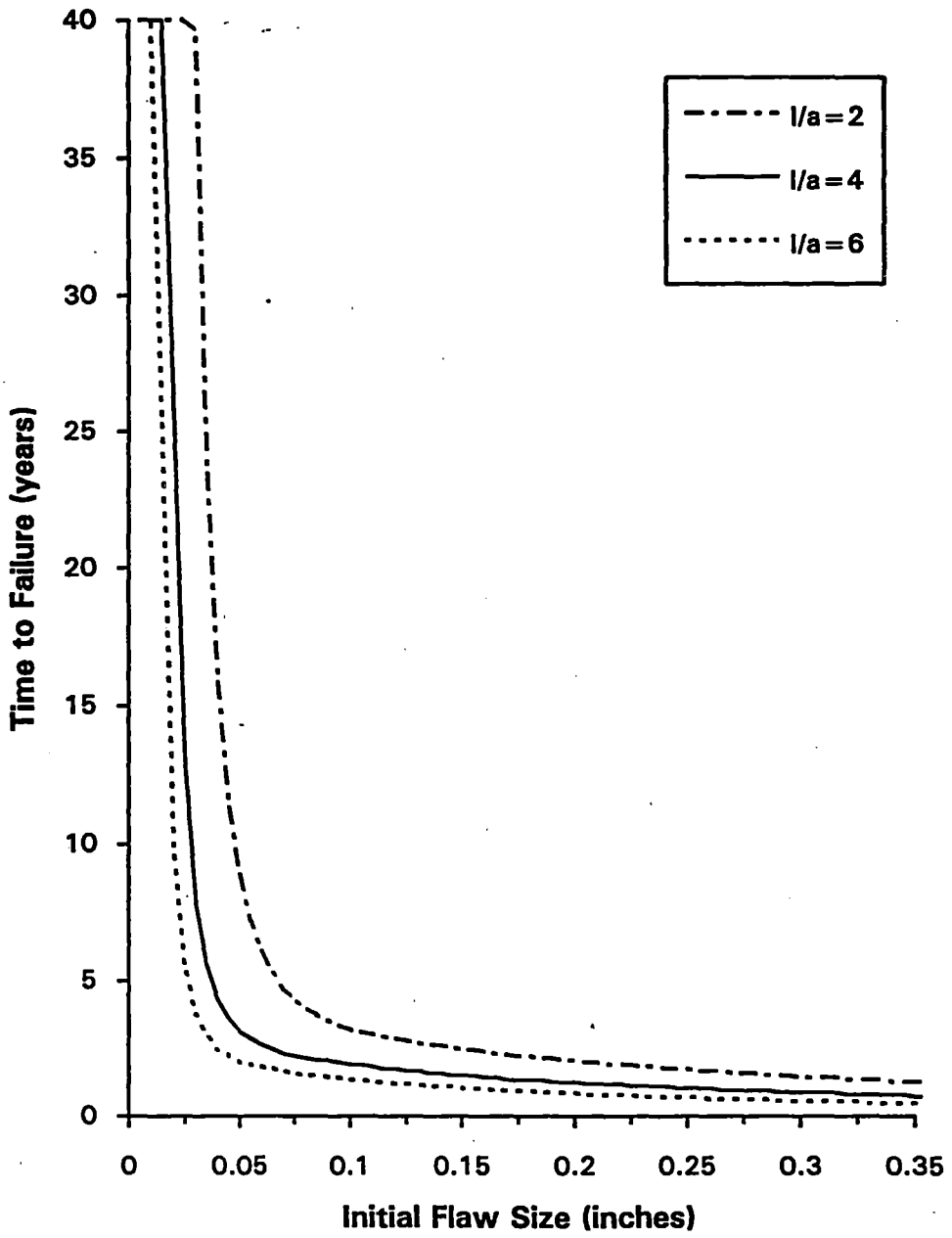

FIGURE 8

REMAINING LIFE VS. INITIAL CRACK DEPTH
FOR THE PRESSURIZER SPRAY NOZZLE SAFE END
CIRCUMFERENTIAL FLAW AT T_{op}=540°F
(Ref. 5)

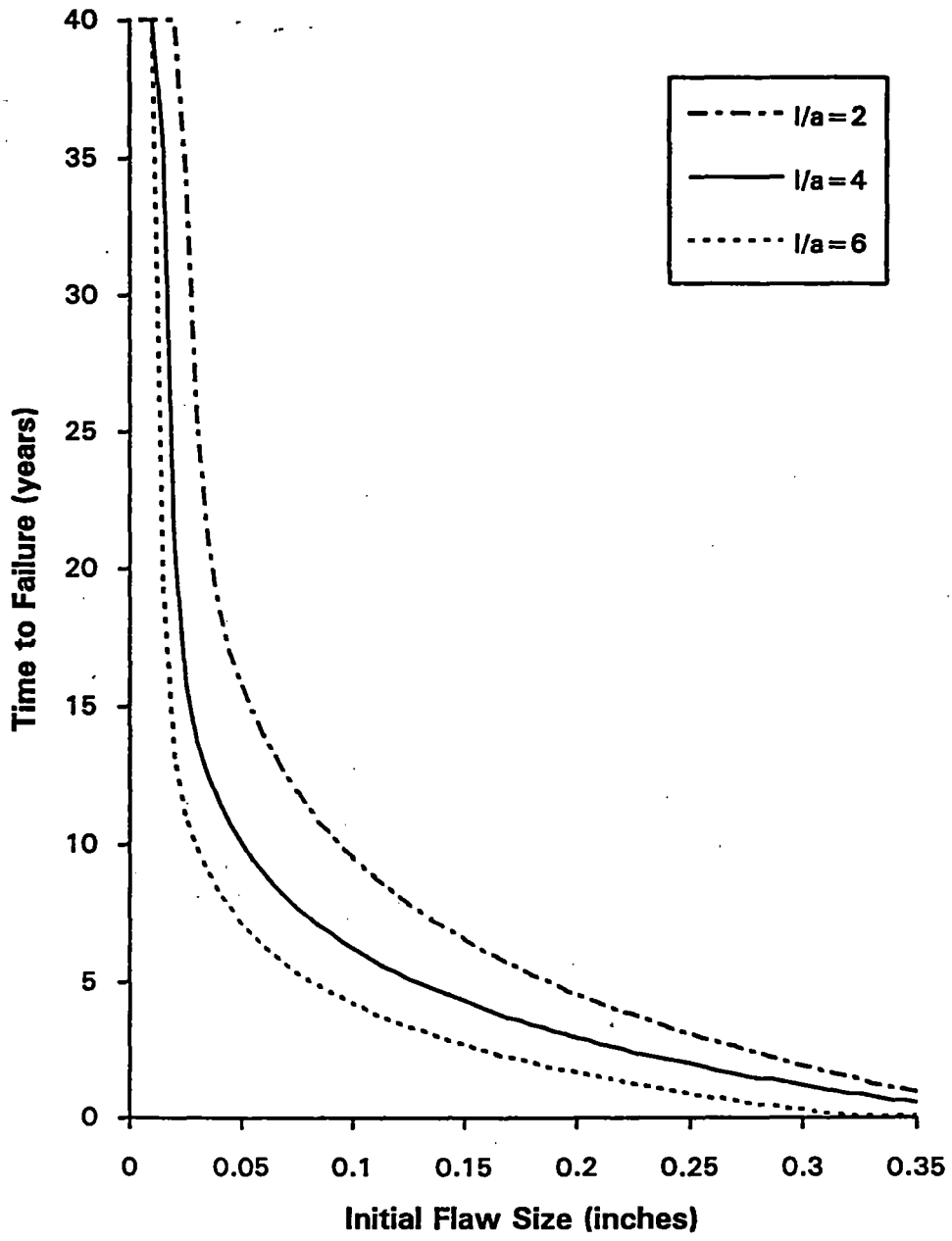

FIGURE 9

REMAINING LIFE VS. INITIAL CRACK DEPTH
FOR THE PRESSURIZER SPRAY NOZZLE SAFE END
CIRCUMFERENTIAL FLAW AT T_{op}=640°F
(Ref. 5)

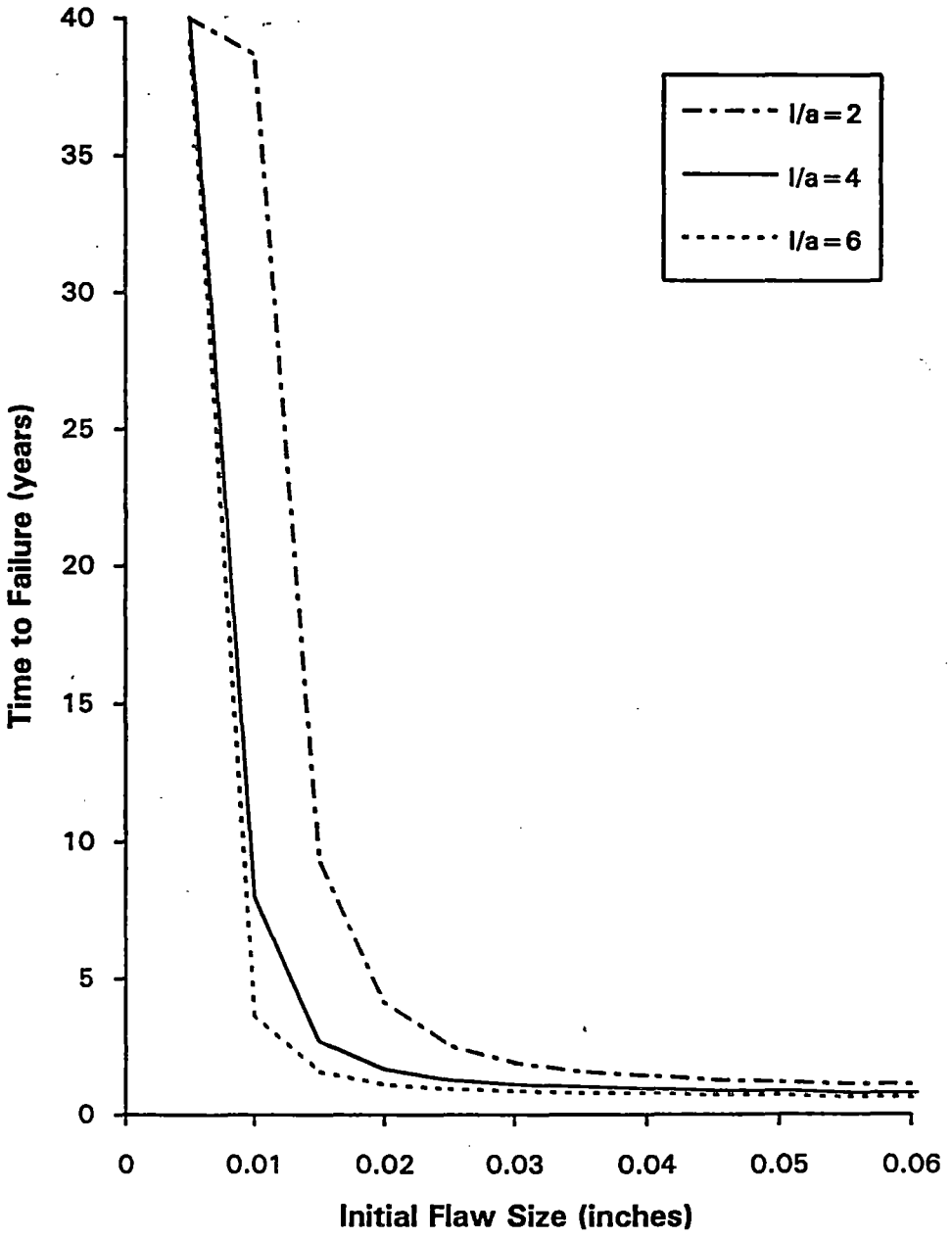

FIGURE 10

REMAINING LIFE VS. INITIAL CRACK DEPTH
FOR THE PRESSURIZER SURGE NOZZLE SAFE END
CIRCUMFERENTIAL FLAW
(Ref. 5)

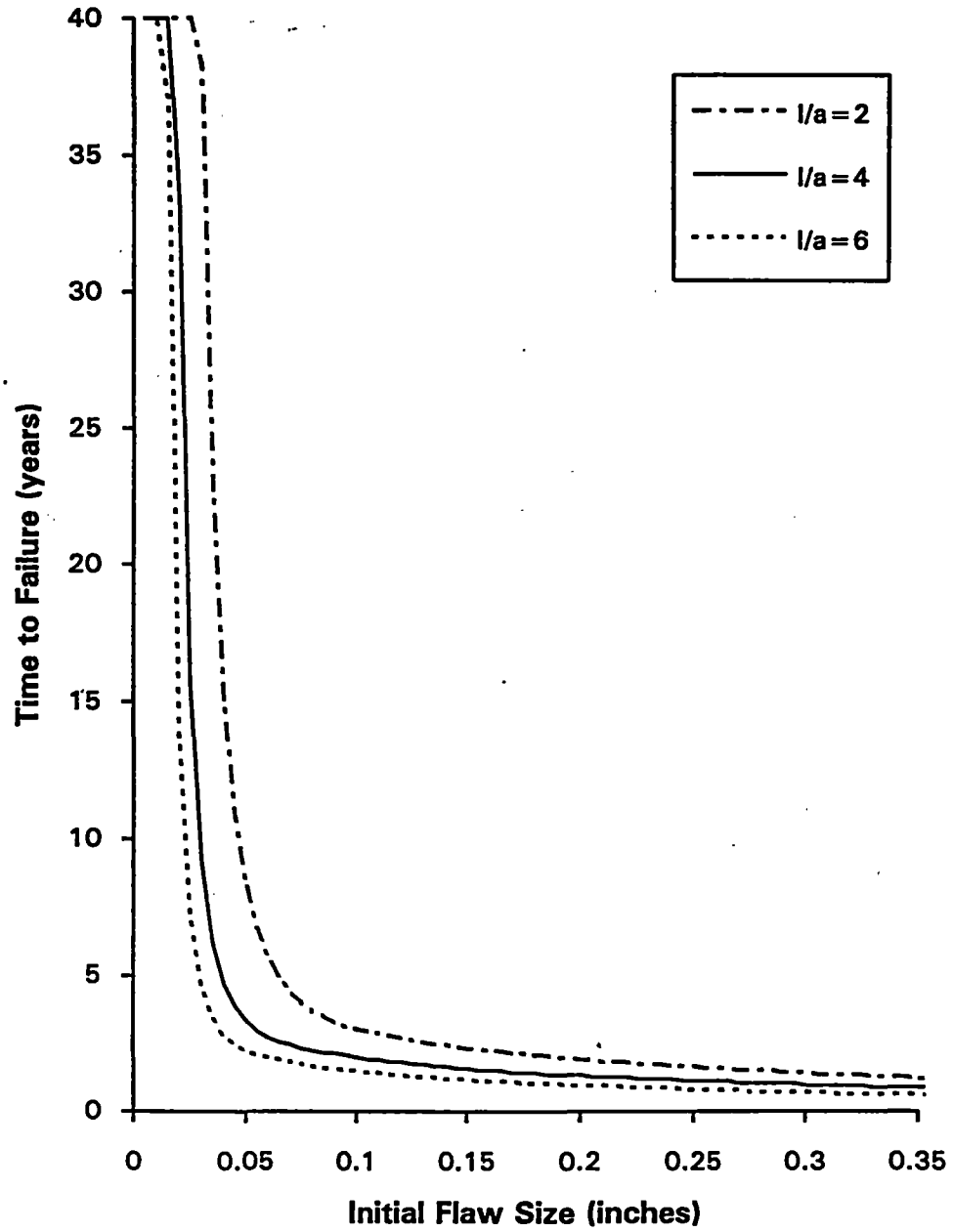

FIGURE 11

REMAINING LIFE VS. INITIAL CRACK DEPTH
FOR THE PRESSURIZER SPRAY NOZZLE SAFE END
CIRCUMFERENTIAL FLAW AT T_{op}=540°F
BASED ON NUREG-0313
(Ref. 5)

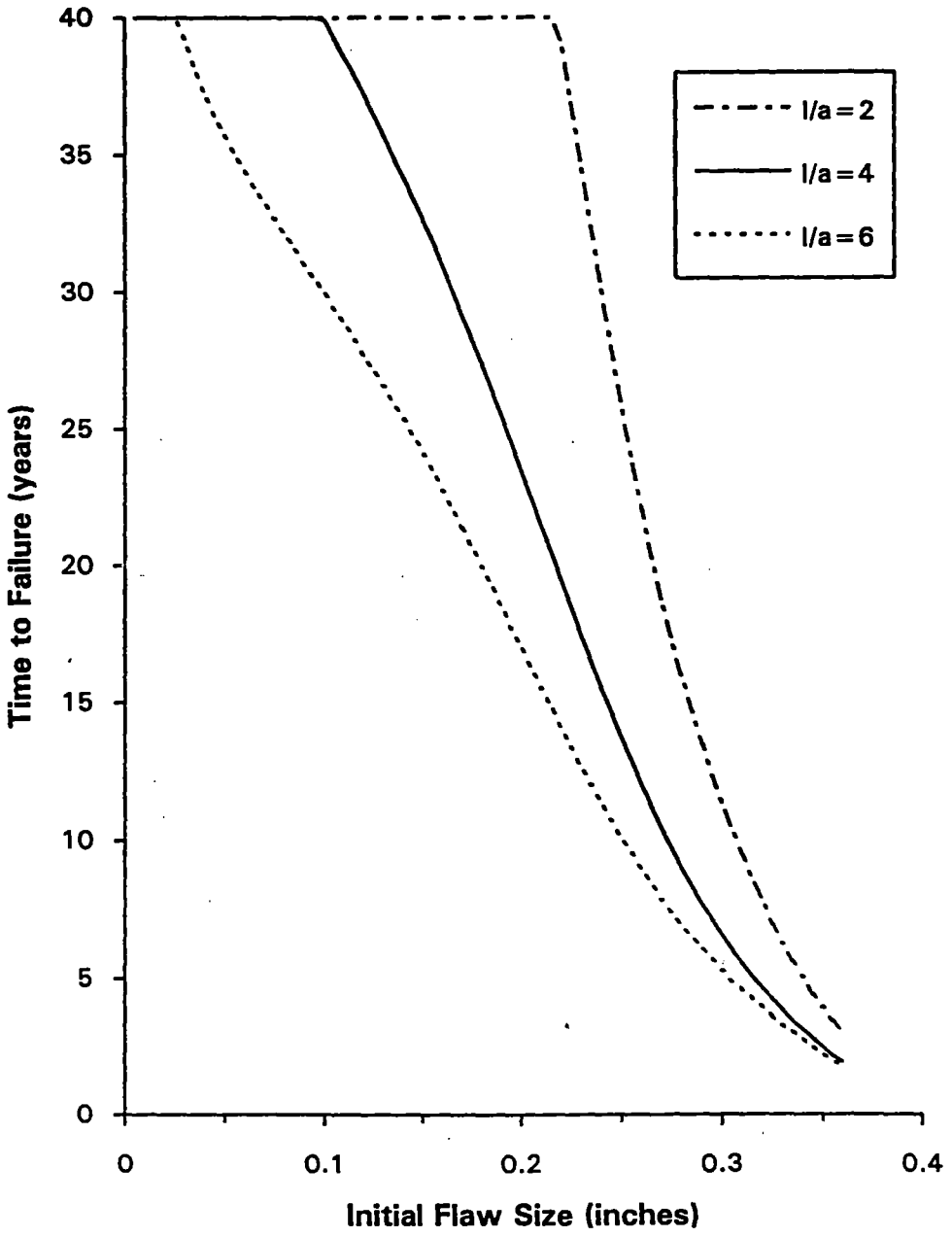

FIGURE 12

REMAINING LIFE VS. INITIAL CRACK DEPTH
FOR THE PRESSURIZER SPRAY NOZZLE SAFE END
CIRCUMFERENTIAL FLAW AT T_{op}=640°F
BASED ON NUREG-0313
(Ref. 5)

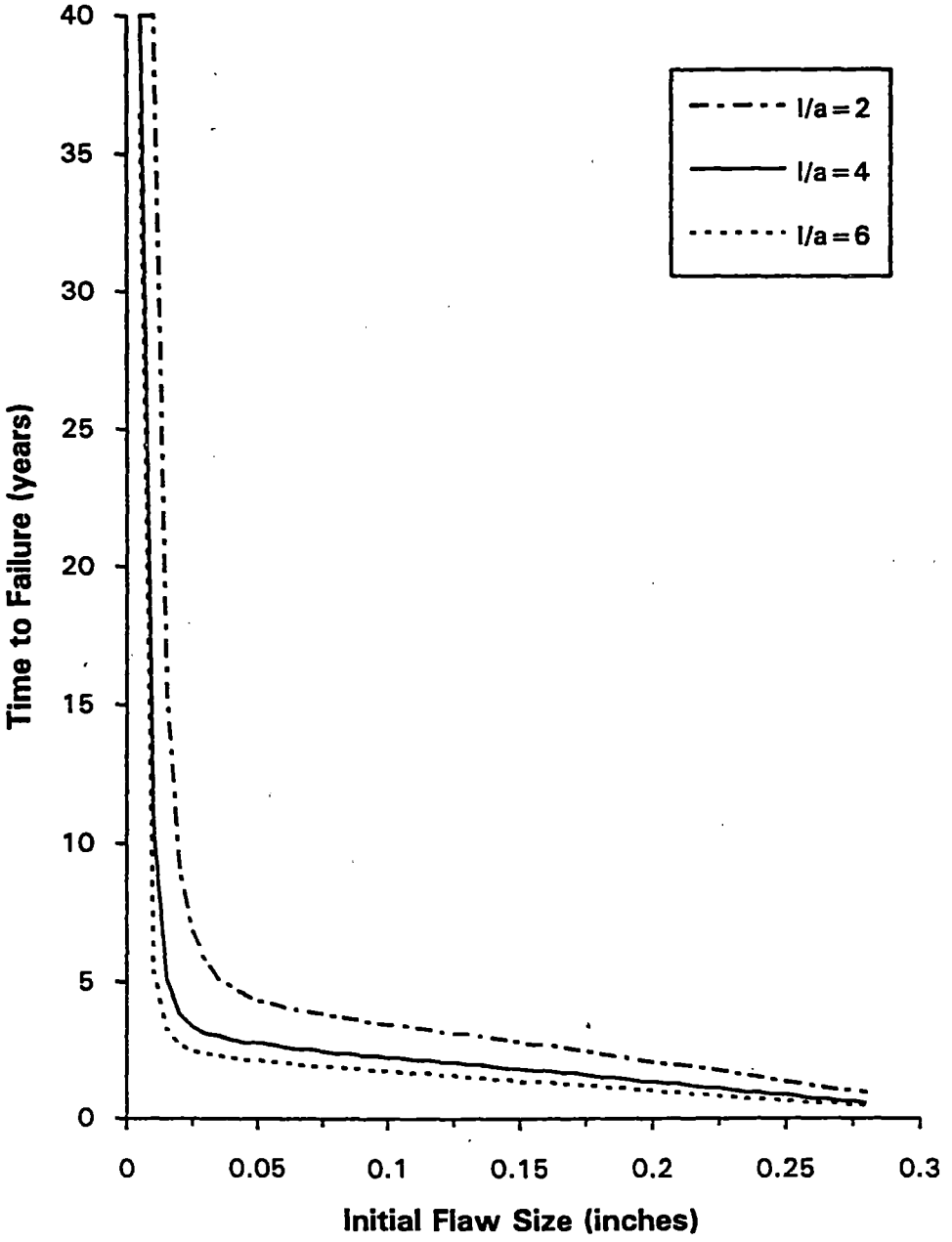

FIGURE 13

REMAINING LIFE VS. INITIAL CRACK DEPTH
FOR THE PRESSURIZER SURGE NOZZLE SAFE END
CIRCUMFERENTIAL FLAW
BASED ON NUREG-0313
(Ref. 5)

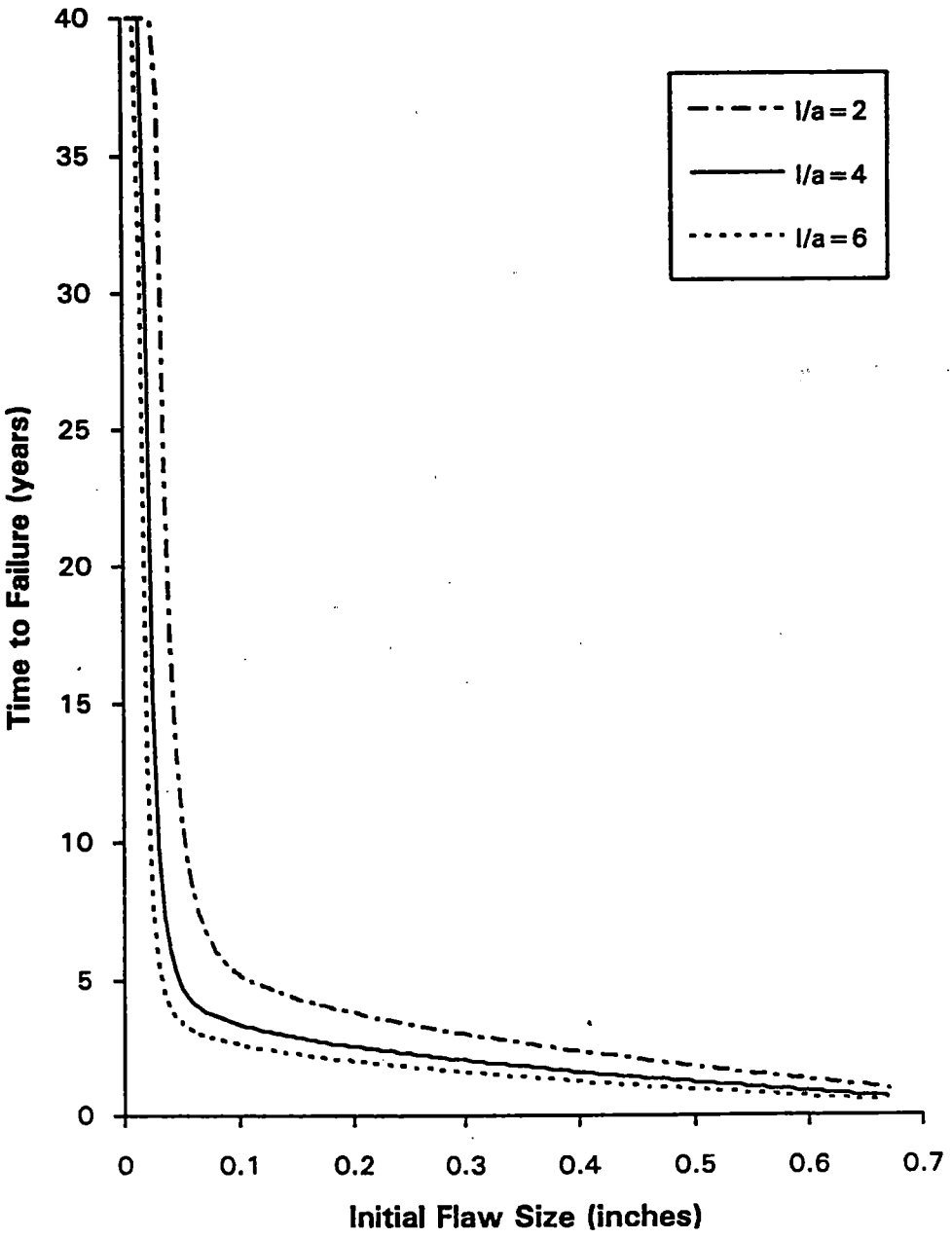

ATTACHMENT 3

Consumers Power Company
Palisades Plant
Docket 50-255

FRACTURE MECHANICS ASSESSMENT OF PALISADES ALLOY 600 COMPONENTS
BWNT CALC No. 32-1235177-00

April 24, 1995

9505030330 950424
PDR ADOCK 05000255
P PDR

B&W NUCLEAR TECHNOLOGIES

CALCULATION SUMMARY SHEET (CSS)

DOCUMENT IDENTIFIER 32-1238965-00

TITLE FM Assessment of Palisades Alloy 600 Components

PREPARED BY:		REVIEWED BY:	
NAME	D.E. Killian	NAME	K.K. Yoon
SIGNATURE	D.E. Killian	SIGNATURE	K.K. Yoon
TITLE	Principal Engineer	TITLE	Technical Consultant
DATE	4/20/95	DATE	4/20/95
COST CENTER	41020	REF. PAGE(S)	58
TM STATEMENT: REVIEWER INDEPENDENCE		K.K. Yoon	

PURPOSE AND SUMMARY OF RESULTS:

PURPOSE:

The purpose of this analysis is to determine the suitability of Palisades Alloy 600 components for safe operation. Postulated internal axial and circumferential flaws are evaluated in accordance with the fracture toughness requirements set by the ASME Boiler and Pressure Vessel Code, Section XI, IWB-3612, considering the potential for crack growth and failure by net section collapse (limit load). The objective is to develop a set of curves from which the allowable time for continued service can be determined for a given flaw size. This is done by evaluating both fatigue crack growth due to design cyclic loading and stress corrosion crack growth due to steady state stresses for each of the Palisades' Alloy 600 components.

SUMMARY OF RESULTS:

Table 6 shows the estimated remaining service life of the Palisades Alloy 600 components, assuming a constant through-wall stress equal to about 125% of the operating yield strength of the material. These results are graphically depicted in Figures 7 through 34. The pressurizer spray nozzle safe end has an estimated service life of 2.64 years assuming a worst case temperature of 640°F. The pressurizer temperature element nozzles can be expected to remain in service for about 7.5 years. All other components can remain in service for 40 years.

An alternate approach, based on the nonlinear distribution for residual axial stress in NUREG-0313, was used for the pressurizer surge and spray nozzle safe ends. These results are shown in Table A-3 and Figures A-4 through A-6. The limiting service life was increased from 2.64 to 5.36 years for the pressurizer spray nozzle safe end at 640°F.

Note: This document is classified as BWNT Non-Proprietary.

THE FOLLOWING COMPUTER CODES HAVE BEEN USED IN THIS DOCUMENT:

CODE / VERSION / REV	CODE / VERSION / REV

THIS DOCUMENT CONTAINS ASSUMPTIONS THAT MUST BE VERIFIED PRIOR TO USE ON SAFETY-RELATED WORK

YES ( ) NO (X)

RECORD OF REVISIONS

Revision	Description of Revision	Date
0	Original Release	4/95

TABLE OF CONTENTS

Section	Title	Page
List of Figures		4
List of Tables		5
1.0	Introduction	6
2.0	Nozzle/Flaw Geometry	6
	2.1 Postulated Flaw Geometries	6
	2.2 Geometry of Alloy 600 Components	9
3.0	Stresses	10
	3.1 Applied Stresses	10
	3.2 Spectrum History	10
4.0	Fracture Mechanics Analysis	11
	4.1 ASME B&PV Code, Section XI, Acceptance Criteria	11
	4.2 Stress Intensity Factor Solutions	12
	4.3 Irwin Plasticity Correction	15
	4.4 Limit Load Solutions	17
	4.5 Initial Flaw Depth	19
	4.6 Fatigue Crack Growth	20
	4.7 Stress Corrosion Crack Growth	22
5.0	Material Properties	25
6.0	Procedure for Assessment of Alloy 600 Components	26
7.0	Results and Conclusions	28
8.0	References	58
Appendix		
A	Alternate Method using Residual Stress Distribution from NUREG-0313	59
B	Verification of FORTRAN Programs	71
C	Computer Input Files	79
D	List of Computer Output Microfiche	85

LIST OF FIGURES

Figure	Title	Page
1.	Semi-Elliptical Internal Axial Flaw	7
2.	Semi-Elliptical Internal Circumferential Flaw	8
3.	The Irwin Plastic Zone Correction.	16
4.	Inconel - Wrought Material - Effect of Temperature and PWR Environment on Fatigue Crack Growth Rates	21
5.	Comparison of Crack Growth Rates as a Function of Temperature	24
6.	Procedure Used to Evaluate the Remaining Service Life of Each of the Palisades' Alloy 600 Components	27
	Allowable Flaw Depth Versus Time to Failure: Yield Stress, Axial Flaw	
7.	Pressurizer TE Nozzles	30
8.	Pressurizer Surge Nozzle Safe End	31
9.	Pressurizer Spray Nozzle Safe End @ 540 deg F	32
10.	Pressurizer Spray Nozzle Safe End @ 640 deg F	33
11.	Hot Leg Surge Nozzle Safe End	34
12.	Hot Leg Shut Down Nozzle Safe End	35
13.	Hot Leg Loop Drain Nozzle	36
14.	Hot Leg Pressure & Sampling Nozzle	37
15.	Hot Leg RTD Nozzle	38
16.	Cold Leg Shut Down Nozzle Safe End	39
17.	Cold Leg Spray Nozzle	40
18.	Cold Leg Charging and Loop Drain Nozzles	41
19.	Cold Leg Pressure & Sampling Nozzle	42
20.	Cold Leg RTD Nozzle	43
	Allowable Flaw Depth Versus Time to Failure: Yield Stress, Circ Flaw	
21.	Pressurizer TE Nozzles	44
22.	Pressurizer Surge Nozzle Safe End	45
23.	Pressurizer Spray Nozzle Safe End @ 540 deg F	46
24.	Pressurizer Spray Nozzle Safe End @ 640 deg F	47
25.	Hot Leg Surge Nozzle Safe End	48
26.	Hot Leg Shut Down Nozzle Safe End	49
27.	Hot Leg Loop Drain Nozzle	50
28.	Hot Leg Pressure & Sampling Nozzle	51
29.	Hot Leg RTD Nozzle	52
30.	Cold Leg Shut Down Nozzle Safe End	53
31.	Cold Leg Spray Nozzle	54
32.	Cold Leg Charging and Loop Drain Nozzles	55
33.	Cold Leg Pressure & Sampling Nozzle	56
34.	Cold Leg RTD Nozzle	57

LIST OF TABLES

Table	Title	Page
1.	Summary of Geometric Dimensions for Palisades' Alloy 600 Components	9
2a.	Axial Flaw Shape Factors Associated with the Deepest Point on the Flaw	12
2b.	Axial Flaw Shape Factors Associated with the Point Near the Surface	13
3.	Circumferential Flaw Shape Factors Associated with the Deepest Point on the Flaw	14
4.	Derivation of Paris Law Coefficients Using Data from Figure 4 for a PWR environment	20
5.	Material Properties Required for Fracture Mechanics Assessment of Palisades' Alloy 600 Components	25
6.	Summary of Time to Failure for an Initial Flaw Depth of 0.010"	29
7.	Summary of Allowable Flaw Depths for One Fuel Cycle (18 months)	29

1.0 Introduction

The purpose of this analysis is to determine the suitability of Palisades Alloy 600 components for safe operation. Postulated internal axial and circumferential flaws are evaluated in accordance with the fracture toughness requirements set by the ASME Boiler and Pressure Vessel Code, Section, XI, IWB-3612, considering the potential for crack growth and failure by net section collapse (limit load). The objective is to develop a set of curves from which the allowable time for continued service can be determined for a given flaw size. This is done by evaluating both fatigue crack growth due to design cyclic loading and stress corrosion crack growth due to steady state stresses for each of the Palisades' Alloy 600 components.

2.0 Nozzle/Flaw Geometry

2.1 Postulated Flaw Geometries

In this analysis, a postulated semi-elliptical internal surface flaw is evaluated with a longitudinal orientation and with a circumferential orientation. As will be seen in Section 4.3, the postulated axial flaw will be evaluated using a third order curve fit of the circumferential stress, while the circumferential flaw will be evaluated using a third order curve fit of the axial stress. Figures 1 and 2 graphically depict the information required to evaluate the postulated flaws.

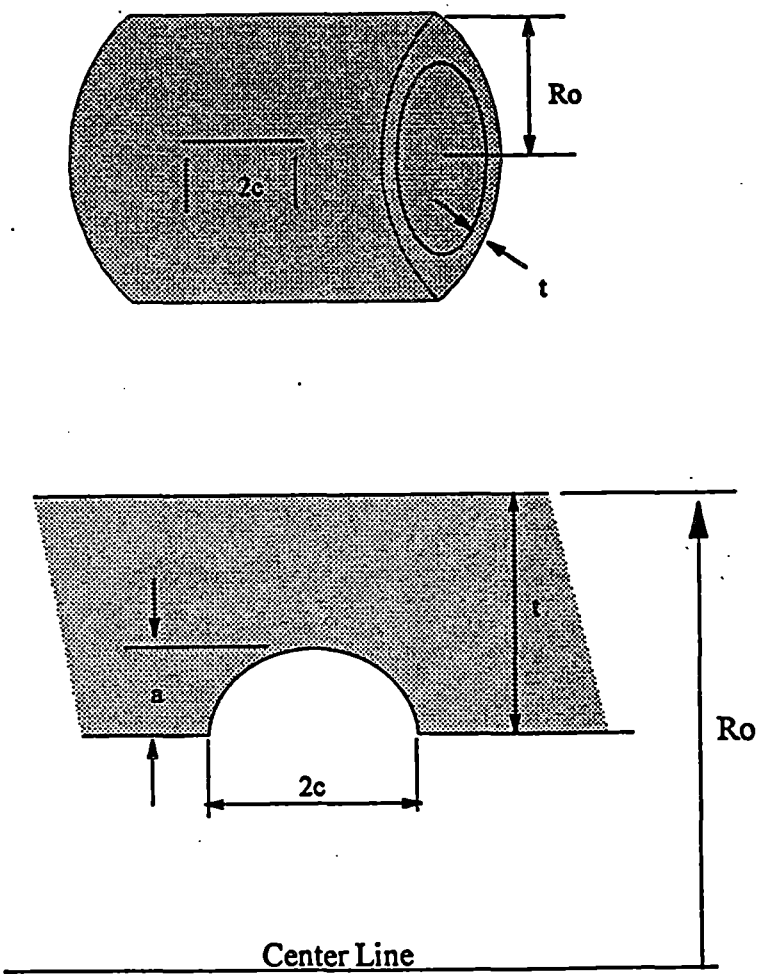

Figure 1. Semi-Elliptical Internal Axial Flaw

Prepared by: D.E. Killian Date: 4/19/95

Reviewed by: K.K. Yoon Date: 4/20/95

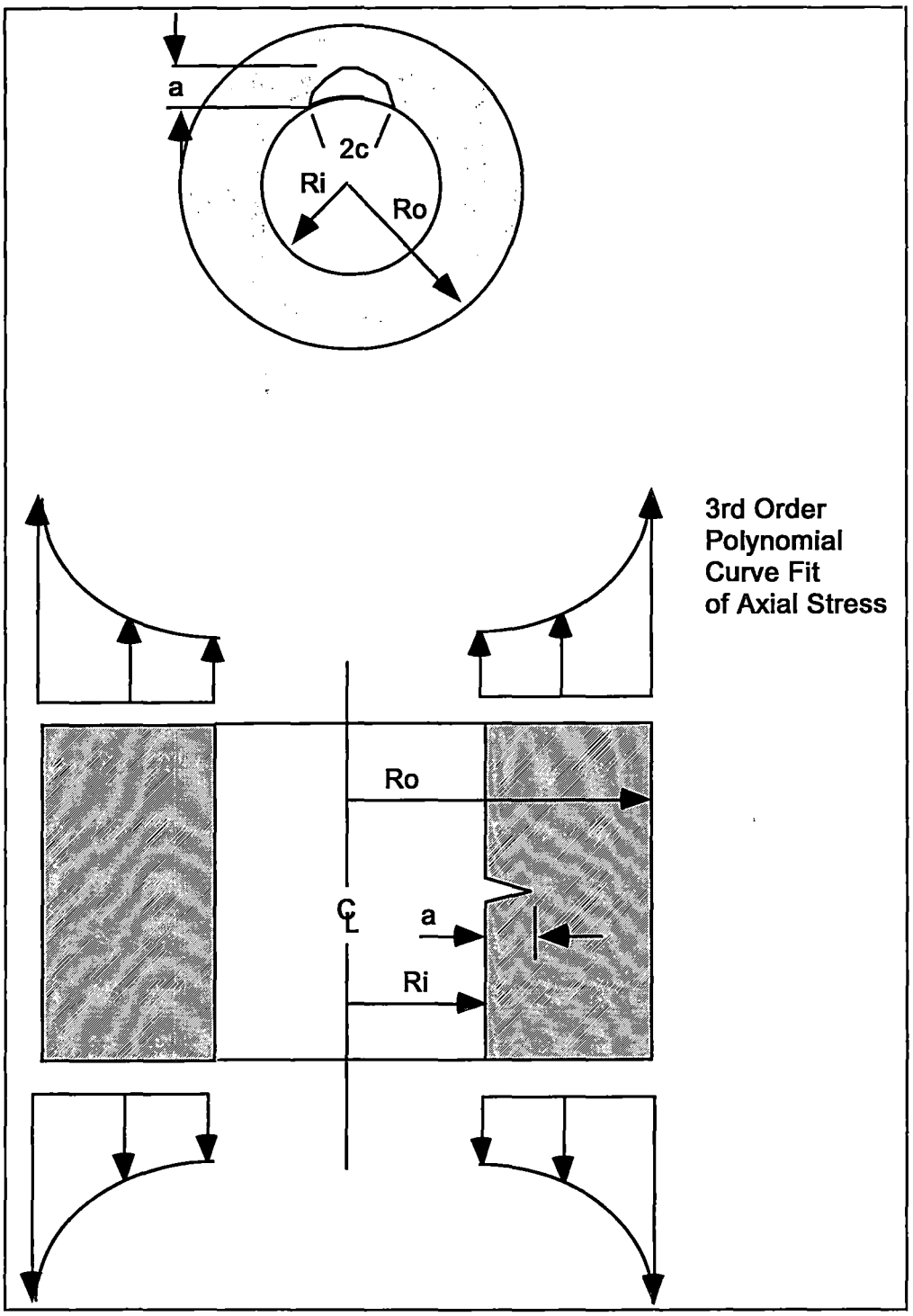

Figure 2. Semi-Elliptical Internal Circumferential Flaw

2.2 Geometry of Alloy 600 Components

The pertinent geometric dimensions are given below in Table 1.

Table 1 Summary of Geometric Dimensions for Palisades' Alloy 600 Components (Ref. 1)

Nozzle/ Safe End	Location	Quantity	OD (in.)	ID (in.)	Penetration Weld
TE-0101 and TE-0102	Pressurizer	1 each	1.315	0.815	Partial
Spray Nozzle Safe End	Pressurizer	1	4.500	3.692	Full
Surge Nozzle Safe End	Pressurizer	1	12.750	10.740	Full
Surge Nozzle Safe End	Hot Leg Piping	1	13.000	10.741	Full
Shut Down Cooling Outlet Nozzle Safe End	Hot Leg Piping	1	12.750	10.741	Full
Loop Drain Nozzle	Hot Leg Piping	1	2.375	1.689	Full
Shut Down Cooling Inlet Nozzle Safe End	Cold Leg Piping	4	13.000	10.741	Full
Pressure & Sampling Nozzle	Hot Leg Piping	10	1.250	0.625	Full
RTD J-Weld Nozzle	Hot Leg Piping	10	1.250	0.377	Partial
Spray Line Outlet Nozzle	Cold Leg Piping	2	3.500	2.693	Full
Charging Nozzle	Cold Leg Piping	2	2.375	1.689	Full
Loop Drain Nozzle	Cold Leg Piping	4	2.375	1.689	Full
Pressure & Sampling Nozzle	Cold Leg Piping	8	1.250	0.625	Full
RTD J-Weld Nozzle	Cold Leg Piping	12	1.250	0.377	Partial

3.0 Stresses

3.1 Applied Stresses

The actual stress distribution for each of the components studied is unknown. However, certain conservative assumptions can be made to ensure that stresses used in predicting the remaining service life of the Palisades Alloy 600 components bound the actual stresses.

The effects of primary stresses, operating stress and geometrical anomalies (i.e. the distortion of TE-0102 during the weld repair process), along with the weld residual stress could produce extremely high stresses. The welding process without a post weld treatment may leave a large residual stress. Since no evaluation was performed to estimate the magnitude of the residual stress, it is postulated that the residual stress is equal to the material yield strength. The material yield strength at room temperature will be used to develop residual stresses at operating temperatures. Based on tabulated yield strengths from Section III of ASME Code, room temperature yield strengths are about 125% of yield strengths at operating temperatures above 500F. It is therefore appropriate and conservative to use room temperature yield strength as the postulated total stress. In the present analysis, this stress will be applied as a constant through-wall stress in both the axial and circumferential directions.

The degree of conservatism associated with the above approach varies from nozzle to nozzle, but can best be characterized by categorizing the nozzles into two main groups according to the type of attachment weld, J-groove partial penetration or full penetration. Nozzles attached to PCS components by J-groove type welds (Pressurizer TE nozzles and PCS Loop RTD nozzles) are not connected to any type of external piping. This in turn virtually eliminates the potential for circumferential PWSCC, since there is no axial stress to either initiate or drive a crack. On the other hand, circumferential PWSCC may very well be the primary mode of failure for full penetration type nozzles with girth butt welded safe ends. For this category, high residual axial stresses may be present at the location of the girth butt weld, and additional operational loads are produced by the attached piping. At the same time, compressive circumferential stress at the root of the weld, typical of butt welded piping components, would tend to decrease the likelihood of axial PWSCC. Recognizing that the potential for PWSCC varies for these two types of welded nozzles (partial and full penetration), it is nevertheless both conservative and convenient to evaluate all nozzles for both axial and circumferential failure modes.

Based on research conducted on large diameter BWR stainless steel piping, it may be particularly conservative to assume a constant value of through-wall axial stress for evaluating girth butt welded safe ends. NUREG-0313 (Ref. 10) presents a nondimensional, nonlinear through-wall stress distribution for axial residual stresses in 12" diameter piping joined by girth butt welds. Although this form of residual stress distribution may not be exactly applicable to weld between small diameter piping and nozzle safe ends, it could be somewhat representative of the actual stress distribution, and as such, is used as an alternate method of analysis in Appendix A.

3.2 Spectrum History

The Palisades plant has 500 heatup and cooldown design cycles (Ref. 1). In calculating fatigue crack growth, the maximum stress (i.e. yield strength) is combined with the minimum stress (i.e. zero at shutdown) to determine a cyclic stress range. It should be noted that the amount of fatigue crack growth was found to contribute only about 1% of the total crack growth as compared to PWSCC. For this reason, and based on experience, it was determined that accounting for smaller transients in the fatigue crack growth analysis for these components was not needed. For stress corrosion crack growth at a given location, the maximum stress state (i.e. room temperature yield strength) is used to evaluate the corrosion crack growth within a given time span.

Predictions of yearly crack growth are based on 12.5 heatup/cooldown cycles per year (500 cycles over a 40 year design life).

4.0 Fracture Mechanics Analysis

A linear elastic fracture mechanics analysis is performed to determine the maximum allowable flaw size that meets IWB-3612 fracture toughness margins and that the assumed semi-elliptical internal surface crack does not grow to through wall. As previously noted, a semi-elliptical internal surface flaw with a longitudinal orientation and with a circumferential orientation will be used as the postulated defects. The following sections outline the fracture mechanics methodology used in this analysis.

4.1 ASME B&PV Code, Section XI, Acceptance Criteria

A flaw is acceptable if the applied stress intensity factor satisfies the following IWB-3612 criterion (Ref. 4) for normal and upset conditions:

$$K_I(a_f) < \frac{K_{Ia}}{\sqrt{10}}$$

where:

$K_I(a_f)$ = the maximum applied stress intensity factor for normal and upset conditions based on final crack depth.

K_{Ia} = crack arrest fracture toughness for the corresponding crack tip temperature.

Since the highest possible stress is being employed in this analysis, the normal/upset and emergency/faulted conditions would use the same stress value for determination of the applied stress intensity factor. Also, as will be demonstrated in Section 5.0, the crack arrest fracture toughness, K_{Ia}, and the crack initiation fracture toughness, K_{Ic}, are the same for this application. Hence, the only difference in the N/U and E/F conditions is in the fracture toughness margins required in IWB-3612. Since the fracture toughness margin is higher in the N/U condition ($\sqrt{10}$) than in the E/F condition ($\sqrt{2}$), the N/U condition is the bounding criteria for satisfying IWB-3612.

4.2 Stress Intensity Factor Solutions

AXIAL FLAW

Maximum Depth Point:

The Mode I stress intensity factor for the deepest point on the semi-elliptical flaw is (Ref. 3):

$$K_I=(\pi t)^{0.5}[\sum_{i=0}^{3} \sigma_i G_i]$$

where σ_i are the coefficients of the stress polynomial describing the hoop stress (σ) variation through the cylinder wall and are defined below.

$$\sigma=\sigma_o+ \sigma_1 (z/t) +\sigma_2 (z/t)^2 + \sigma_3 (z/t)^3$$

z is the distance measured from the inner surface of the cylinder wall and t is the cylinder wall thickness. The G_i are the shape factors associated with the coefficients of the stress polynomial and may be expressed by the following general form:

$$G_i = A_0 + (A_1\alpha_i + A_2\alpha_i^2 + A_3\alpha_i^3 + A_4\alpha_i^4 + A_5\alpha_i^5) / [0.102(R_i/t) - 0.02]^{0.05}$$

$$\alpha_i = (a/t)/(a/c)^m$$

The values of A_0 through A_5 and m are given in Table 2a. The R_i is cylinder inner radius. The 2c and a are the flaw length and flaw depth at the deepest point of the flaw respectively.

Table 2a. Axial Flaw Shape Factors Associated with the Deepest Point on the Flaw (Ref. 3)

	A_0	A_1	A_2	A_3	A_4	A_5	m
G_0	0.0	1.7767	-2.5975	2.7520	-1.3237	0.2363	0.58
G_1	0.0	0.1045	0.4189	0.000	0.0	0.0	0.22
G_2	0.0	0.02038	-.00397	0.42126	0.0	0.0	0.10
G_3	0.0	0.07283	-.36006	0.66883	0.0	0.0	0.05

AXIAL FLAW

Point Near Surface:

The Mode I stress intensity factor for the point near the surface on the semi-elliptical flaw is (Ref. 3):

$$K_I=(\pi t)^{0.5}[\sum_{i=0}^{3} \sigma_i G_{si}]$$

where

$$G_{si} = G_i * [A_6 + A_7(a/t)^2] (a/c)^r$$

The G_{si} are the shape factors associated with the point near the surface of the flaw. The G_i are the shape factors associated with the deepest point on the flaw, defined on the previous page. The A_6, A_7 and r are defined in Table 2b.

Table 2b. Axial Flaw Shape Factors Associated with the Point Near the Surface (Ref. 3)

	A_6	A_7	r
G_{s0}	1.06	0.28	0.41
G_{s1}	0.25	0.20	0.26
G_{s2}	0.07	0.16	0.06
G_{s3}	0.085	0.02	0.0

CIRCUMFERENTIAL FLAW

The Mode I stress intensity factor for the deepest point on the semi-elliptical flaw is (Ref. 3):

$$K_I=(\pi t)^{0.5}[\sum_{i=0}^{3} \sigma_i(a/t)^i G_i]$$

where σ_i are the coefficients of the stress polynomial describing the axial stress (σ) variation through the cylinder wall and are defined below.

$$\sigma=\sigma_o+ \sigma_1 (z/t) +\sigma_2 (z/t)^2 + \sigma_3 (z/t)^3$$

z is the distance measured from the inner surface of the cylinder wall and t is the cylinder wall thickness. The G_i are the shape factors associated with the coefficients of the stress polynomial and may be expressed by the following general form:

$$G_i = A_1\alpha_i + A_2\alpha_i^2 + A_3\alpha_i^3 + A_4\alpha_i^4 + A_5\alpha_i^5 + A_6\alpha_i (R/t - 5)$$

$$\alpha_i = (a/t)/(a/c)^m$$

The values of A_1 through A_6 and m are given in Table 3. The R is the mean radius of the cylinder. The 2c and a are the flaw length measured at the cylinder inner surface and flaw depth at the deepest point of the flaw, respectively.

Table 3. Circumferential Flaw Shape Factors Associated with the Deepest Point on the Flaw (Ref. 3)

	A_1	A_2	A_3	A_4	A_5	A_6	m
G_0	1.8143	-1.9881	1.4382	-0.4680	0.056696	0.0067	0.50
G_1	1.0959	-0.9874	0.5399	-0.09303	0.0	0.0	0.38
G_2	1.1836	-2.3347	2.9756	-1.7652	0.39483	0.0	0.30
G_3	1.0029	-2.0160	2.5627	-1.4951	0.32759	0.0	0.25

Note: A_6 is set equal to zero for R/t < 5.

4.3 Irwin Plasticity Correction

Linear elastic stress analysis of sharp crack-like defects predicts infinite stresses at the crack tip. However, in real materials, stresses at the crack tip are finite because the crack tip radius is finite. To account for crack tip plasticity, a simple estimation of the elastic-plastic boundary is made using the elastic stress analysis. This approach is called the Irwin plasticity correction and is applicable up to the point where moderate crack tip yielding occurs.

When yielding occurs, stresses must redistribute in order to satisfy equilibrium. The shaded region in Figure 3 bounded by the yield stress and the elastic stress field curve represents forces that would be present in an elastic material but cannot be carried in the elastic-plastic material because the stress cannot exceed yield. The plastic zone must increase in size to accommodate these forces. Note that the redistributed stress in the elastic region is higher than elastic only stress, implying a higher effective stress intensity factor. Irwin accounted for this increase in K by defining an effective crack length that is slightly longer than the actual crack size. He found that a good approximation of K_{eff} can be obtained by placing the tip of the effective crack in the center of the plastic zone. Thus, the effective crack length is defined as the sum of the actual crack size and a plastic zone correction:

$$a_{eff}=a+r_y$$

Under plane strain conditions, this effective increase in crack length is defined by (Ref. 9):

$$r_y=\frac{1}{1+(P/P_o)^2}\frac{1}{6\pi}\frac{(n-1)}{(n+1)}\left(\frac{K_I(a)}{\sigma_{YS}}\right)^2$$

where:

P	=	Applied load
P_o	=	Limit load
n	=	strain hardening coefficient
$K_I(a)$	=	stress intensity factor based on actual crack length
σ_{YS}	=	yield stress

The effective stress intensity factor is then obtained by inserting a_{eff} into the K expression for the geometry of interest.

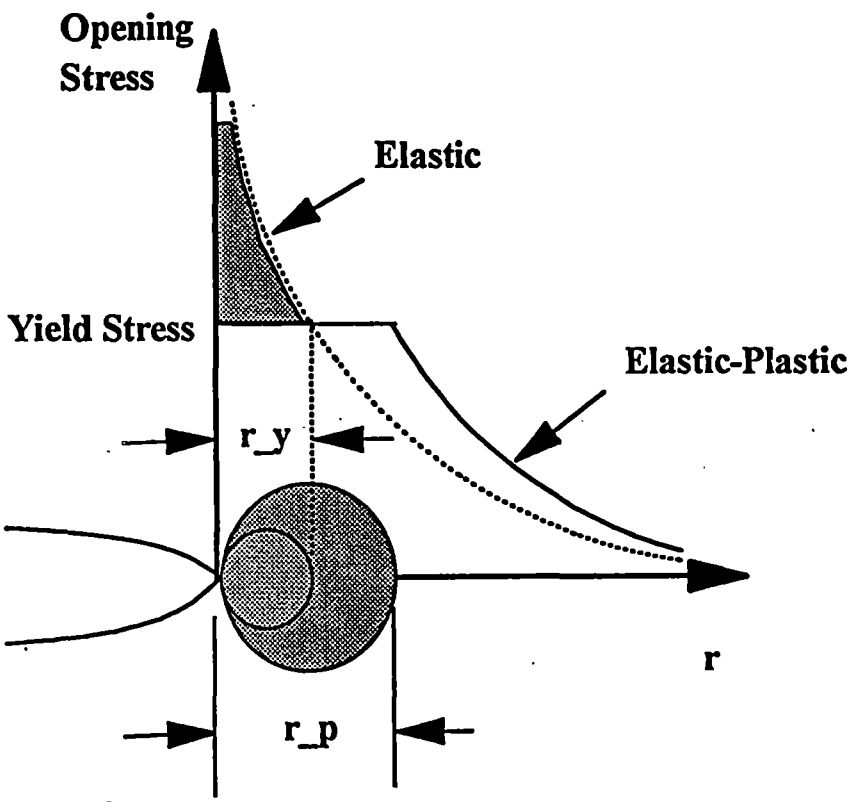

Figure 3. The Irwin Plastic Zone Correction

4.4 Limit Load Solutions

In addition to failure by brittle fracture, a net section collapse failure needs to be assessed. The safest approach in a fracture mechanics assessment is to adopt an analysis that spans the entire range from linear elastic to fully plastic behavior. Such an analysis accounts for the two extremes of brittle fracture and plastic collapse.

AXIAL FLAW - Internal, Semi-Elliptical Longitudinal Flaw

The limit load pressure, p_o, for an internal, semi-elliptical longitudinal flaw is calculated by (Ref. 3):

$$p_o = \sigma_{flow} \frac{t}{R_o} \frac{1-x}{1-\frac{x}{M}}$$

$$x = \frac{a}{t}$$

$$M = \sqrt{1+\frac{1.61c^2}{Rt}}$$

$$\sigma_{flow} = \frac{\sigma_{yield} + \sigma_{ultimate}}{2}$$

$$R = \frac{R_i + R_o}{2}$$

where a = the crack depth,
c = half the crack length
and t = the cylinder wall thickness.

The design pressure, p_d, for all the Palisades' Alloy 600 components examined is 2500 psi. (Ref. 1) Since no margin of safety is applied to the limit load condition, the component will not fail by plastic collapse if

$$p_d < p_o$$

CIRCUMFERENTIAL FLAW

Two limit load solutions are used for the circumferential flaws. The solution for a internal, semi-elliptical circumferential flaw is used for nozzles with $R_o/t \geq 5$. A more conservative solution for a internal, 360° circumferential flaw is used for $R_o/t < 5$, where the semi-elliptical flaw solution is not valid.

Since external piping loads are not generally available for these nozzles, the limit load solutions for circumferential flaws will be conservatively compared to an applied axial load that is equivalent to a constant through-wall axial stress equal to the material yield strength at operating temperature; that is,

$$P_y < P_o$$

where

$$P_y = \sigma_{yield}\,\pi\,(R_o^2 - R_i^2)$$

Internal, Semi-Elliptical Circumferential Flaw Limit Load Solution

The limit load solution for an internal, semi-elliptical circumferential flaw is (Ref. 3):

$$P_o = 2\pi R t \sigma_{flow}\,[\,2\alpha/\pi - (x\theta/\pi)\,(2 - 2\zeta + x\zeta)/(2 - \zeta)\,]$$

where

$$\alpha = \arccos(A_1 \sin\theta)$$

$$A_1 = \frac{x\,[\,(1-\zeta)(2-2\zeta+x\zeta) + (1-\zeta+x\zeta)^2\,]}{2\,[\,1 + (2-\zeta)(1-\zeta)\,]}$$

$$x = \frac{a}{t}$$

$$\theta = \frac{\pi c}{4 R_i}$$

$$\zeta = \frac{t}{R_o}$$

Internal, 360° Circumferential Flaw Limit Load Solution

The limit load solution for an internal, 360° circumferential flaw is (Ref. 3):

$$P_o = \frac{2\pi}{\sqrt{3}} \sigma_{flow} [R_o^2 - (R_i + a)^2]$$

The particular limit load solution used for each nozzle is listed below, based on the R_o/t ratio.

Nozzle	R_o/t	Limit Load Solution
Pzr TE-0101 and TE-0102	2.63	360° uniform depth
Pzr Spray SE	5.57	semi-elliptical flaw
Pzr Surge SE	6.34	semi-elliptical flaw
HL Surge SE	5.75	semi-elliptical flaw
HL Shut Down SE	6.35	semi-elliptical flaw
HL Loop Drain	3.46	360° uniform depth
CL Shut Down SE	5.75	semi-elliptical flaw
HL Pressure & Sampling	2.00	360° uniform depth
HL RTD	1.43	360° uniform depth
CL Spray	4.34	360° uniform depth
CL Charging	3.46	360° uniform depth
CL Loop Drain	3.46	360° uniform depth
CL Pressure & Sampling	2.00	360° uniform depth
CL RTD	1.43	360° uniform depth

4.5 Initial Flaw Depth

The leading industry thoughts on the initiation crack size is that machining or fabrication process leaves a thin layer of high residual stress at the surface. Some quantitative measurements have been made using the X-ray diffraction technique followed by hardness tests. Boursier (Ref. 2) has shown the existence of a residual stress field up to a depth of 0.003 inch. Measurements taken from the mockups of Alloy 600 nozzles indicate that the highest residual stress occurs at 0.002 inch; however, it could reach 50 ksi at about the 0.010 inches, depending on the surface finish. An initial crack size of 0.010 inch will be used for the crack growth analysis.

4.6 Fatigue Crack Growth

The fatigue crack growth due to design cyclic loading was calculated using the Paris Law, similar to that given in Article A-4000 of Section XI of the ASME Boiler and Pressure Vessel Code (Ref. 4),

$$\frac{da}{dN} = C(\Delta K)^n$$

where C and n are dependent on the material and environmental conditions, and ΔK is the difference between K due to the maximum primary stress and K due to the minimum primary stress. The minimum primary stress is 0 psi at shutdown, hence, ΔK is the K due to maximum primary stress.

The fatigue crack growth rate data (da/dN) for Alloy 600 in a PWR environment can be seen in Figure 4. The coefficients for the Paris crack growth law are derived in Table 4.

Table 4. Derivation of Paris Law Coefficients Using Data from Figure 4 for a PWR Environment

$$\frac{da}{dN} = C(\Delta K)^n$$

$$\log(\frac{da}{dN}) = \log C + n(\log(\Delta K))$$

da/dN (mm/cycle)	ΔK (MPa√m)	da/dN (in/cycle)	ΔK (ksi√in)
6.706E-4	30	2.640E-5	27.30
1.724E-4	20	6.800E-6	18.20

Setting up two equations for two unknowns:

-4.5785= log C + 1.436 n
-5.4048= log C + 1.266 n

The required coefficients are:

C = 4.09E-10
n = 3.349 for use with units of inches and ksi√in.

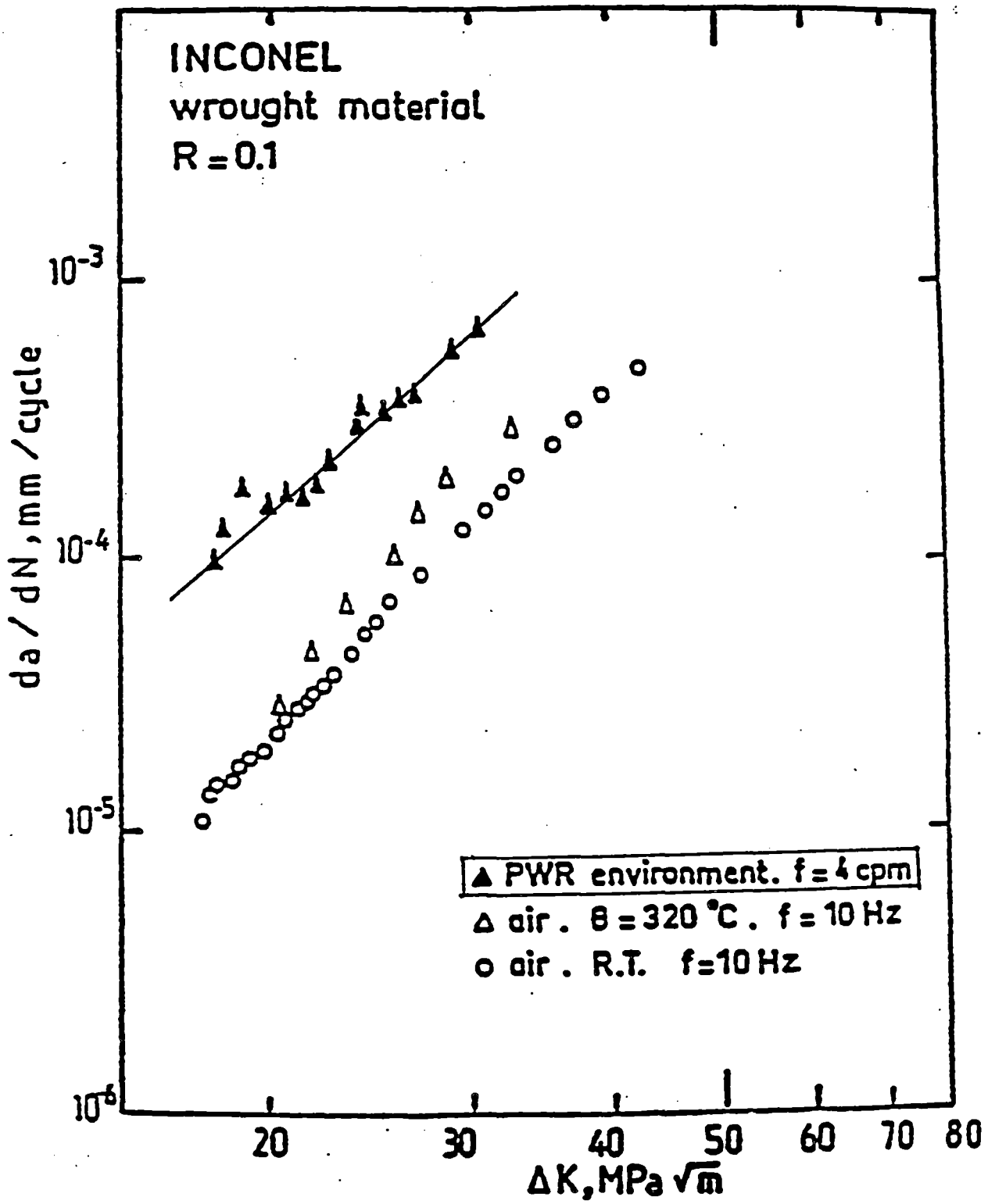

Figure 4. Inconel - Wrought Material - Effect of Temperature and PWR Environment on Fatigue Crack Growth Rates (from Reference 5)

4.7 Stress Corrosion Crack Growth

The corrosion crack growth was calculated using Scott's (Ref. 6) model with an activation energy of 33 Kcal/mole. This crack growth rate model was developed based on industry data for the stress corrosion cracking of Alloy 600 steam generator (SG) tubing. This model is considered the most conservative model available for Alloy 600 PWSCC on SG tubing. An appropriate temperature correction is incorporated to account for the difference in operating temperature between the different Alloy 600 components and SG tubes.

Scott's crack growth rate equation for 330°C (626°F) is:

$$\frac{da}{dt} = C_o(K_I - K_{I_{scc}})^n \frac{m}{\text{sec}}$$

where

n	= 1.16
K_{Iscc}	= 9 MPa$\sqrt{}$m is assumed
K_I	= applied stress intensity factor, in units of MPa$\sqrt{}$m
C_o (330°C)	= 2.8e-12

This equation includes a factor of five to account for the effect of cold work on crack growth rate.

It should be noted that an explicit threshold stress intensity factor is required before crack propagation occurs in this correlation. In order to permit investigation of shallow flaws, a correlation based on the original Scott model was developed without the explicit threshold. It is the following relation that will be utilized in this analysis:

$$\frac{da}{dt} = D_o(2.89E{-}13\ K_I^{1.678})^x \frac{m}{\text{sec}}$$

where K_I = applied stress intensity factor, in units of MPa$\sqrt{}$m, and

$$1.0 \le x = 1.3539(K_I)^{-0.11}$$

and D_o is the temperature correction parameter.

The Alloy 600 components operate at a temperature of 540°F in the cold leg piping, 590°F in the hot leg piping and 640°F in the pressurizer (Ref. 1). Since it is well known that crack growth rate is strongly affected by temperature, a temperature adjustment for analysis of the Alloy 600 components is necessary. A temperature correction was obtained from laboratory and field data for SCC growth rates for Alloy 600 in primary water environments. An activation energy of 33 Kcal/mole for crack growth was used to adjust crack growth rate for the different operating temperatures, as shown below.

da/dt (Operating Temperature) = da/dt (Test Temperature - 330°C) * D_o

$$D_o = \frac{e^{(\frac{-Q}{RT_2})}}{e^{(\frac{-Q}{RT_1})}}$$

where

Q	=	33 Kcal/mole = 138.072 Kjoules/mole
R	=	8.3143 joules/K-mole
T_1	=	Test Temperature
T_2	=	Operating Temperature of the Alloy 600 Component

The temperature adjusted crack growth rates utilized in this analysis for Alloy 600 components are:

$$\frac{da}{dt} = 1.41973\ (2.89E\text{-}13\ K_I^{1.678})^x\ \frac{m}{\text{sec}}\ @\ 640^oF$$

$$\frac{da}{dt} = 0.38902\ (2.89E\text{-}13\ K_I^{1.678})^x\ \frac{m}{\text{sec}}\ @\ 590^oF$$

$$\frac{da}{dt} = 0.09365\ (2.89E\text{-}13\ K_I^{1.678})^x\ \frac{m}{\text{sec}}\ @\ 540^oF$$

Figure 5 illustrates the temperature dependance of these PWSCC crack growth equations, along with P. Scott's original curve. In English units, these equations are:

$$\frac{da}{dt} = 55.895\ (3.386E\text{-}13\ K_I^{1.678})^x\ \frac{in}{\text{sec}}\ @\ 640^oF$$

$$\frac{da}{dt} = 15.316\ (3.386E\text{-}13\ K_I^{1.678})^x\ \frac{in}{\text{sec}}\ @\ 590^oF$$

$$\frac{da}{dt} = 3.687\ (3.386E\text{-}13\ K_I^{1.678})^x\ \frac{in}{\text{sec}}\ @\ 540^oF$$

where K_I = applied stress intensity factor, in units of ksi$\sqrt{}$in, and x is defined as above.

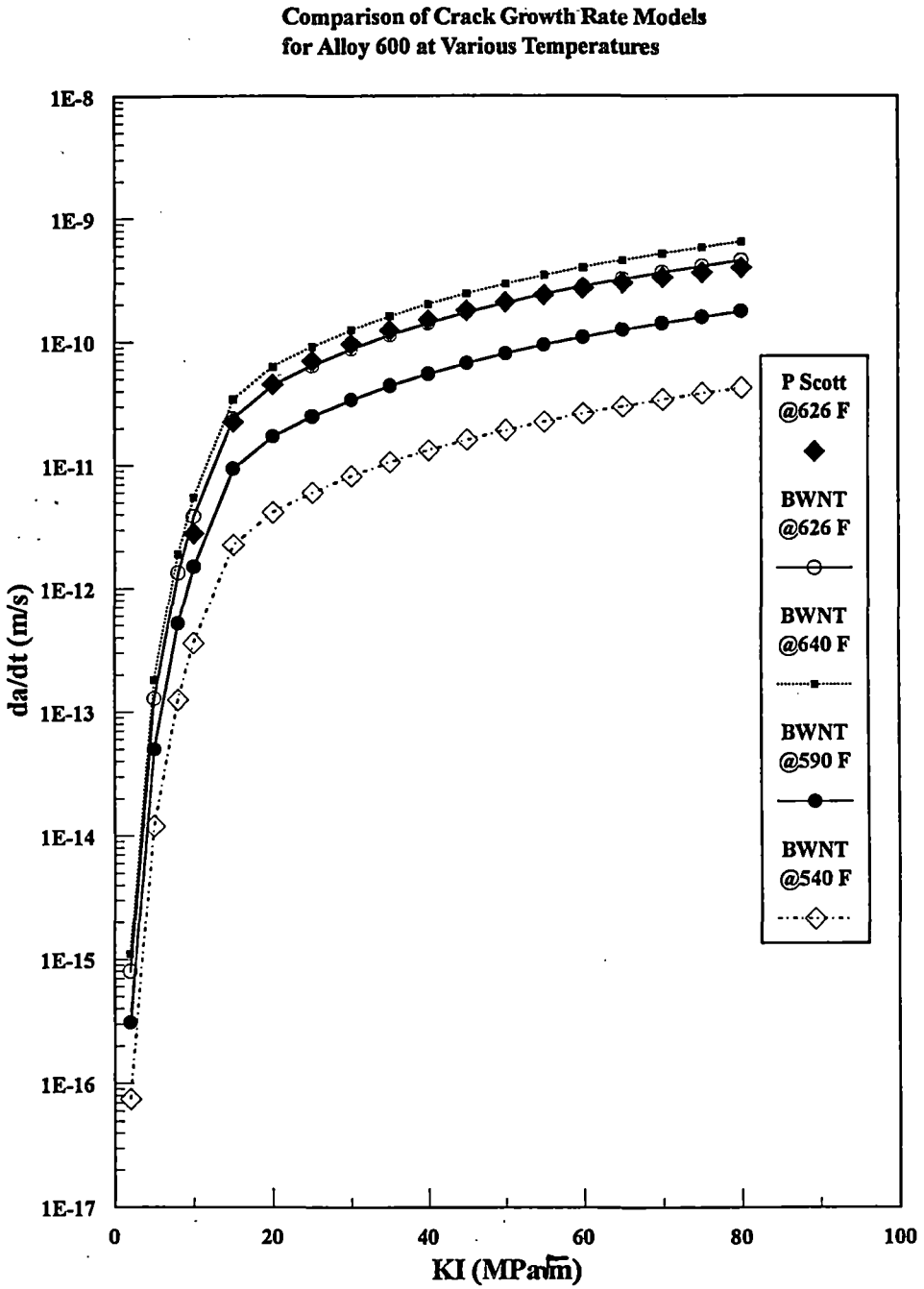

Figure 5. Comparison of Crack Growth Rates as a Function of Temperature

Prepared by: D.E. Killian Date: 4/19/95

Reviewed by: K.K. Yoon Date: 4/20/95

5.0 Material Properties

All components examined are made of Alloy 600 (Ref. 1).

The code flaw evaluation procedure, IWB 3612, is based on linear elastic fracture mechanics. In this application for Alloy 600 at a temperature above 500°F, this material is very ductile and no cleavage fracture can occur. In this evaluation, equivalent K_{Ic} and K_{Ia} values are derived J_{Ic} value from a J-resistance curve. J_{Ic} is defined as the initiation point of ductile tearing, J being at J_c level. The J_{Ic} is converted to K_{jc} by the following equation in a LEFM frame of definition: $K_{jc} = [J_{Ic}E/(1-\nu^2)]^{1/2}$. In addition, observing that ductile tearing can not be sustained without increasing crack driving force, K_{jc} value obtained from this relationship can be considered as a crack arrest toughness in the absence of additional crack driving force. Therefore, $K_{jc} = K_{Ic} = K_{Ia}$.

The fracture toughness, J_c, for Alloy 600 was from Table 3 of Ref. 7. For unirradiated specimens tested at 427°C (800°F), J_c was 575 kJ/m^2, and at 24°C (75°F) J_c was 382 kJ/m^2. Using linear interpolation and the plane strain correlation, the fracture toughness is evaluated at 540°F (hot leg piping), 590°F (cold leg piping), and 640°F(pressurizer). The fracture toughness utilized in each component is shown below in Table 5.

The following table summarizes the Alloy 600 material properties required for the fracture mechanics assessment.

Table 5. Material Properties Required for Fracture Mechanics Assessment of Palisades' Alloy 600 Components

ID	Component	Yield Stress (ksi) [Ref. 1]	Ultimate Stress (ksi) [Ref. 1]	Operating Temp (°F) [Ref. 1]	K_{Ic} (ksi$\sqrt{}$in) [Ref. 7]
1	Pzr TE-0101	46.2	98.2	640	310.18
1	Pzr TE-0102	46.2	98.2	640	310.18
2	Pzr Surge SE	51.2	100.3	640	310.18
3	Pzr Spray SE (Note 1)	77.5	114.0	540	302.33
4				640	310.18
5	HL Surge SE	51.2	100.3	590	306.28
6	HL Shut Down SE	51.2	100.3	590	306.28
7	HL Loop Drain	37.1	93.2	590	306.28
8	HL Press & Sampling	39.8	94.7	590	306.28
9	HL RTD	48.0	99.0	590	306.28
10	CL Shut Down SE	51.2	100.3	540	302.33
11	CL Spray	37.1	93.2	540	302.33
12	CL Charging	37.1	93.2	540	302.33
12	CL Loop Drain	37.1	93.2	540	302.33
13	CL Press & Sampling	39.8	94.7	540	302.33
14	CL RTD	48.0	99.0	540	302.33

Note 1: The correct value of normal spray flow is critical to the PWSCC assessment. For flows of 50 to 70 gpm it is can be assumed that the safe end temperature is equal to the cold leg temperature (540°F). If the flow is only 1.5 gpm, the flow is too low to cool the safe end and an assumed temperature equal to the pressurizer temperature (640°F) is required (Ref. 1). To perform a bounding assessment, an analysis will be completed at both temperatures for the pressurizer spray nozzle safe end.

6.0 Procedure for Assessment of Alloy 600 Components

Based on information depicted in the previous sections, two FORTRAN programs, AX.F and CIRC.F, were created to evaluate the remaining service life of each of the Palisades' Alloy 600 components assuming both an axial flaw and a circumferential flaw. Figure 6 presents a logic diagram for these programs.

The BWNT administrative procedure for preparing engineering calculations (Ref. 11) permits the use of computer programs written for execution on personal computers, provided the programs are documented and verified. The program listings for AX.F and CIRC.F can be found in Appendices B and C, respectively, of Reference 15, the proprietary version of the present fracture mechanics assessment. Both programs are verified in Appendix B of this document.

The input files used with programs AX.F and CIRC.F are listed in Appendix C of this document. The output files are contained in Reference 15 in the form of computer output microfice. These files are listed in Appendix D of this document.

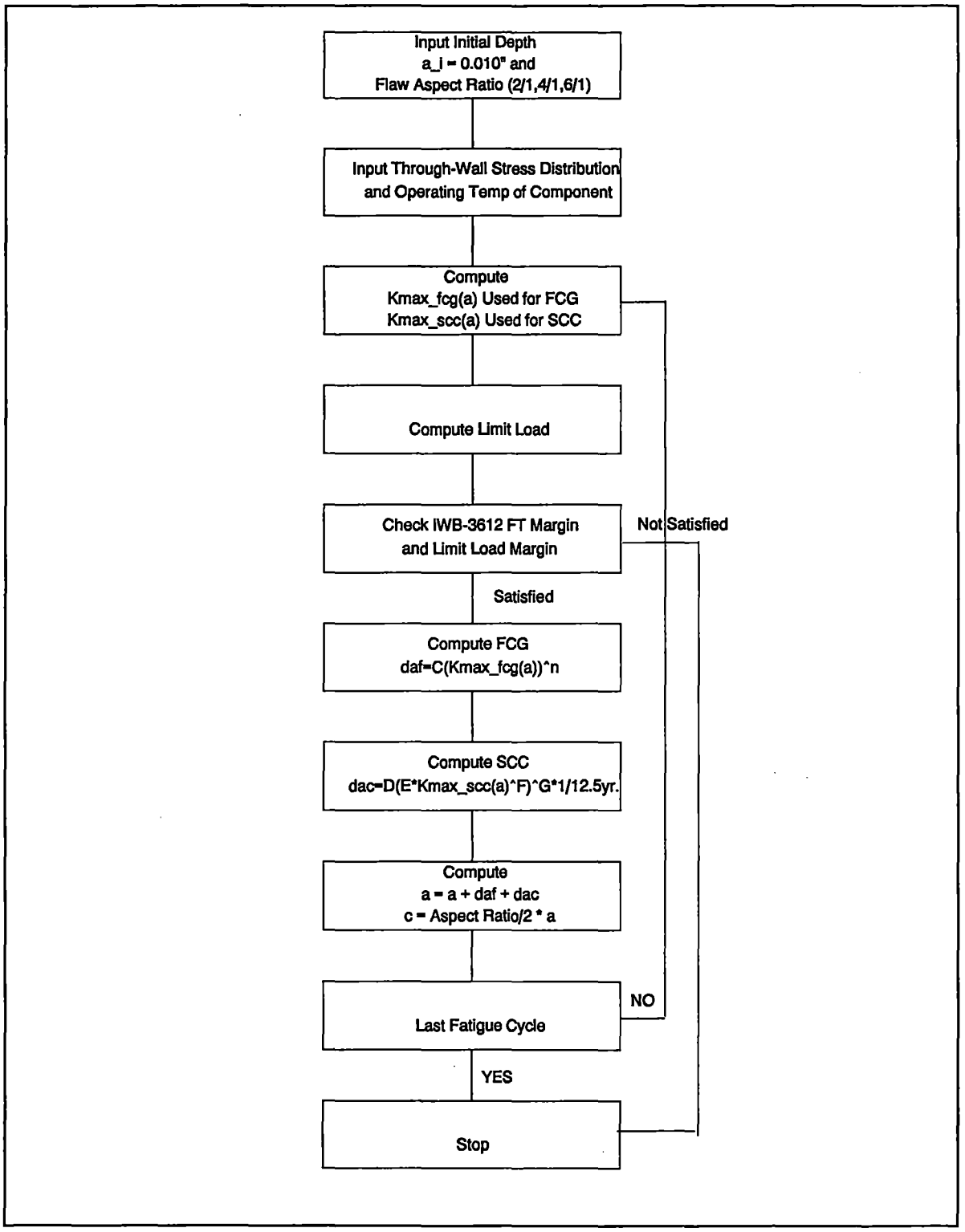

Figure 6. Procedure Used to Evaluate the Remaining Service Life of Each of the Palisades' Alloy 600 Components

7.0 Results and Conclusions

Table 6 shows the estimated remaining service life of the Palisades' Alloy 600 components. These results are graphically depicted in Figures 7 through 34.

General Observations

- The amount of fatigue crack growth as compared to stress corrosion cracking is extremely small. (Fatigue crack growth accounts for approximately 1% of total crack growth)

- Figures 7 through 20 (Axial) and 21 through 34 (Circumferential) demonstrate the allowable flaw size for each of the components for both axial and circumferential flaws. This is primarily intended to serve as an acceptance criteria in the event that a flaw is found in one of the components during an inspection. If the flaw is below the time-to-failure curve for the required length-to-depth ratio, the flaw is acceptable for the next fuel cycle. Table 7 contains the allowable flaw depths that can be justified for one fuel cycle (18 months) of continued operation.

- Nozzles attached to PCS components by J-groove type welds (Pressurizer TE nozzles and PCS Loop RTD nozzles) are not connected to any type of external piping. This in turn virtually eliminates the potential for circumferential PWSCC, since there is no axial stress to either initiate or drive a crack. On the other hand, circumferential PWSCC may very well be the primary mode of failure for full penetration type nozzles with girth butt welded safe ends. For this category, high residual axial stresses may be present at the location of the girth butt weld, and additional operational loads are produced by the attached piping. At the same time, compressive circumferential stress at the root of the weld, typical of butt welded piping components, would tend to decrease the likelihood of axial PWSCC.

Component Specific Observations

- The wall thickness of the pressurizer temperature element nozzles is only 0.25". Hence, if any flaw exists that is exposed to the primary water, PWSCC may be a significant concern. Still, for the conservative length-to-depth ratio of 6, it would take about 7.5 years for an axial flaw and 13 years for a circumferential flaw to grow to a critical size.

- Of all the components examined in this study, only the pressurizer surge nozzle has undergone post-weld heat treatment (Ref. 1). To be conservative, the yield stress was still utilized for the stress distribution for this component. Even still, the remaining service life of this component exceeds the design life of the plant.

- As previously reported, the assumed temperature of the pressurizer spray nozzle safe end is extremely important for a PWSCC assessment. (The SCC growth rate differs by a factor of 15 between 540°F (Cold Leg) and 640°F (Pressurizer).) If the temperature is assumed to be that of the cold leg, the component should be able to remain in-service without failure for about 35 years. However, if the pressurizer temperature is used, the component could only be expected to last less than 3 years.

- All other components can be expected to remain in service for 40 years without failure.

Table 6. Summary of Time to Failure for an Initial Flaw Depth of 0.010"

Note: Total through-wall stress distribution set equal to room temperature yield strength.

ID	Component	Thick. (in.)	Axial Flaw Time to Failure (years) l/a=2	l/a=4	l/a=6	Circumferential Flaw Time to Failure (years) l/a=2	l/a=4	l/a=6
1	Pzr TE-0101	0.25	40.00	20.16	7.68	40.00	32.48	13.04
1	Pzr TE-0102	0.25	40.00	20.16	7.68	40.00	32.48	13.04
2	Pzr Surge SE	1.005	40.00	40.00	40.00	40.00	40.00	40.00
3	Pzr Spray SE @540°F	0.404	40.00	40.00	35.12	40.00	40.00	40.00
4	@640°F	0.404	37.12	6.32	2.64	38.64	8.00	3.60
5	HL Surge SE	1.1295	40.00	40.00	40.00	40.00	40.00	40.00
6	HL Shut Down SE	1.0045	40.00	40.00	40.00	40.00	40.00	40.00
7	HL Loop Drain	0.343	40.00	40.00	40.00	40.00	40.00	40.00
8	HL Press & Sampling	0.3125	40.00	40.00	40.00	40.00	40.00	40.00
9	HL RTD	0.4365	40.00	40.00	40.00	40.00	40.00	40.00
10	CL Shut Down SE	1.1295	40.00	40.00	40.00	40.00	40.00	40.00
11	CL Spray	0.4035	40.00	40.00	40.00	40.00	40.00	40.00
12	CL Charging	0.343	40.00	40.00	40.00	40.00	40.00	40.00
12	CL Loop Drain	0.343	40.00	40.00	40.00	40.00	40.00	40.00
13	CL Press & Sampling	0.3125	40.00	40.00	40.00	40.00	40.00	40.00
14	CL RTD	0.4365	40.00	40.00	40.00	40.00	40.00	40.00

Table 7. Summary of Allowable Flaw Depths for One Fuel Cycle (18 months)

Notes: 1. Total through-wall stress distribution set equal to room temperature yield strength.
2. Flaw depths are in inches.

ID	Component	Thick. (in.)	Axial Flaw Allowable Flaw Depth l/a=2	l/a=4	l/a=6	Circumferential Flaw Allowable Flaw Depth l/a=2	l/a=4	l/a=6
1	Pzr TE-0101	0.25	0.065	0.035	0.020	0.050	0.030	0.025
1	Pzr TE-0102	0.25	0.065	0.035	0.020	0.050	0.030	0.025
2	Pzr Surge SE	1.005	0.270	0.135	0.075	0.270	0.145	0.085
3	Pzr Spray SE @540°F	0.404	0.285	0.215	0.155	0.320	0.270	0.205
4	@640°F	0.404	0.035	0.015	0.010	0.035	0.020	0.015
5	HL Surge SE	1.1295	0.645	0.470	0.320	0.775	0.550	0.390
6	HL Shut Down SE	1.0045	0.605	0.435	0.300	0.680	0.510	0.365
7	HL Loop Drain	0.343	0.255	0.200	0.165	0.170	0.155	0.140
8	HL Press & Sampling	0.3125	0.215	0.165	0.135	0.155	0.135	0.125
9	HL RTD	0.4365	0.265	0.185	0.130	0.200	0.170	0.150
10	CL Shut Down SE	1.1295	0.835	0.695	0.520	1.015	0.810	0.630
11	CL Spray	0.4035	0.360	0.330	0.305	0.235	0.230	0.225
12	CL Charging	0.343	0.305	0.280	0.260	0.205	0.200	0.195
12	CL Loop Drain	0.343	0.305	0.280	0.260	0.205	0.200	0.195
13	CL Press & Sampling	0.3125	0.275	0.250	0.230	0.190	0.185	0.180
14	CL RTD	0.4365	0.375	0.325	0.255	0.260	0.250	0.240

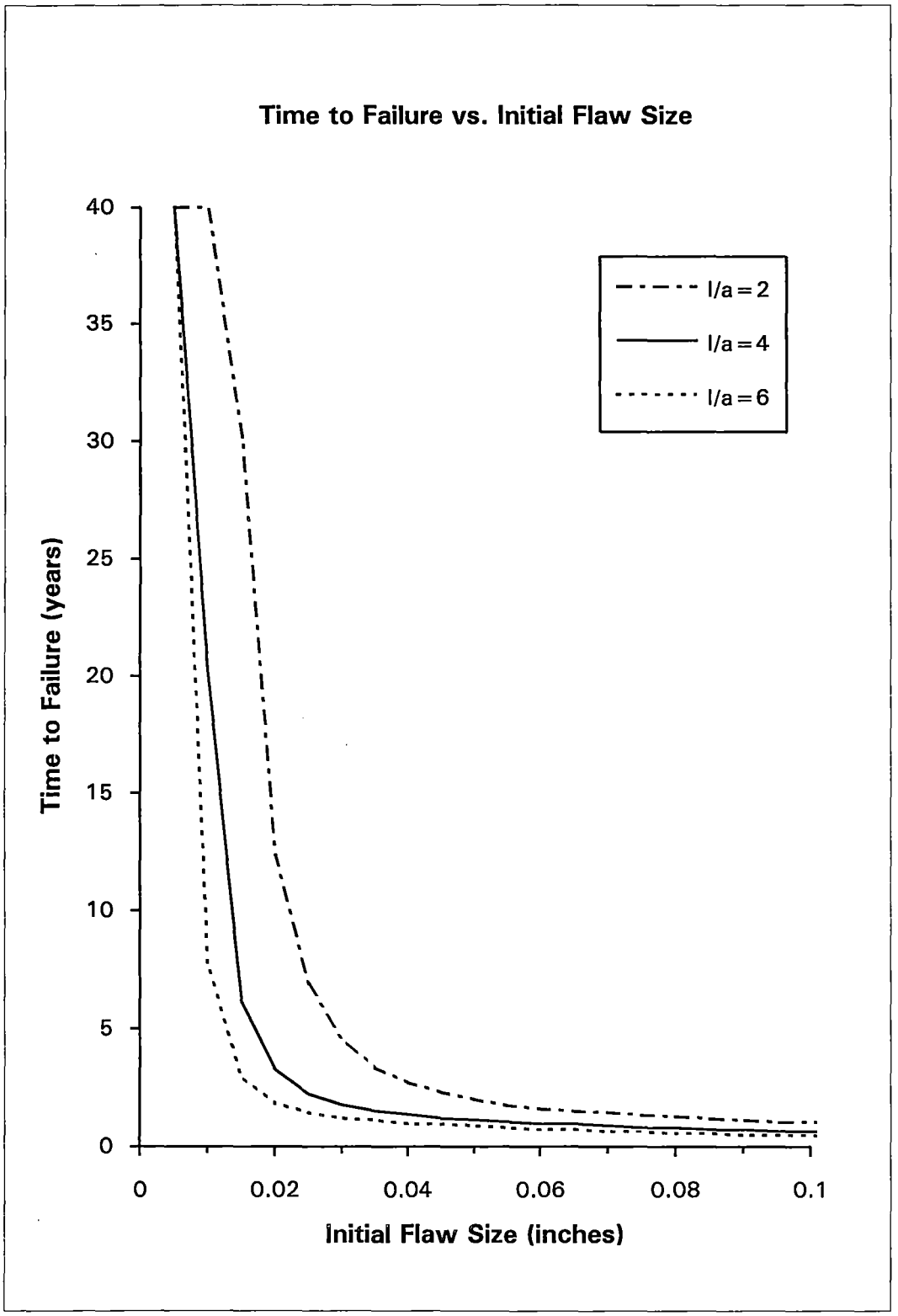

Figure 7. Time to Failure for Pressurizer TE Nozzles: Axial Semi-Elliptical Inside Surface Flaws with Constant Through-Wall Yield Stress

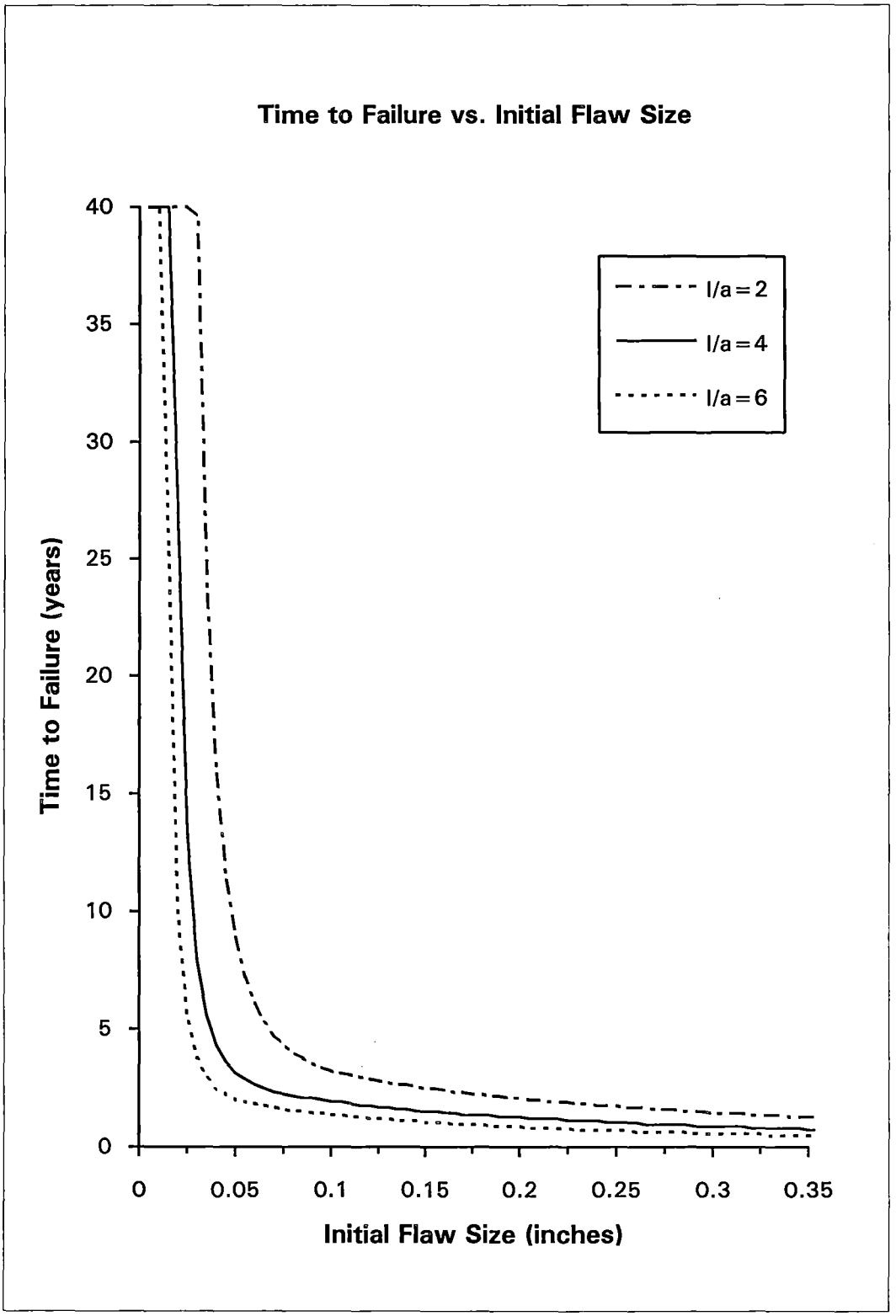

Figure 8. Time to Failure for Pressurizer Surge Nozzle Safe End: Axial Semi-Elliptical Inside Surface Flaws with Constant Through-Wall Yield Stress

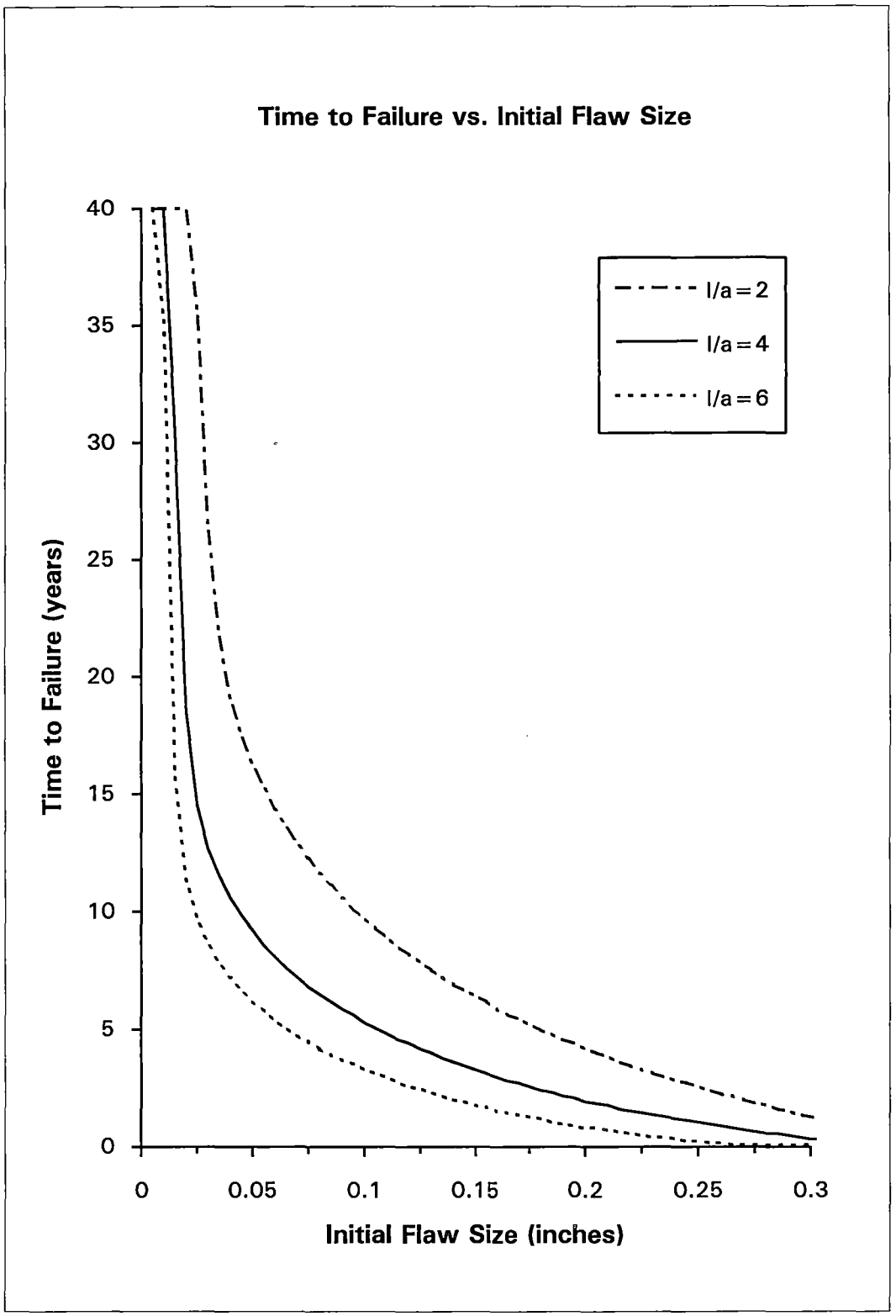

Figure 9. Time to Failure for Pressurizer Spray Nozzle Safe End at 540F: Axial Semi-Elliptical Inside Surface Flaws with Constant Through-Wall Yield Stress

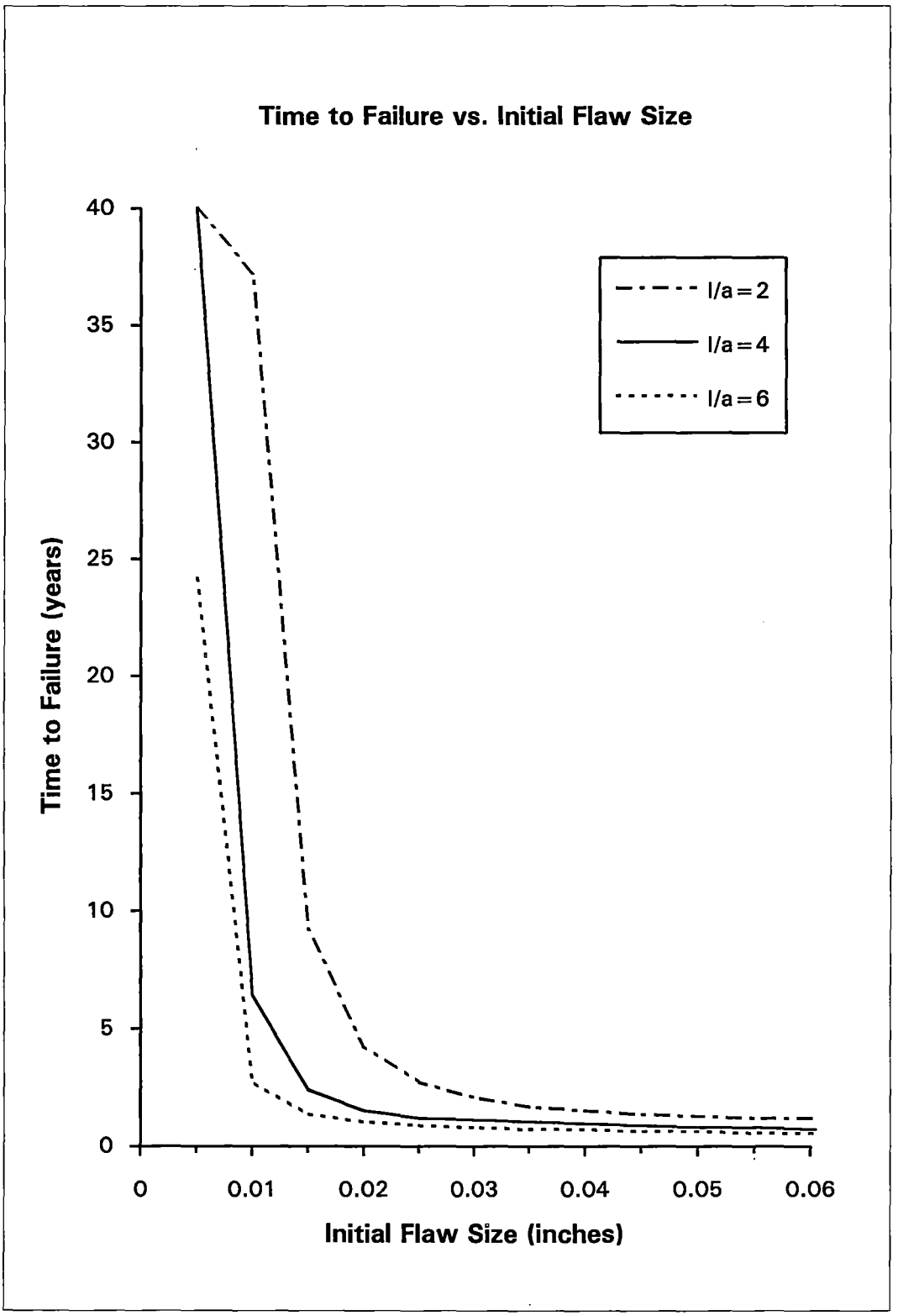

Figure 10. Time to Failure for Pressurizer Spray Nozzle Safe End at 640F: Axial Semi-Elliptical Inside Surface Flaws with Constant Through-Wall Yield Stress

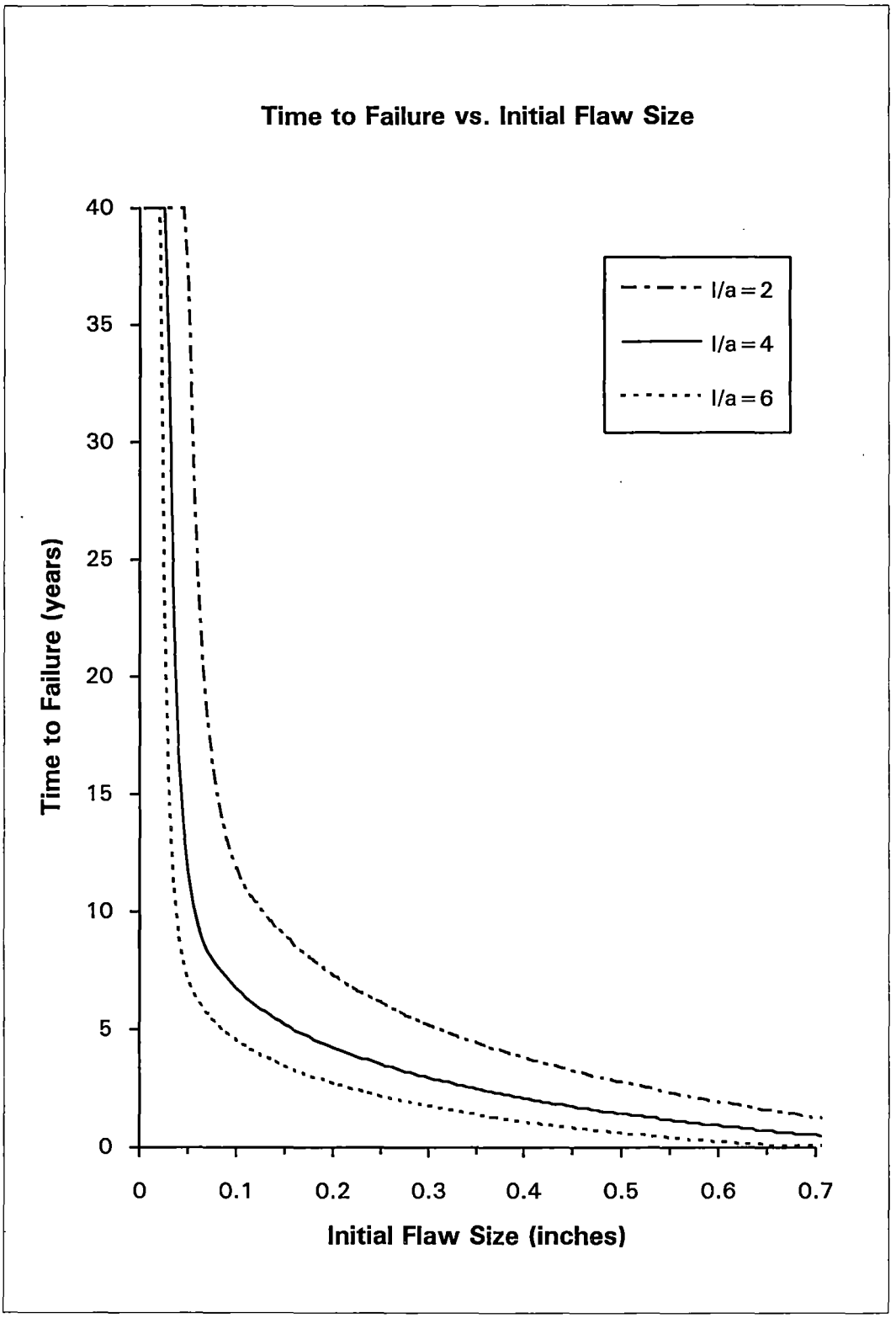

Figure 11. Time to Failure for Hot Leg Surge Nozzle Safe End: Axial Semi-Elliptical Inside Surface Flaws with Constant Through-Wall Yield Stress

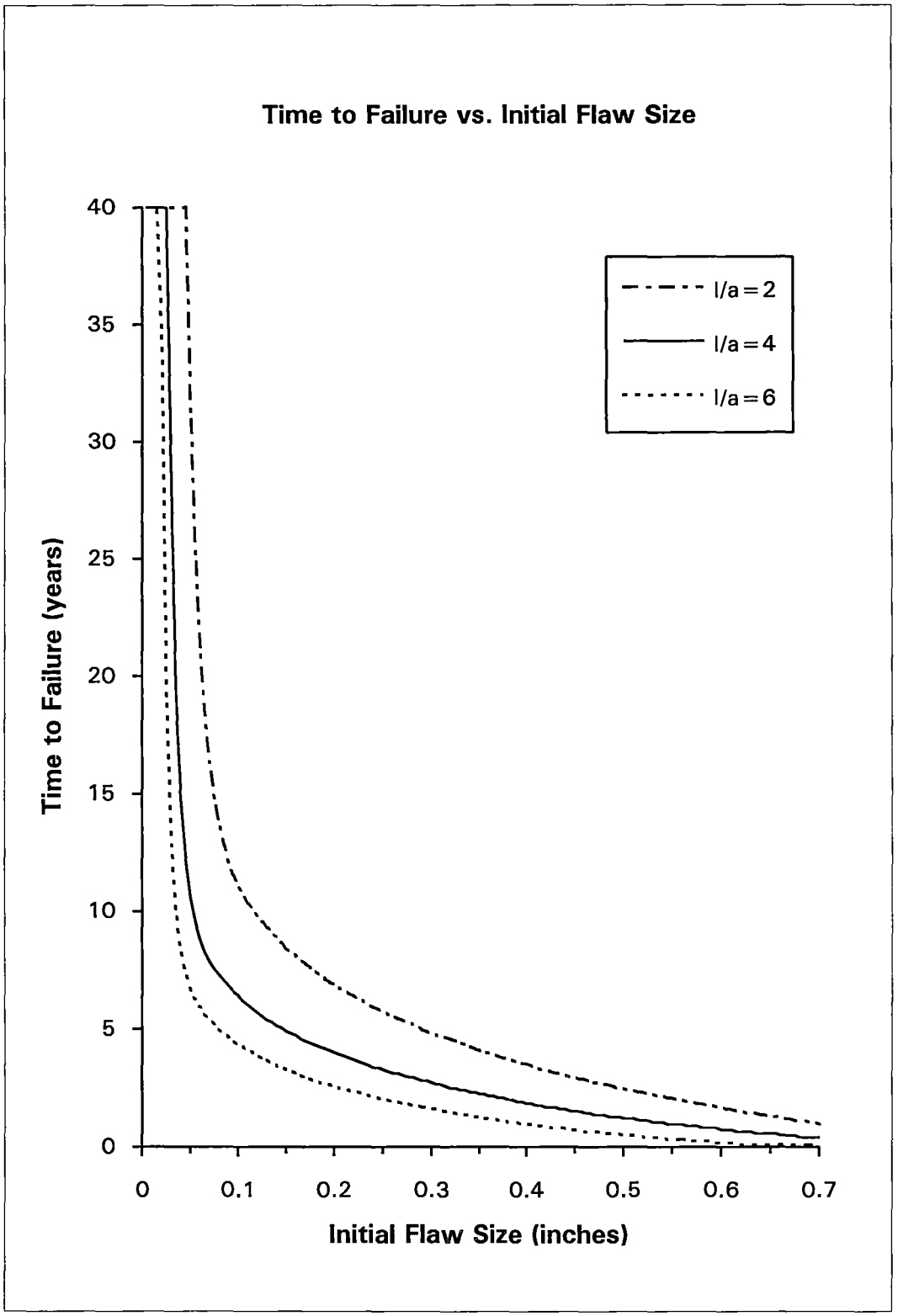

Figure 12. Time to Failure for Hot Leg Shut Down Nozzle Safe End: Axial Semi-Elliptical Inside Surface Flaws with Constant Through-Wall Yield Stress

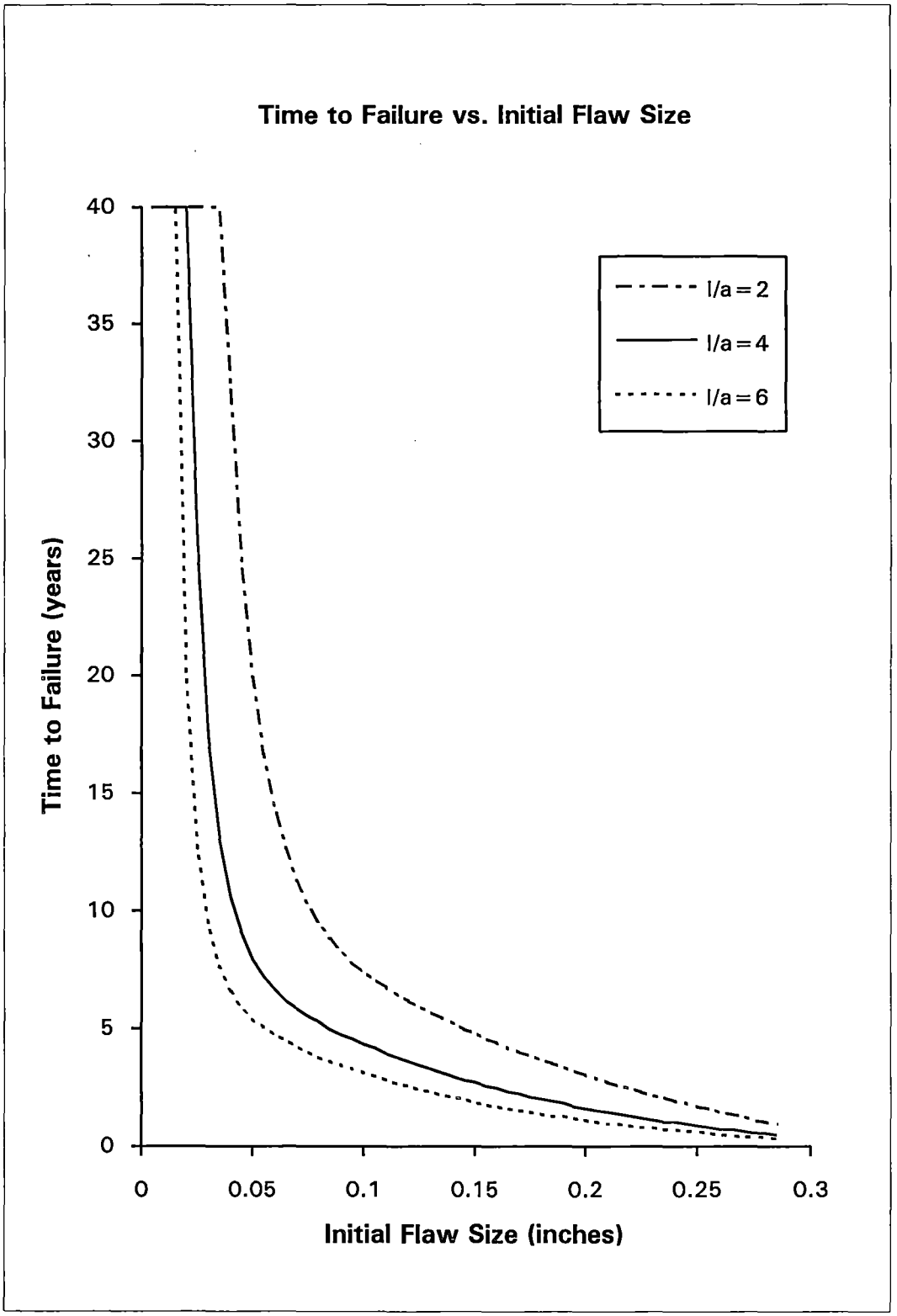

Figure 13. Time to Failure for Hot Leg Loop Drain Nozzle: Axial Semi-Elliptical Inside Surface Flaws with Constant Through-Wall Yield Stress

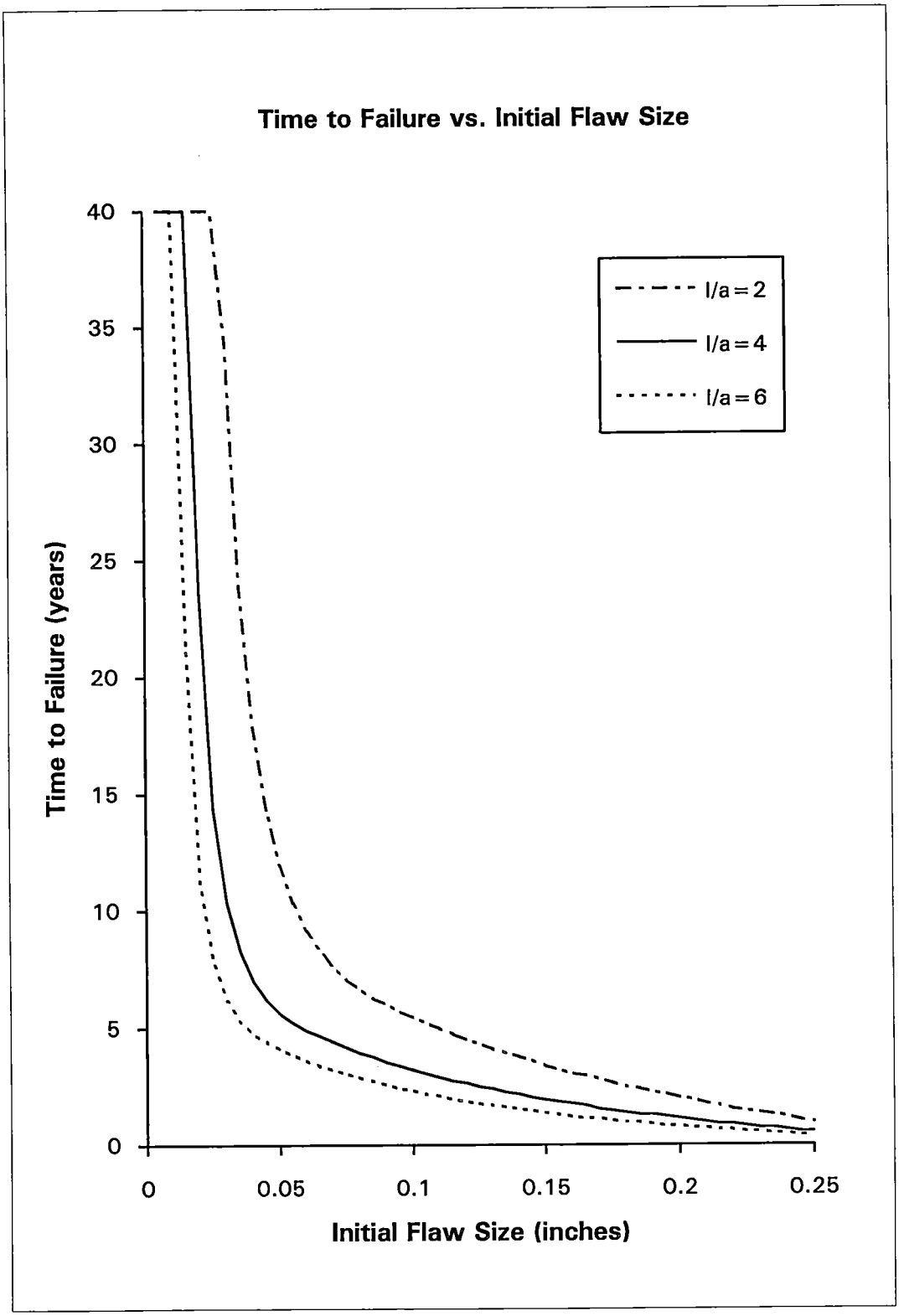

Figure 14. Time to Failure for Hot Leg Pressure & Sampling Nozzle: Axial Semi-Elliptical Inside Surface Flaws with Constant Through-Wall Yield Stress

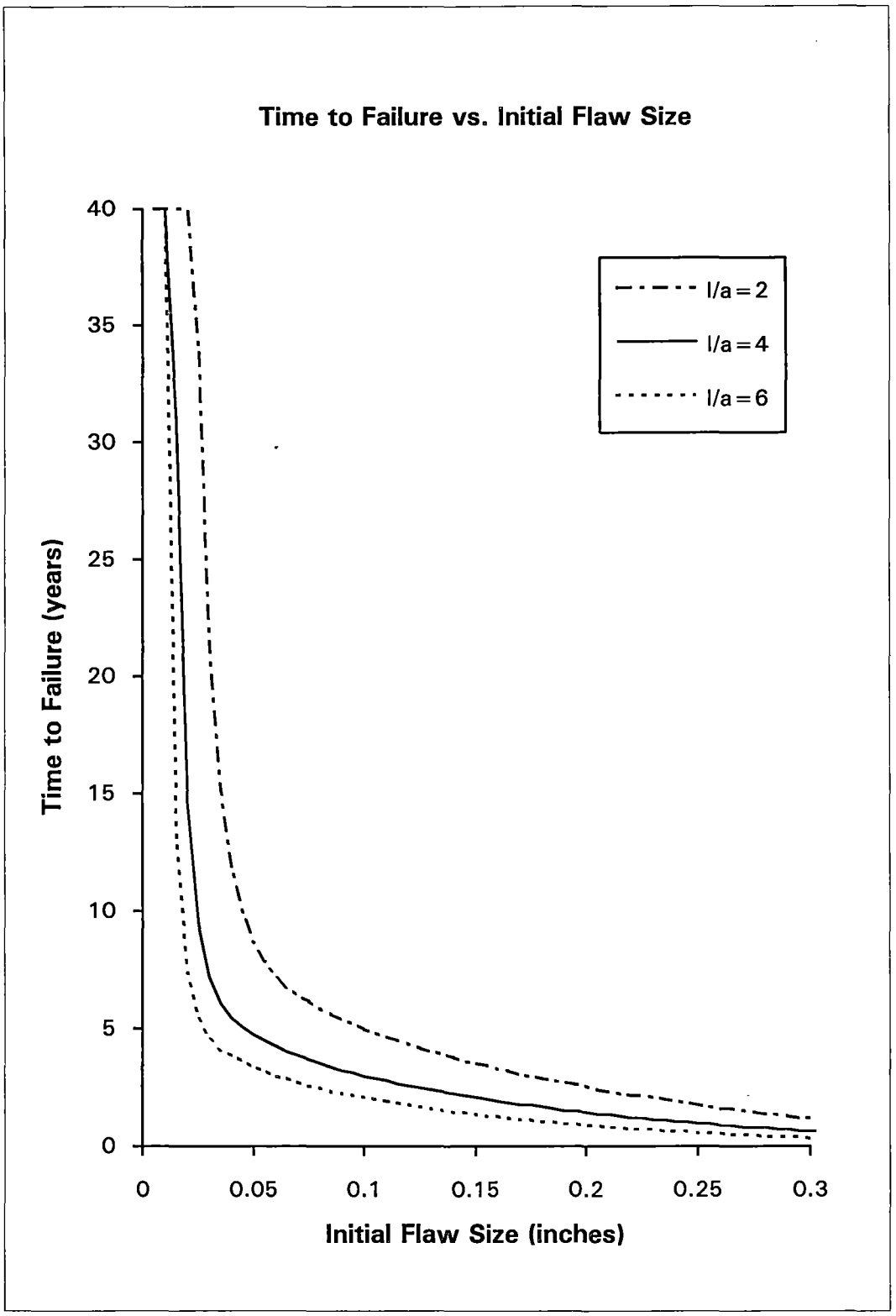

Figure 15. Time to Failure for Hot Leg RTD Nozzle: Axial Semi-Elliptical Inside Surface Flaws with Constant Through-Wall Yield Stress

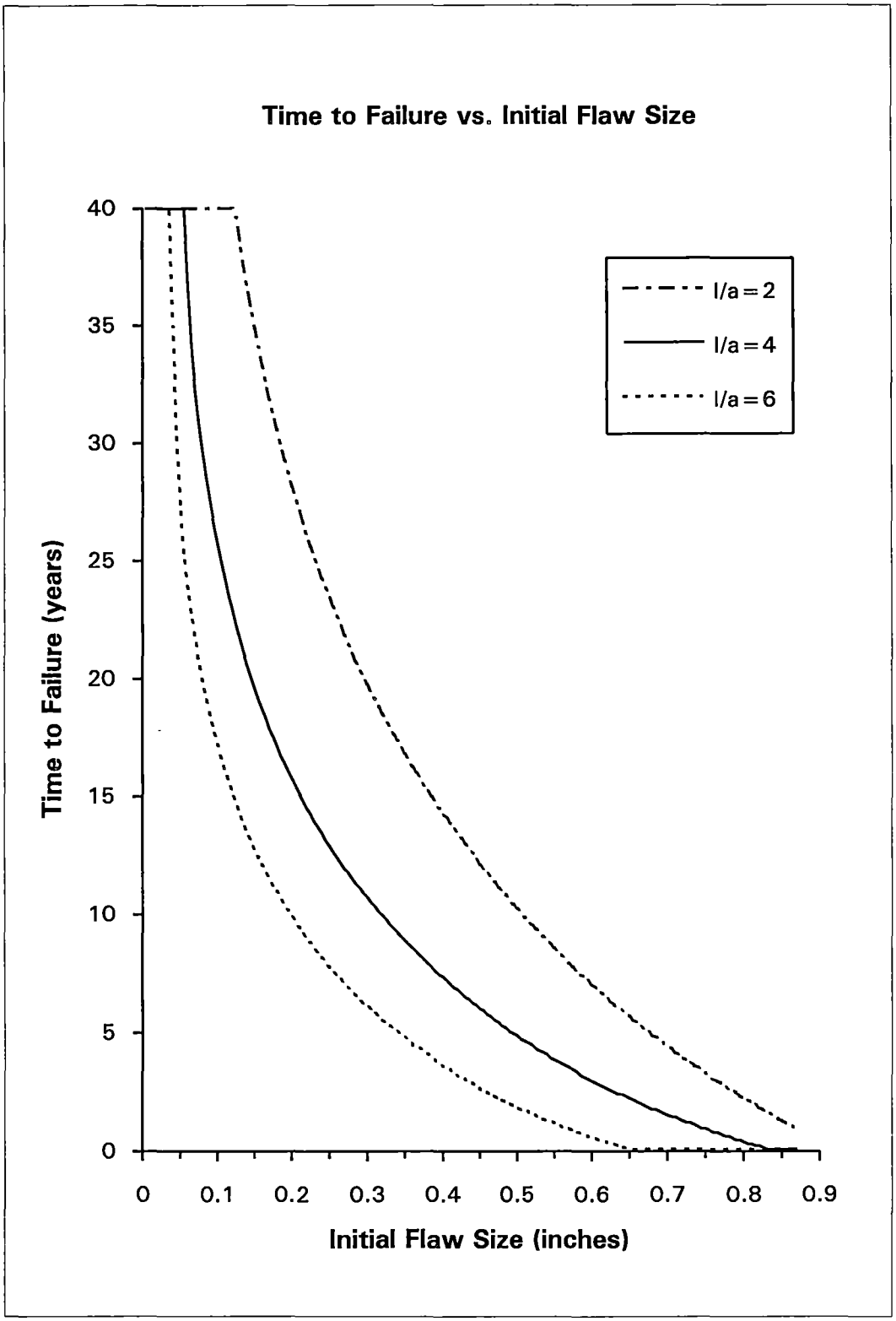

Figure 16. Time to Failure for Cold Leg Shut Down Nozzle Safe End: Axial Semi-Elliptical Inside Surface Flaws with Constant Through-Wall Yield Stress

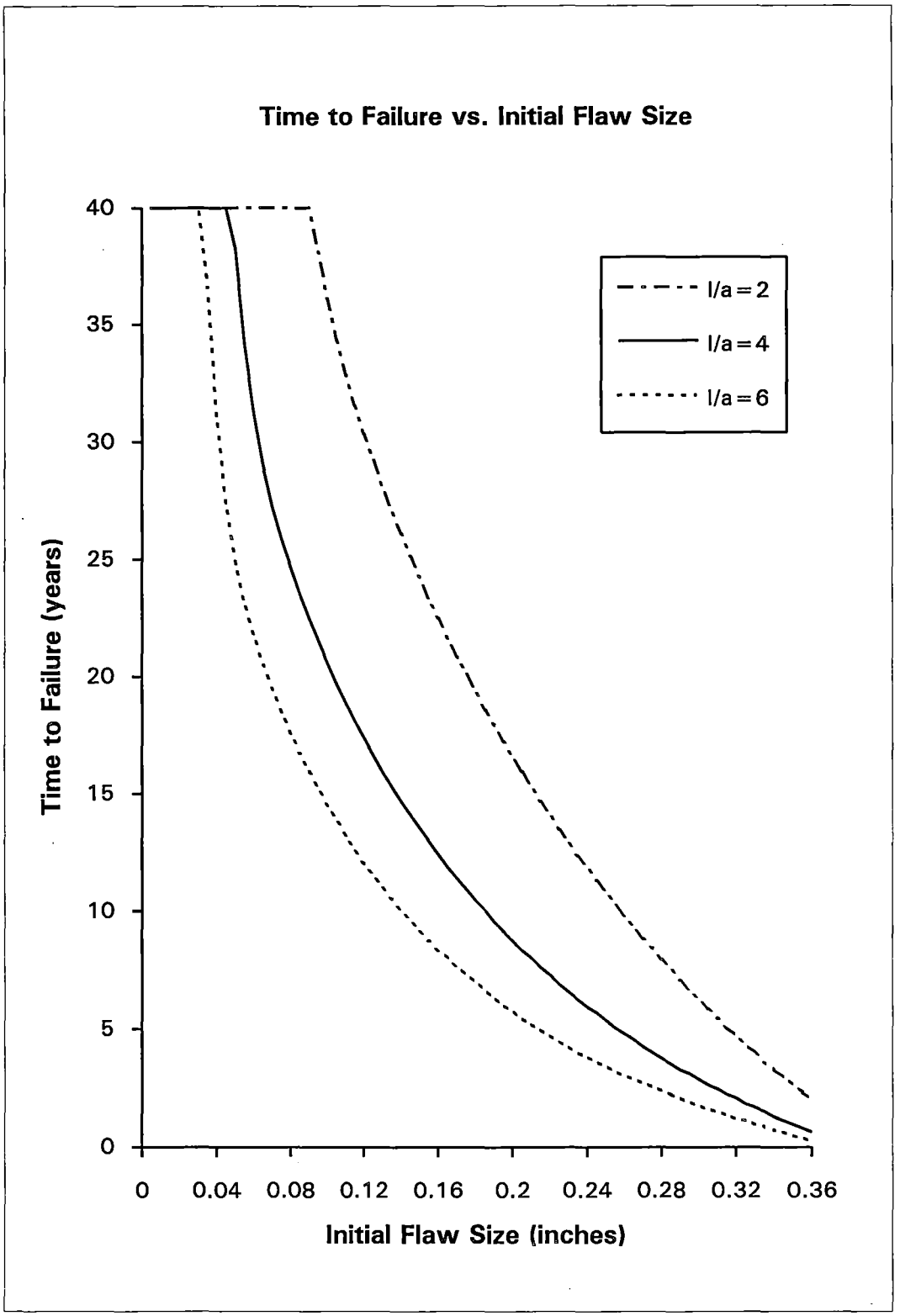

Figure 17. Time to Failure for Cold Leg Spray Nozzle: Axial Semi-Elliptical Inside Surface Flaws with Constant Through-Wall Yield Stress

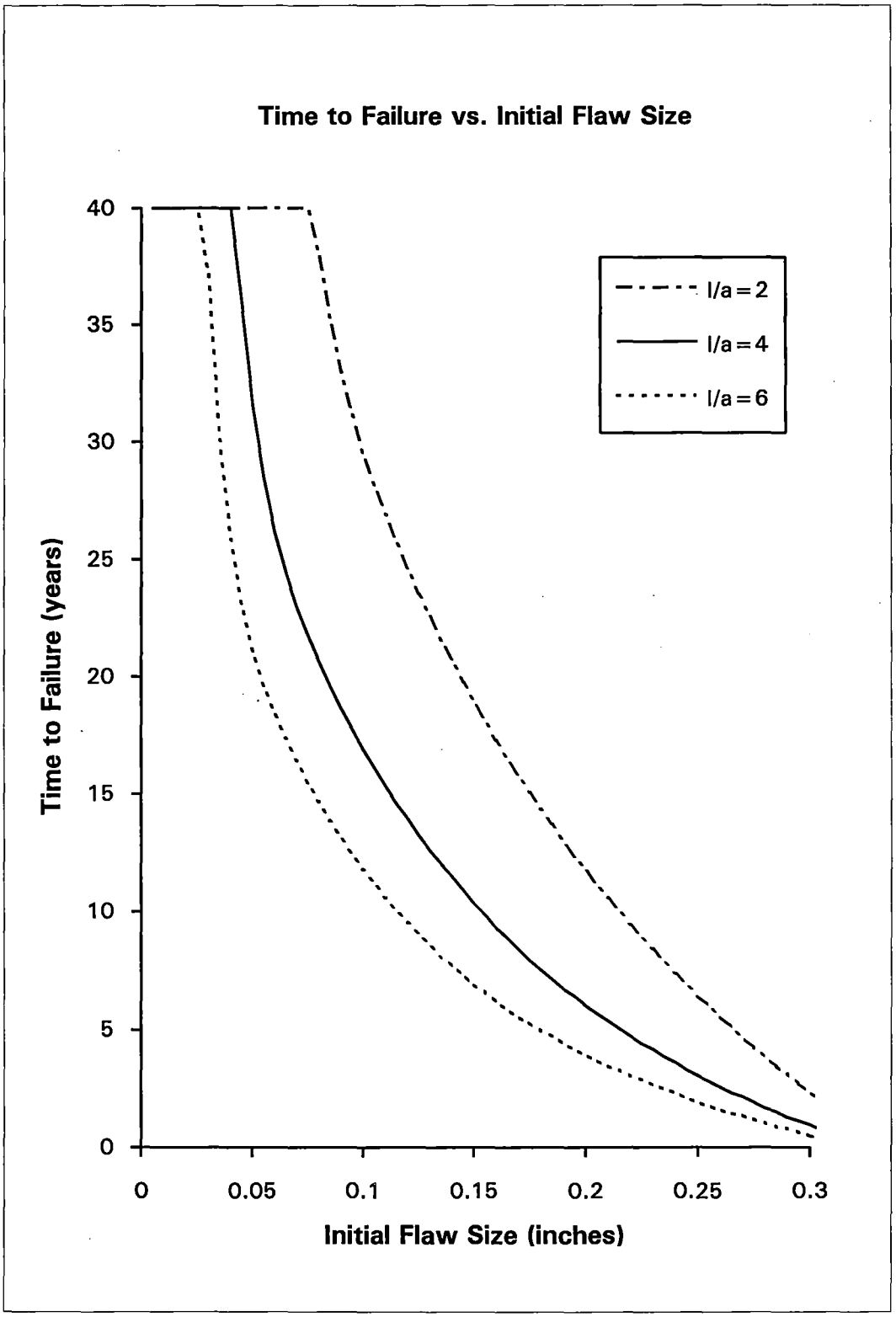

Figure 18. Time to Failure for Cold Leg Charging and Loop Drain Nozzles: Axial Semi-Elliptical Inside Surface Flaws with Constant Through-Wall Yield Stress

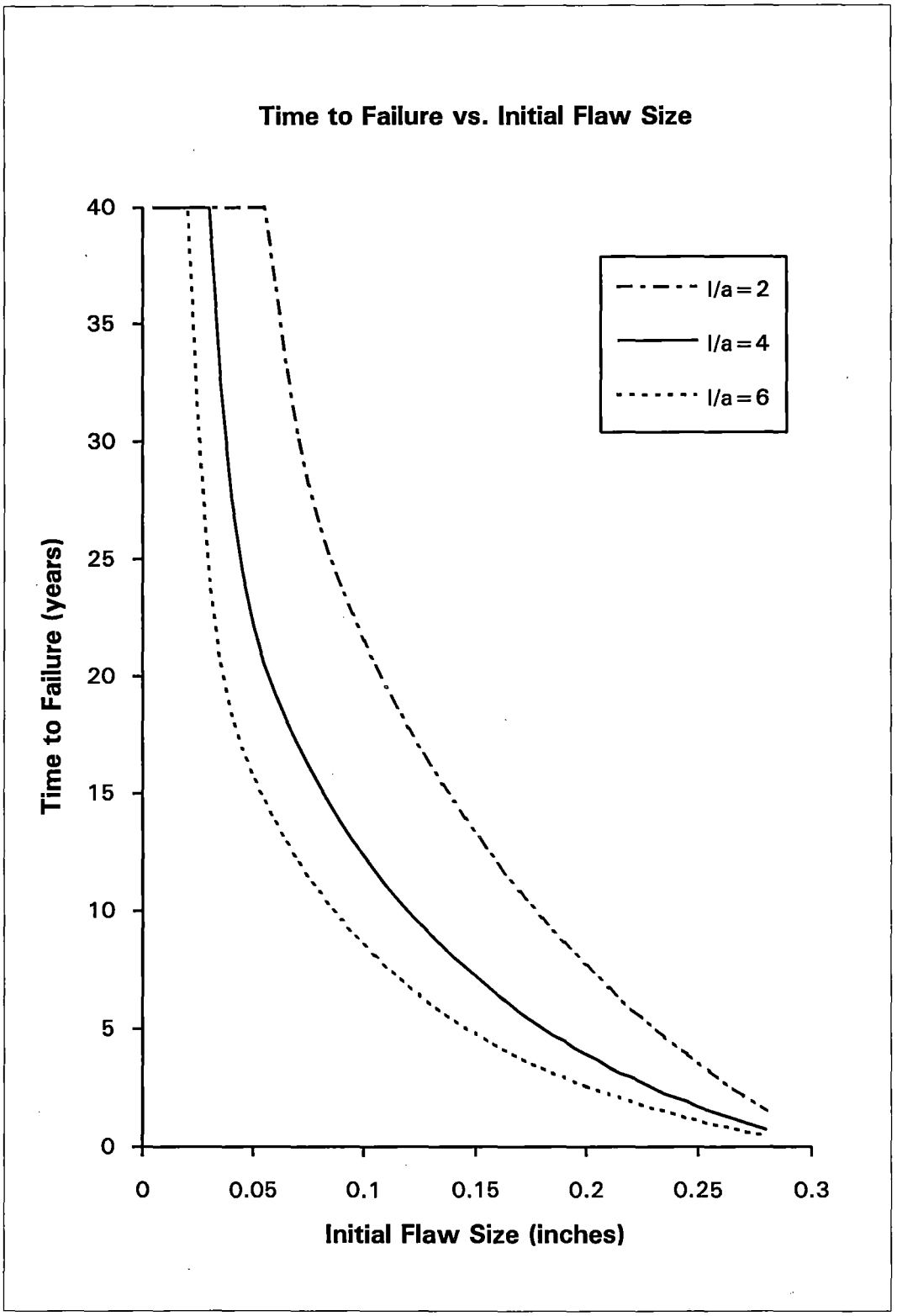

Figure 19. Time to Failure for Cold Leg Pressure & Sampling Nozzle: Axial Semi-Elliptical Inside Surface Flaws with Constant Through-Wall Yield Stress

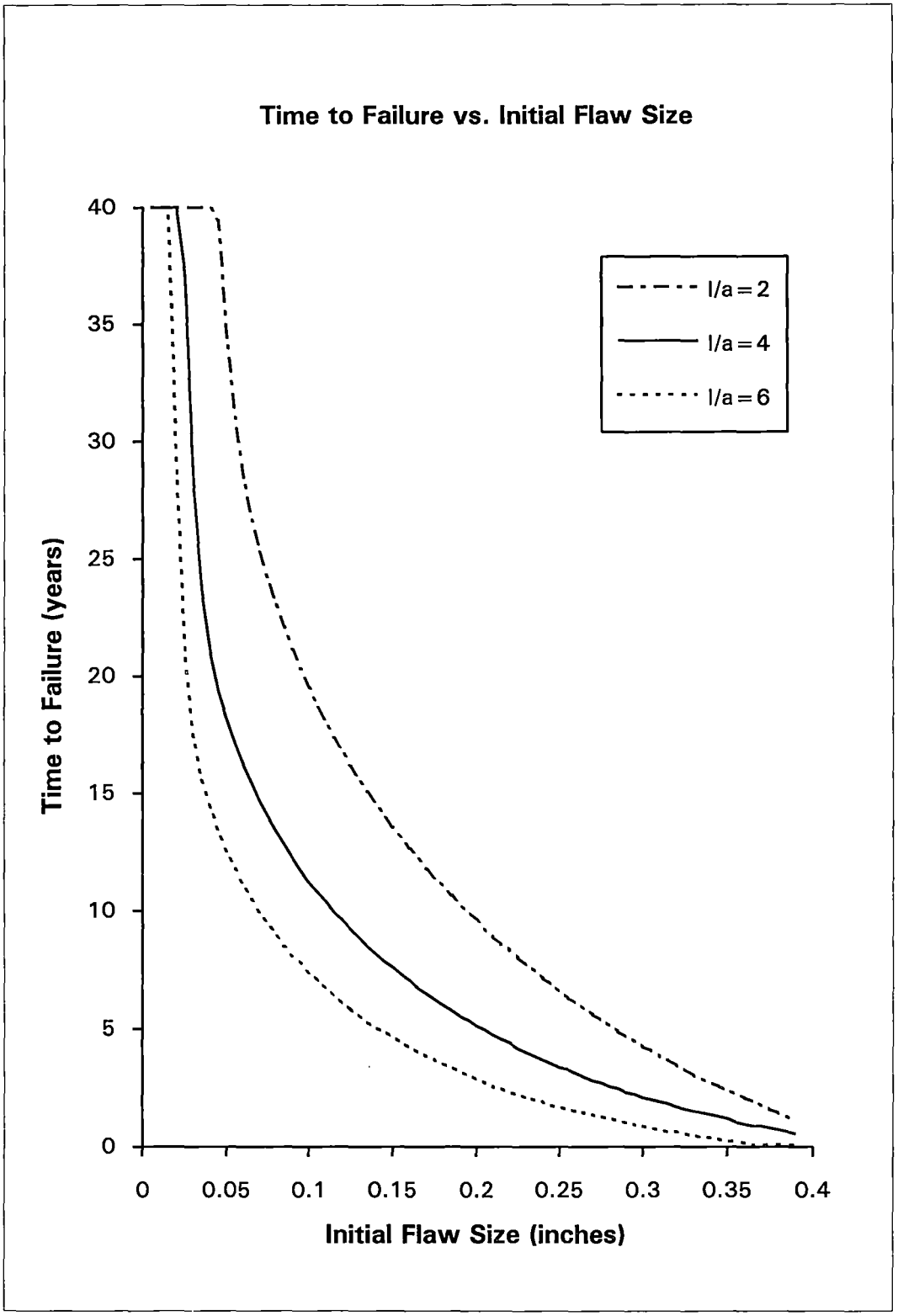

Figure 20. Time to Failure for Cold Leg RTD Nozzle: Axial Semi-Elliptical Inside Surface Flaws with Constant Through-Wall Yield Stress

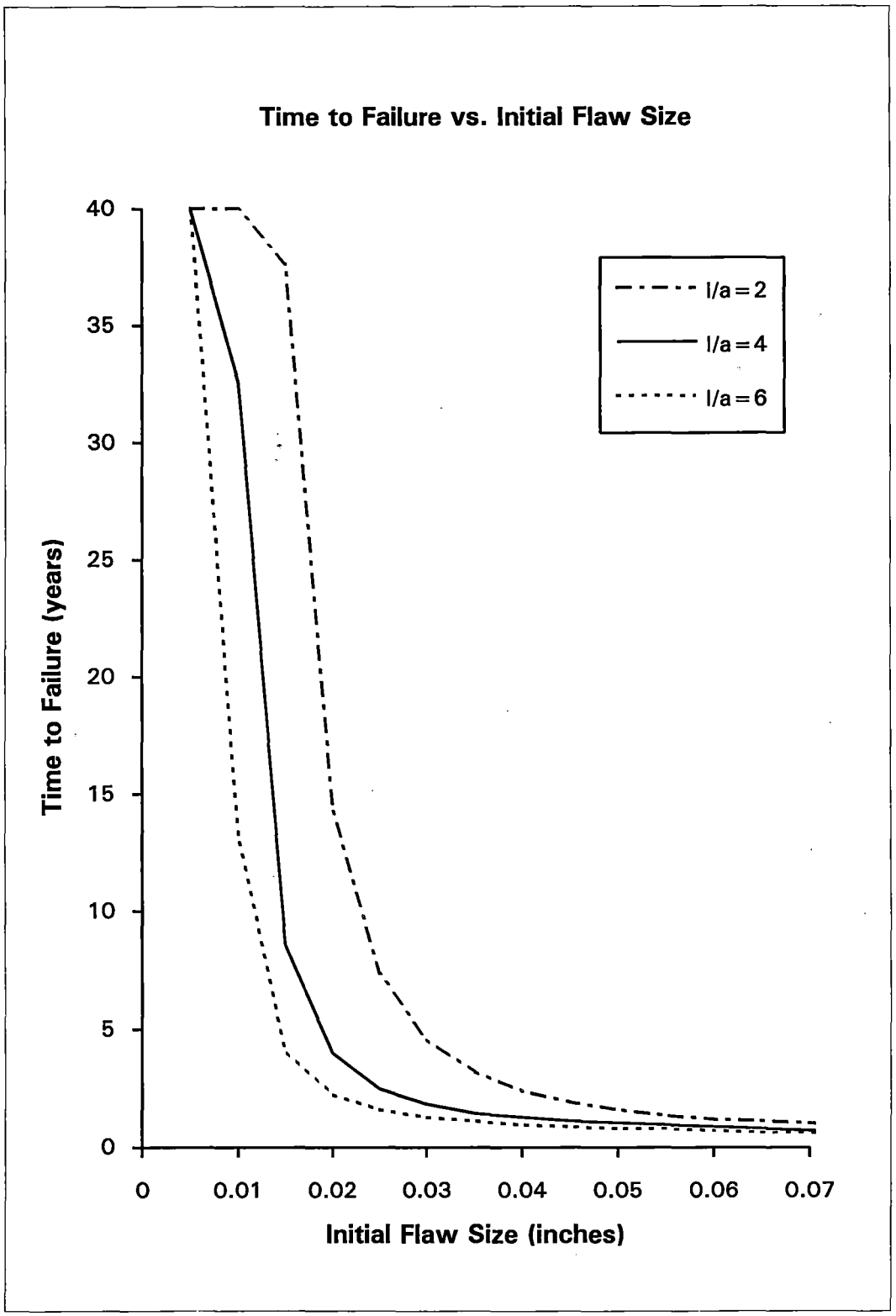

Figure 21. Time to Failure for Pressurizer TE Nozzles: Circumferential Semi-Elliptical Inside Surface Flaws with Constant Through-Wall Yield Stress

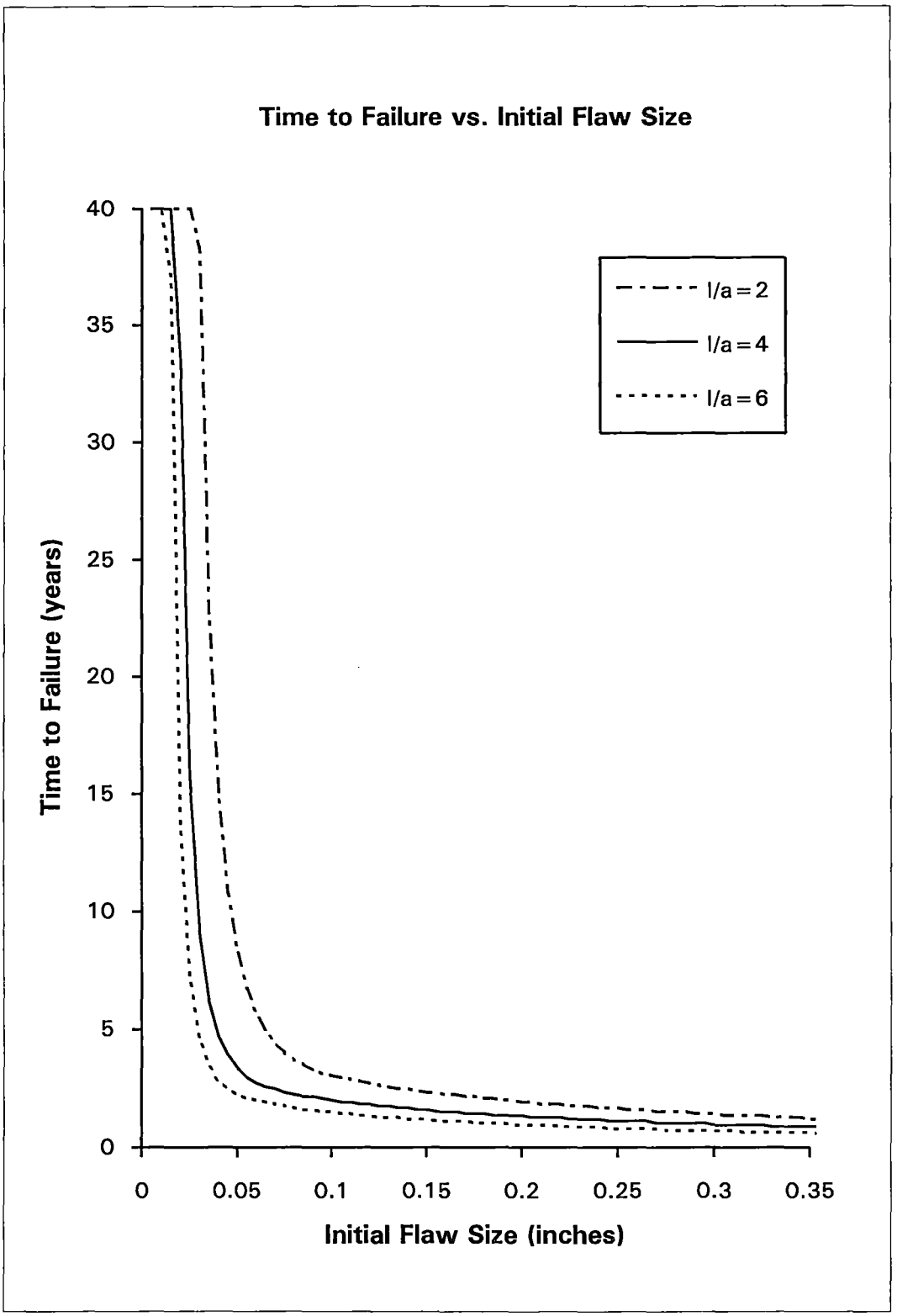

Figure 22. Time to Failure for Pressurizer Surge Nozzle Safe End: Circumferential Semi-Elliptical Inside Surface Flaws with Constant Through-Wall Yield Stress

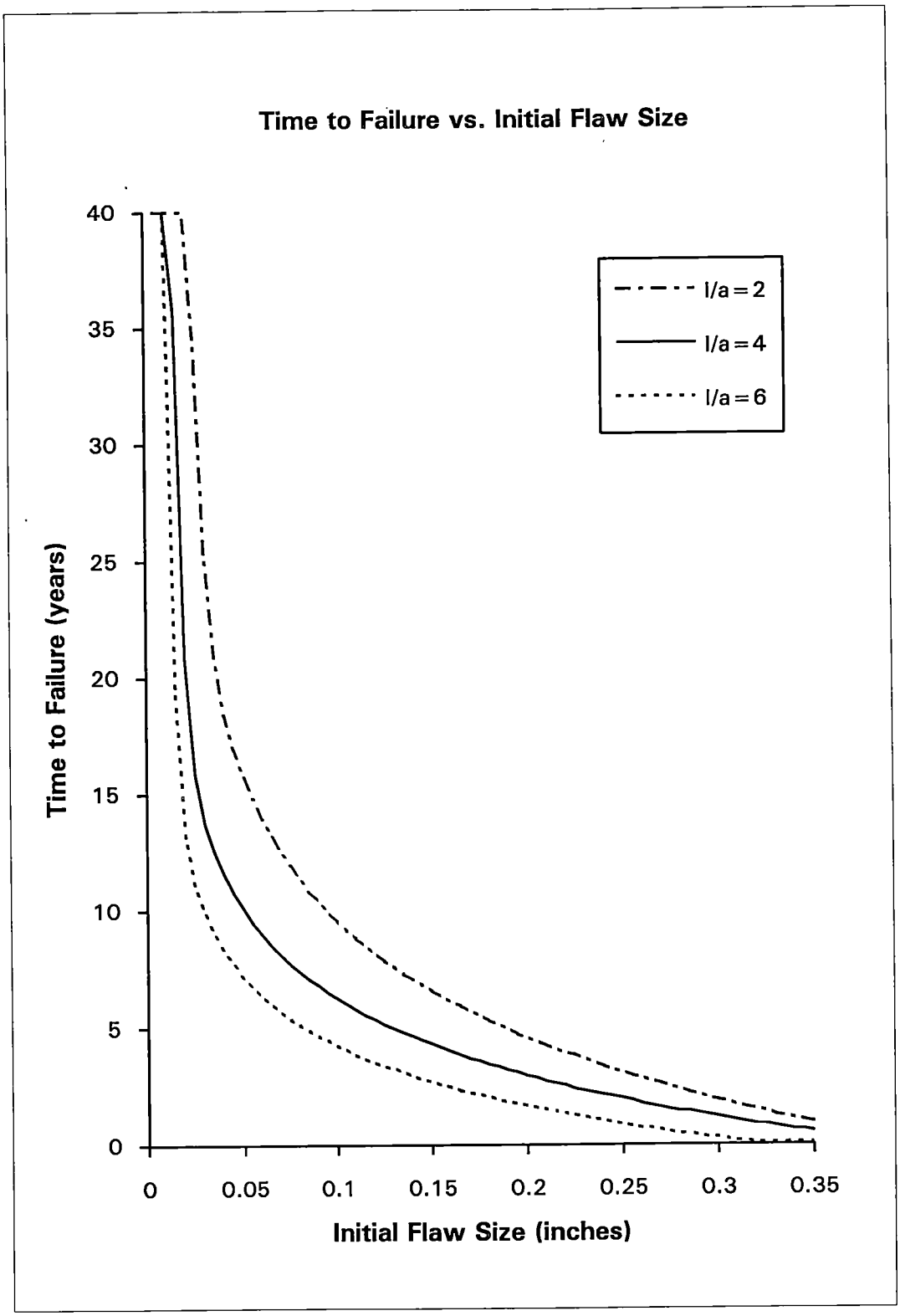

Figure 23. Time to Failure for Pressurizer Spray Nozzle Safe End at 540F: Circumferential Semi-Elliptical Inside Surface Flaws with Constant Through-Wall Yield Stress

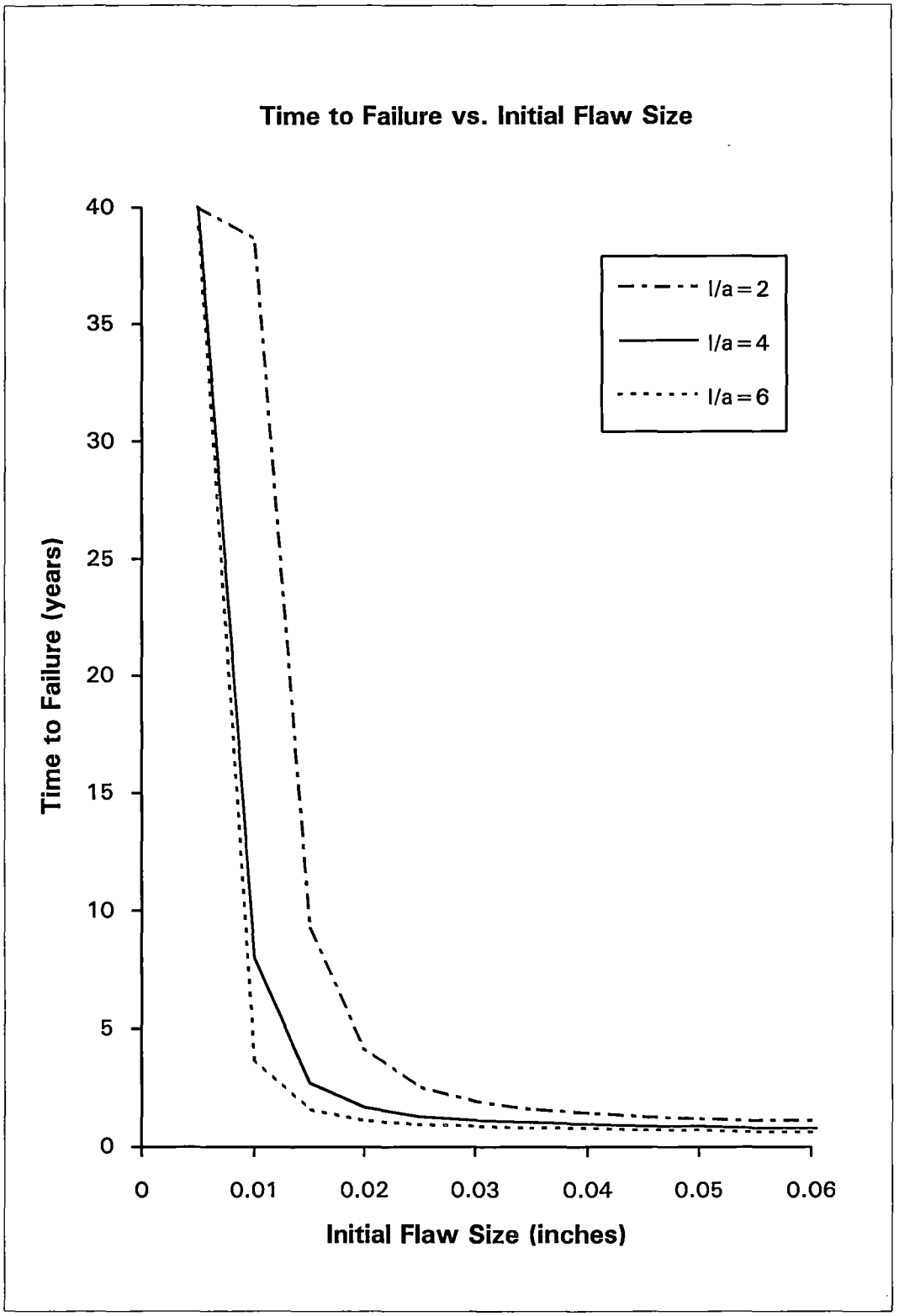

Figure 24. Time to Failure for Pressurizer Spray Nozzle Safe End at 640F: Circumferential Semi-Elliptical Inside Surface Flaws with Constant Through-Wall Yield Stress

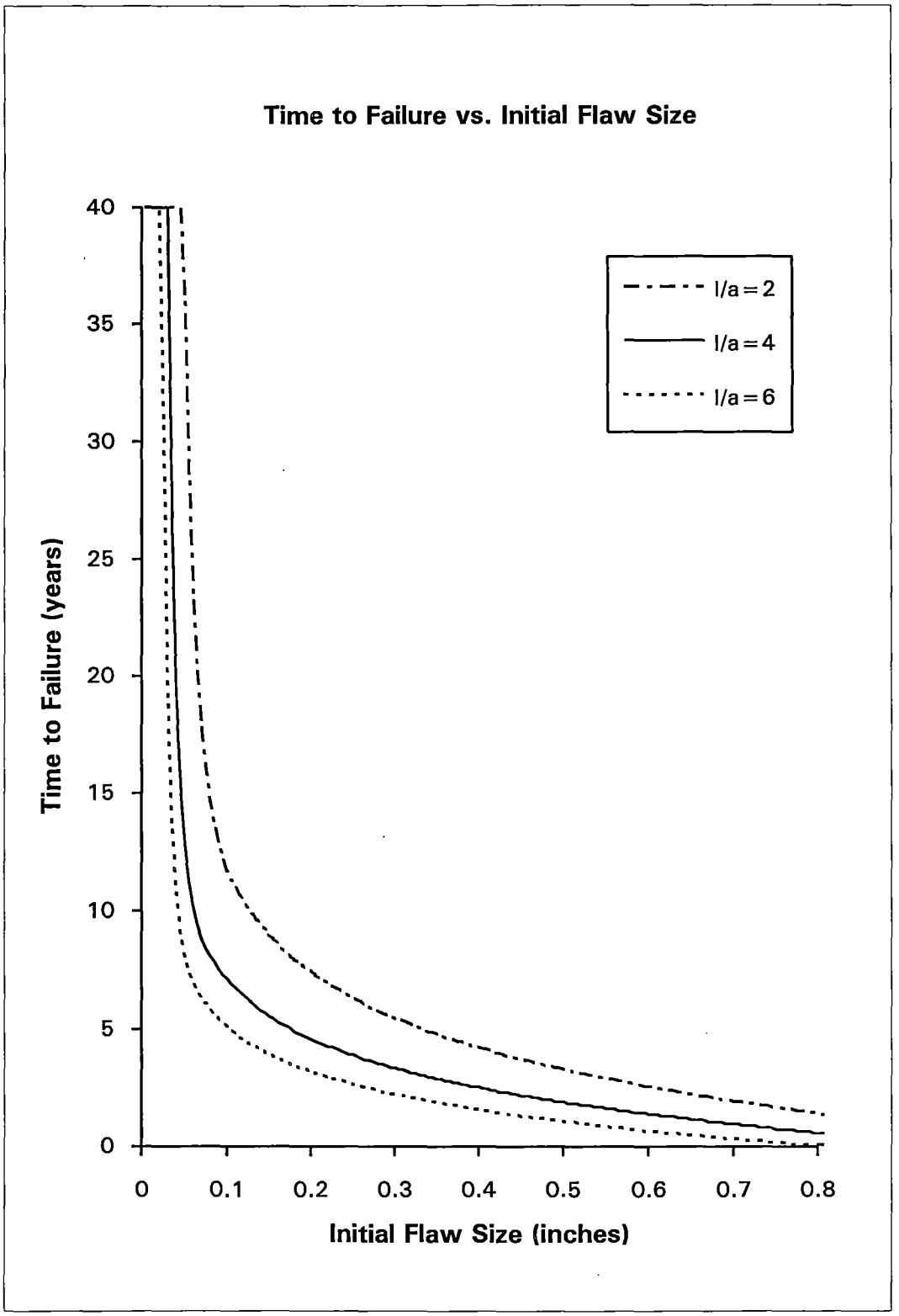

Figure 25. Time to Failure for Hot Leg Surge Nozzle Safe End: Circumferential Semi-Elliptical Inside Surface Flaws with Constant Through-Wall Yield Stress

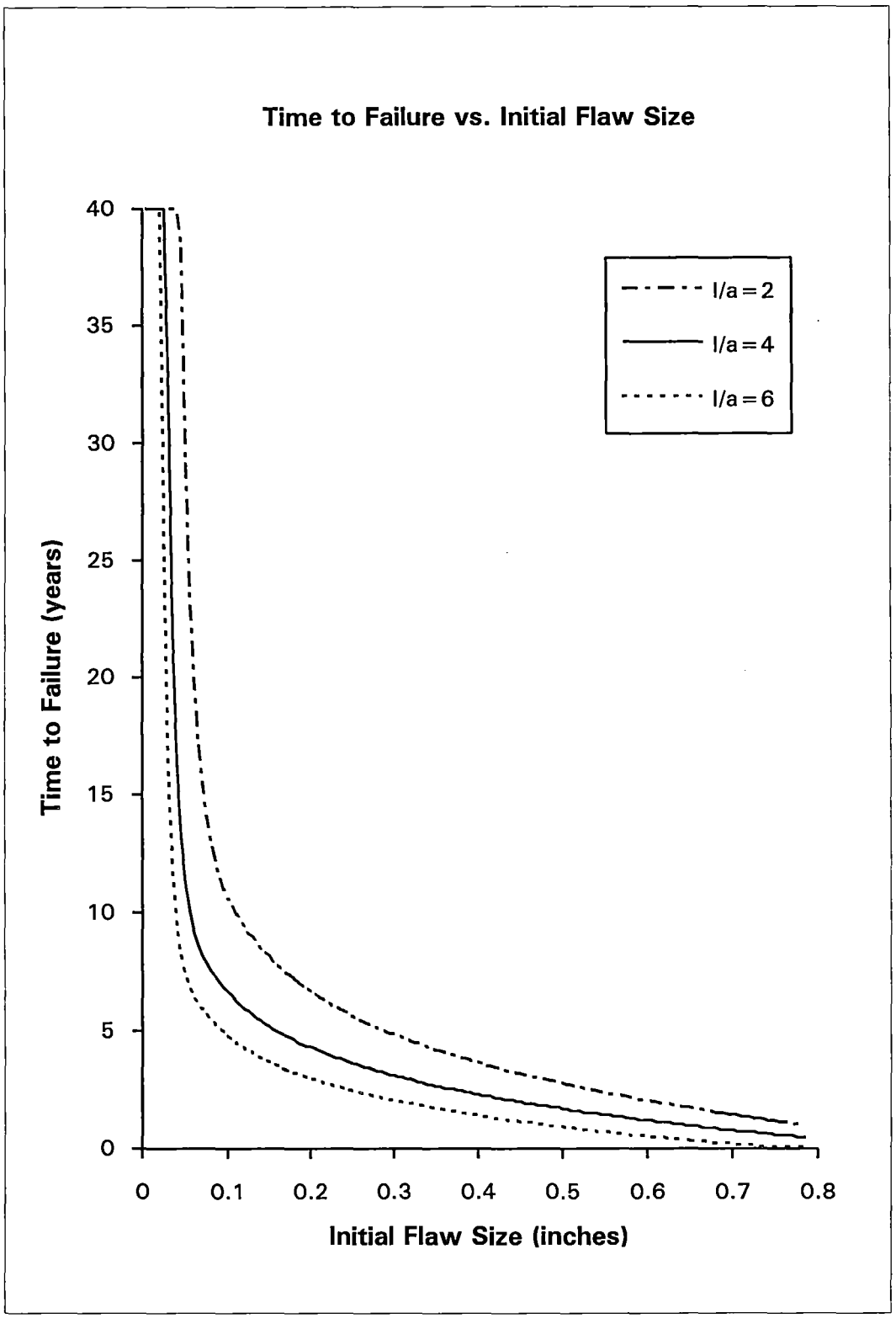

Figure 26. Time to Failure for Hot Leg Shut Down Nozzle Safe End: Circumferential Semi-Elliptical Inside Surface Flaws with Constant Through-Wall Yield Stress

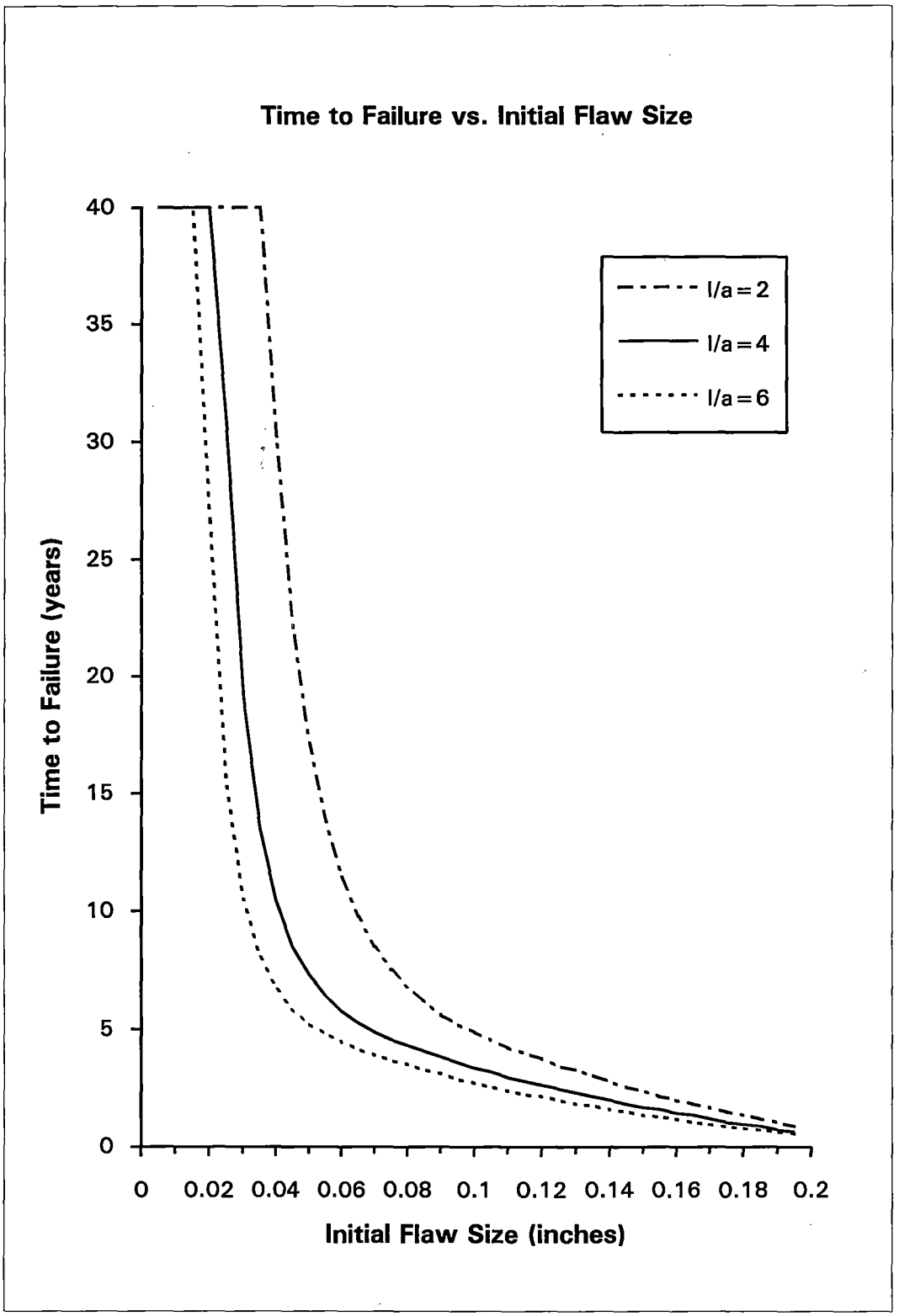

Figure 27. Time to Failure for Hot Leg Loop Drain Nozzle: Circumferential Semi-Elliptical Inside Surface Flaws with Constant Through-Wall Yield Stress

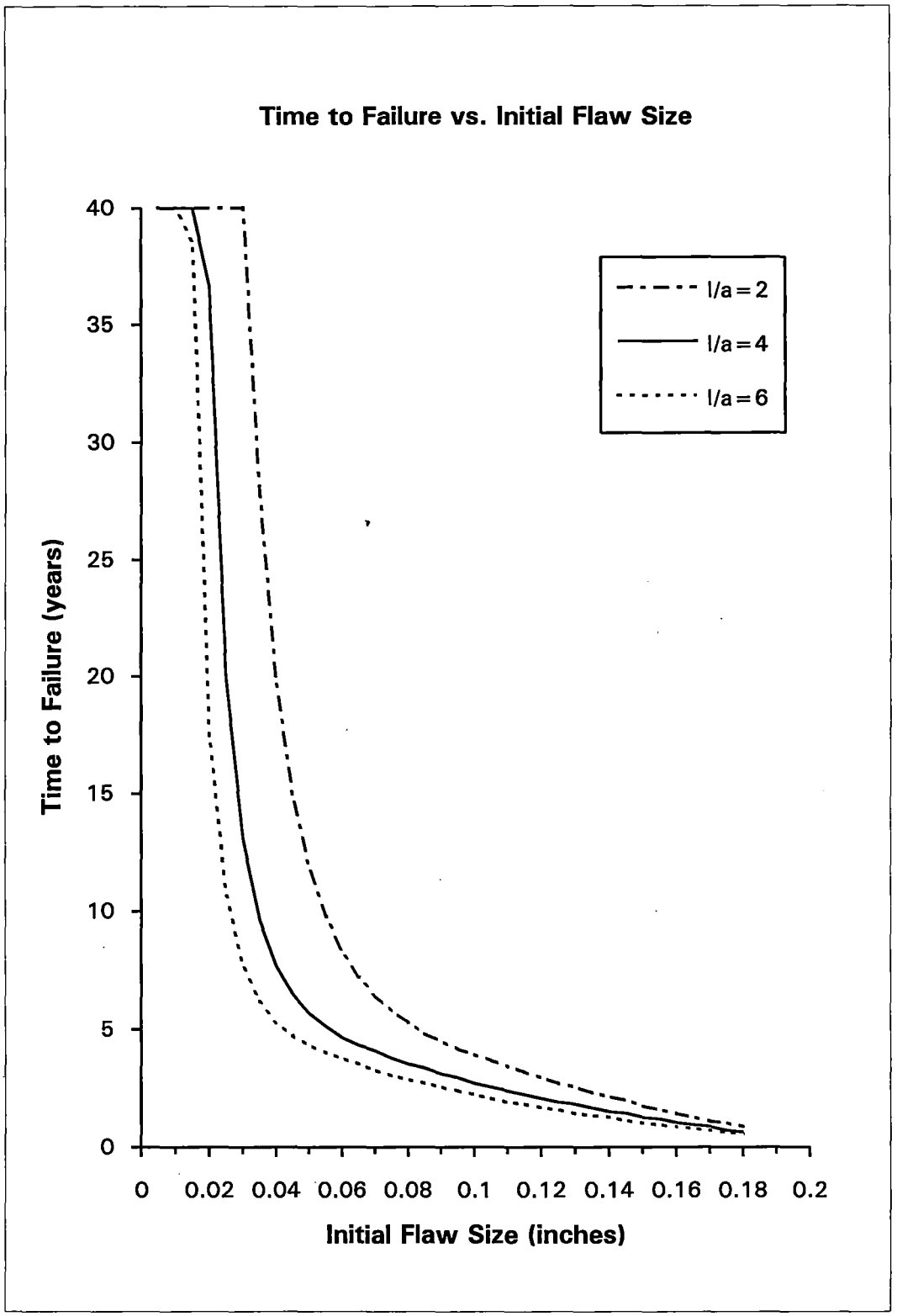

Figure 28. Time to Failure for Hot Leg Pressure & Sampling Nozzle: Circumferential Semi-Elliptical Inside Surface Flaws with Constant Through-Wall Yield Stress

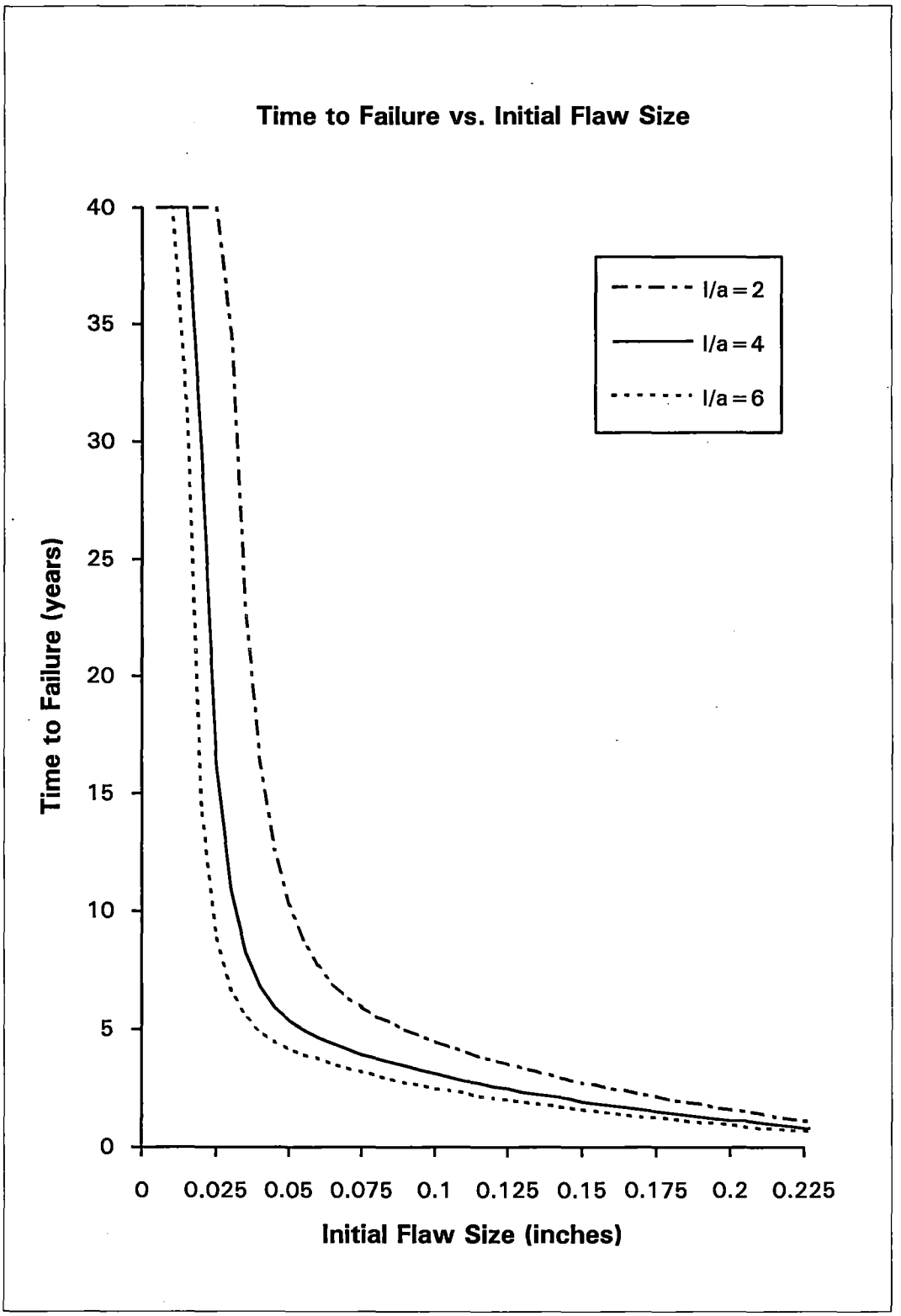

Figure 29. Time to Failure for Hot Leg RTD Nozzle: Circumferential Semi-Elliptical Inside Surface Flaws with Constant Through-Wall Yield Stress

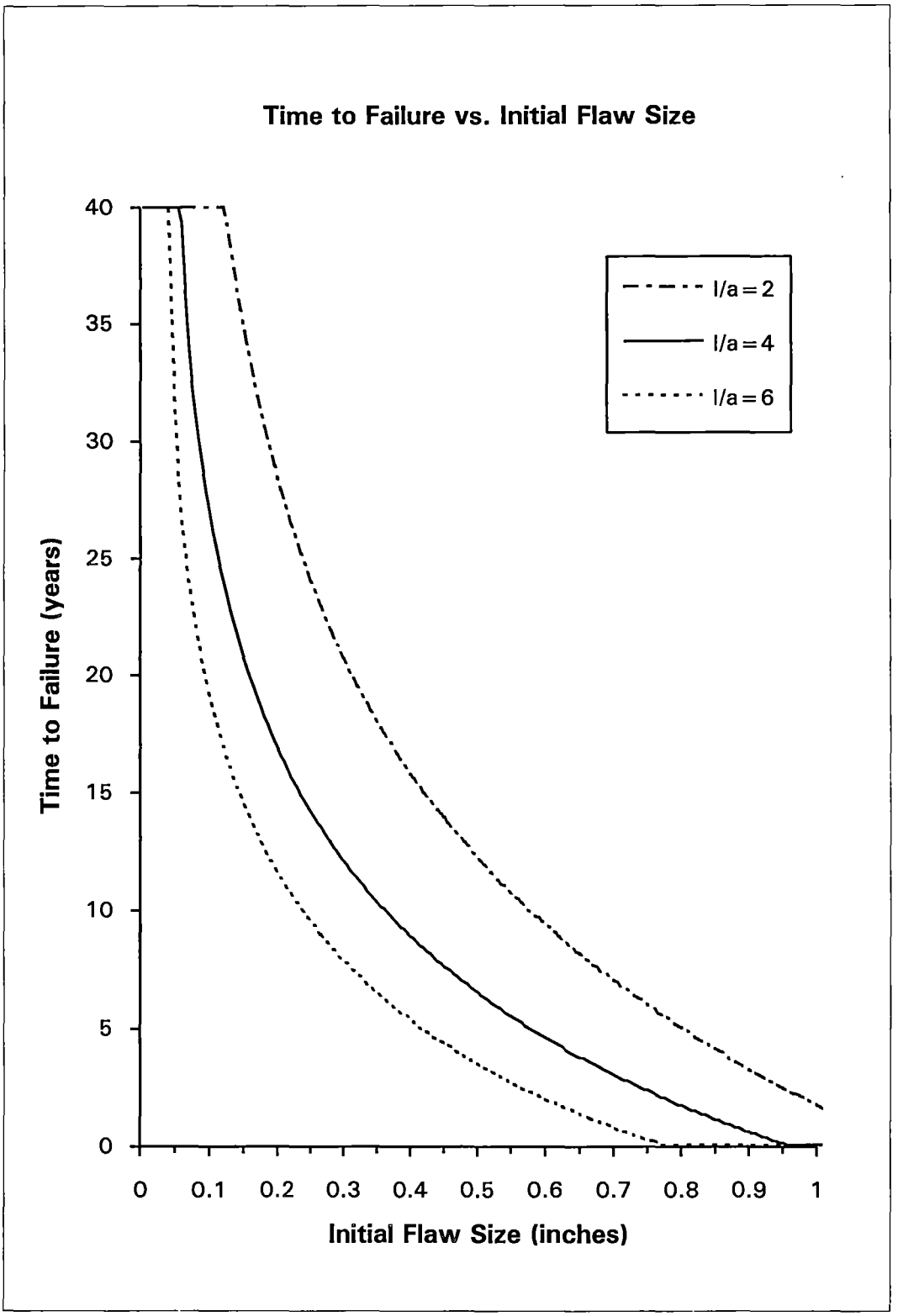

Figure 30. Time to Failure for Cold Leg Shut Down Nozzle Safe End: Circumferential Semi-Elliptical Inside Surface Flaws with Constant Through-Wall Yield Stress

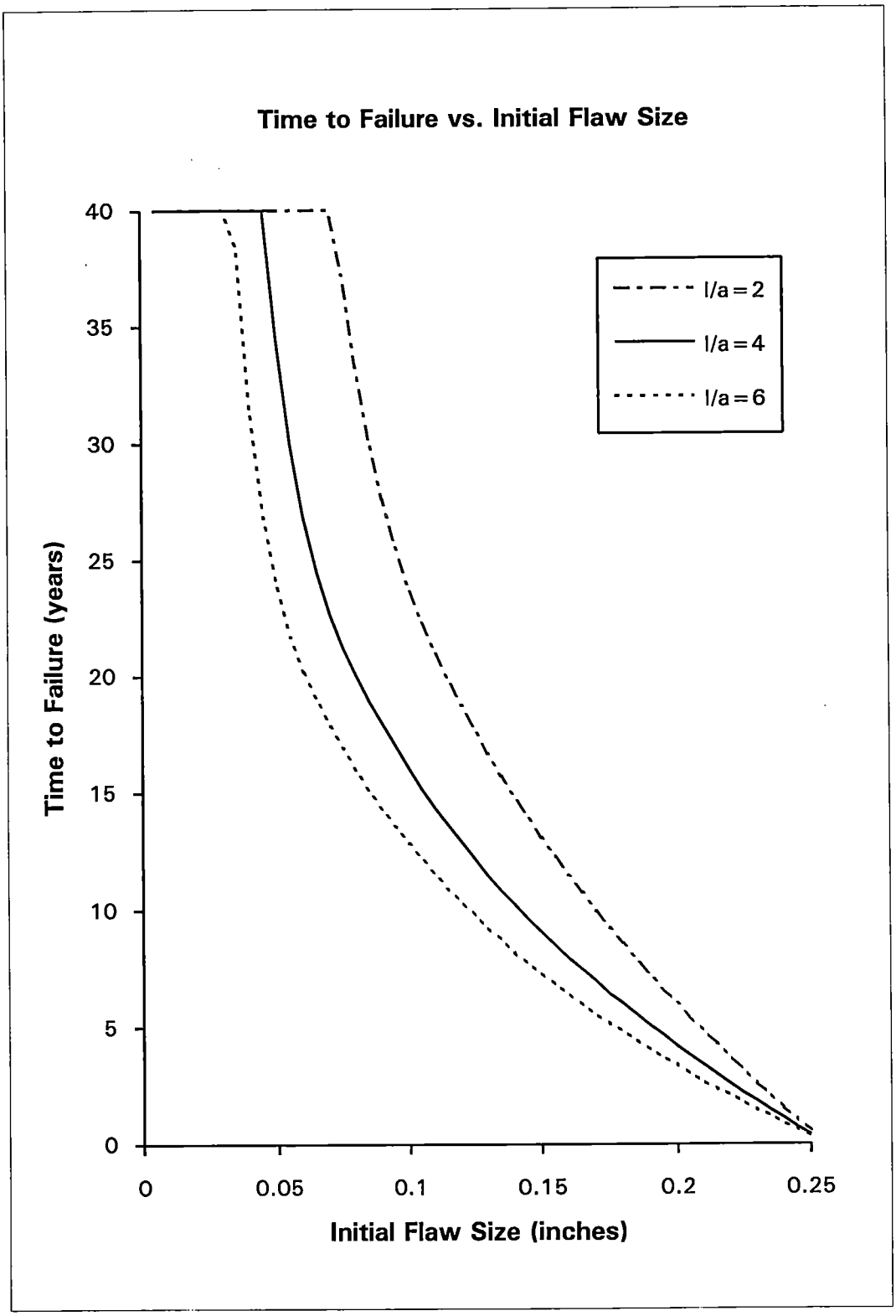

Figure 31. Time to Failure for Cold Leg Spray Nozzle: Circumferential Semi-Elliptical Inside Surface Flaws with Constant Through-Wall Yield Stress

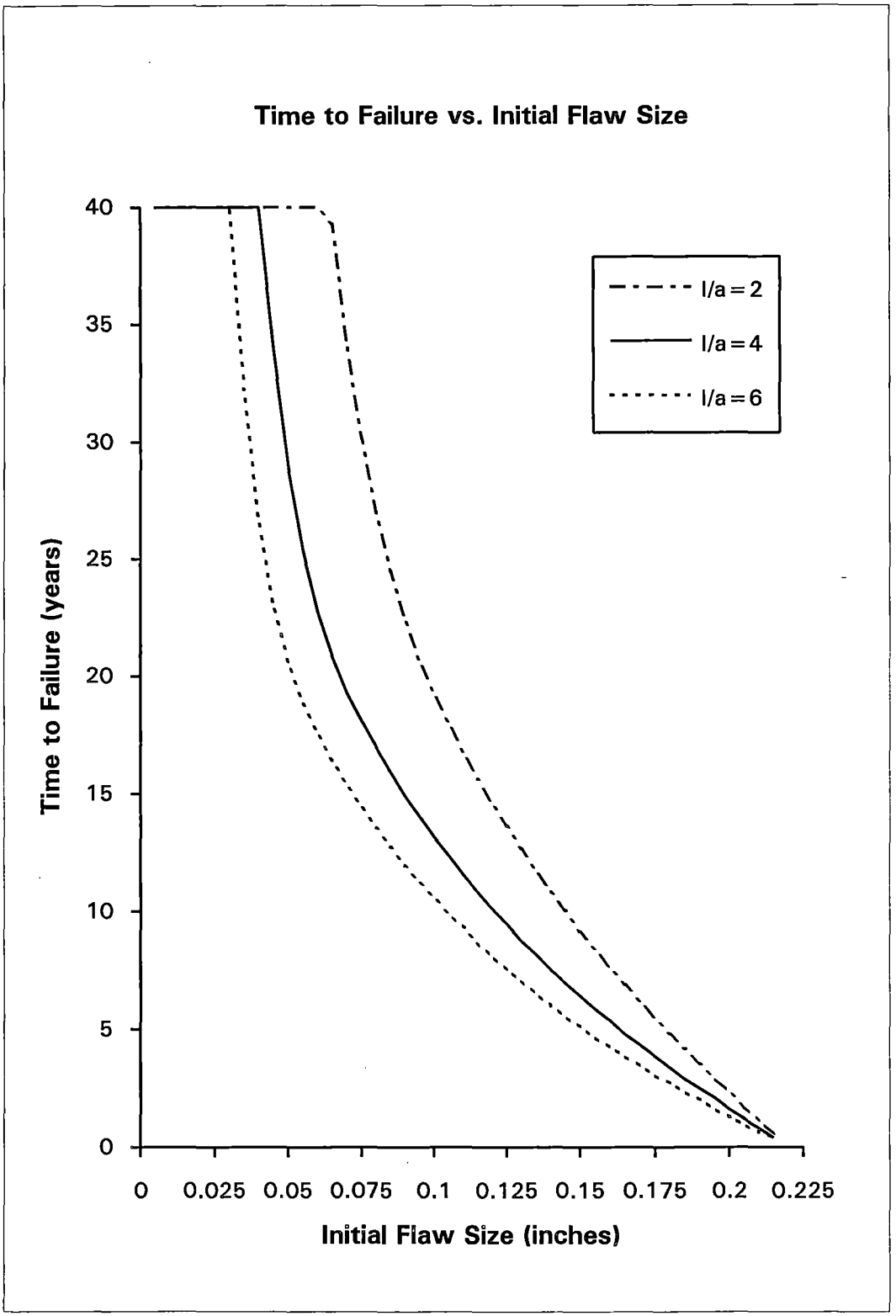

Figure 32. Time to Failure for Cold Leg Charging and Loop Drain Nozzles: Circumferential Semi-Elliptical Inside Surface Flaws with Constant Through-Wall Yield Stress

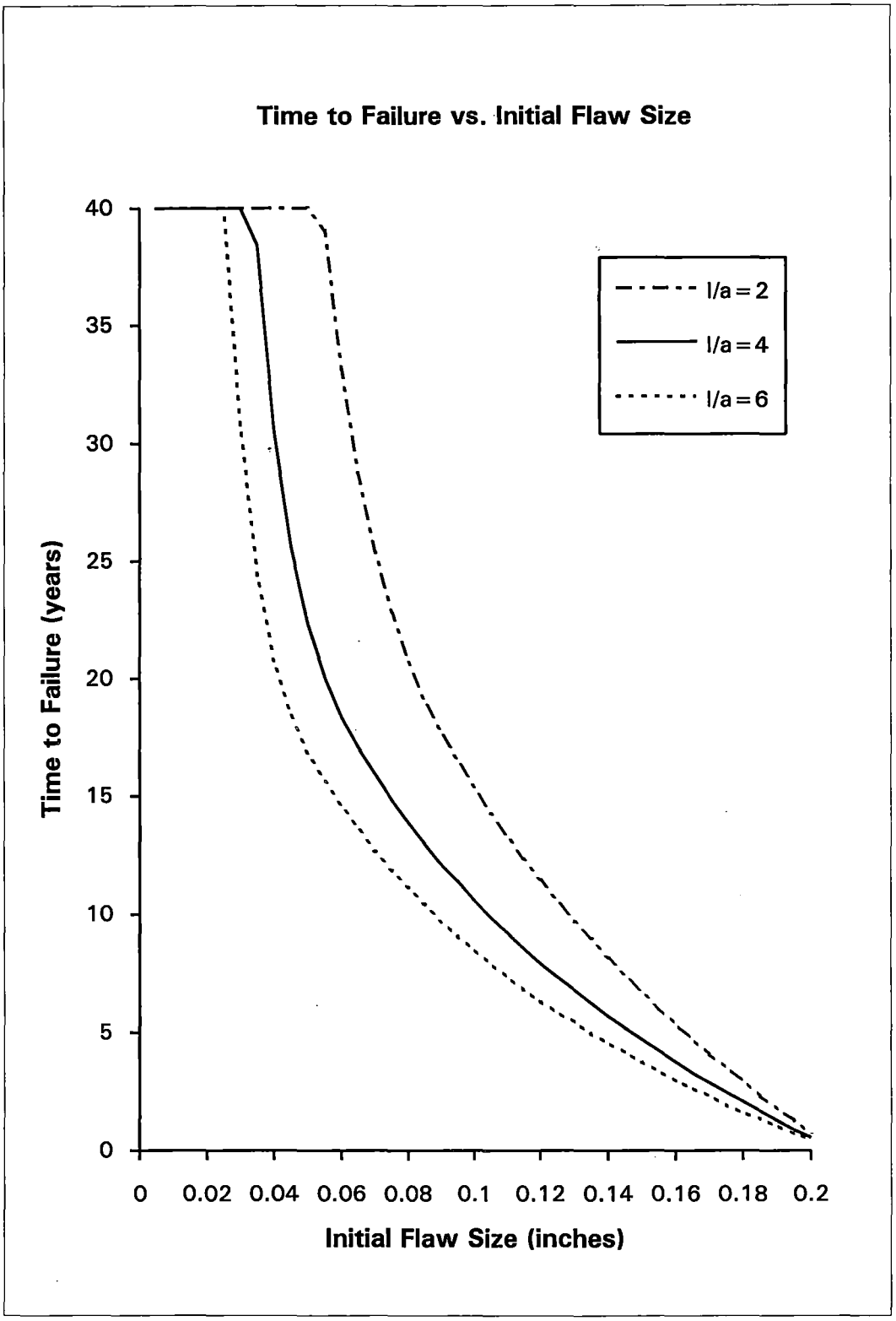

Figure 33. Time to Failure for Cold Leg Pressure & Sampling Nozzle: Circumferential Semi-Elliptical Inside Surface Flaws with Constant Through-Wall Yield Stress

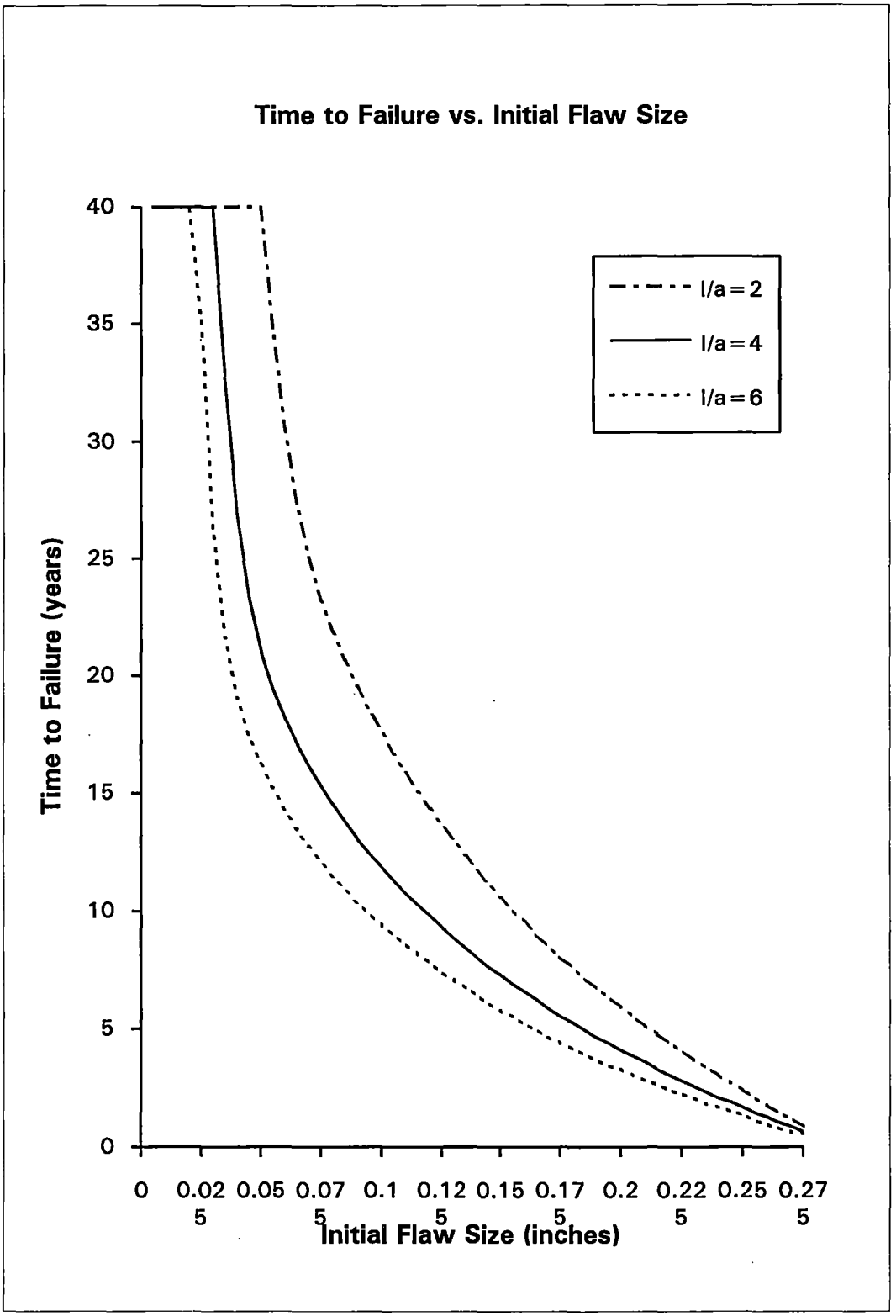

Figure 34. Time to Failure for Cold Leg RTD Nozzle: Circumferential Semi-Elliptical Inside Surface Flaws with Constant Through-Wall Yield Stress

8.0 References

1. BWNT Document 51-1235040-00, "Alloy 600 Program - Inputs."

2. Boursier, J., et al., "Stress Corrosion Cracking of Alloy 600 in Water: Influence of Strain Rate on the Different Stages of Cracking," EUROCORR '92, June 1992.

3. Zahoor, A., "Ductile Fracture Handbook", EPRI-Report NP-6301-D, Electric Power Research Institute, Palo Alto, CA, 1990.

4. ASME Boiler and Pressure Vessel Code, Section XI, 1986 Edition.

5. Amzallag, C., Baudry, G. and Bernard, J.L., IAEA Specialists Meeting on Subcritical Crack Growth, Freiburg, West Germany, May 13-15, 1981, p. 229.

6. Scott, P.M., "An Analysis of Primary Water Stress Corrosion Cracking in PWR Steam Generators," Presented at the OCED Meeting, Brussels, Belgium, September 16-20, 1991.

7. Mills, W.J., "Fracture Toughness of Two Ni-Fe-Cr Alloys," Hanford Engineering Development Laboratory Document HEDL-SA-3309, April 1985.

8. Anderson, T.L., "Fracture Mechanics: Fundamentals and Applications," CRC Press, Boca Raton, FL, 1991.

9. Kumar, V., et. al, "An Engineering Approach for Elastic-Plastic Fracture Analysis," EPRI NP-1931, July 1981.

10. Hazelton, W.S. and Koo, W.H., "Technical Report on Material Selection and Processing Guidelines for BWR Coolant Pressure Boundary Piping," Final Report, NUREG-0313, Rev. 2, January 1988.

11. BWNT Procedure BWNT-0402-01, Rev. 29, "Preparing and Processing BWNT Calculations," June 1, 1994.

12. ASME Boiler and Pressure Vessel Code, Section III, 1986 Edition.

13. CPCo Document P-MECH-CALC-021, Rev. 0, "Stress and Fatigue Evaluation of the Pressurizer Surge Nozzle for Consumers Power Company, Palisades Nuclear Plant."

14. CPCo Document EA-SP-03361-01, Rev. 4, "Pipe Stress Analysis for Pressurizer Spray System Piping."

15. BWNT Document 32-1235177-00, "FM Assessment of Palisades Alloy 600 Components" (BWNT proprietary).

References 13 and 14 are not available for entering into the BWNT Record Center but may be referenced as permitted by BWNT procedure BWNT-0402-01, Appendix 2. These documents are available through CPCo.

Approval: 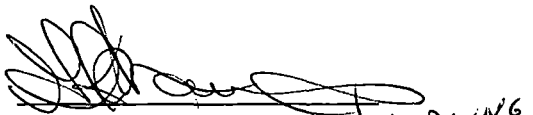
FOR R.R. Steinke G.K. WARDLING

Prepared by: D.E. Killian Date: 4/19/95

Reviewed by: K.K. Yoon Date: 4/20/95

Appendix A Alternate Method using Residual Stress Distribution from NUREG-0313

A.1 Analytical Procedure

Recognizing that the use of a constant through-wall stress distribution for axial residual weld stresses is conservative for the evaluation of circumferential flaws in girth butt welded components, an alternate method is utilized in this appendix to take advantage of a postulated nonlinear stress distribution at two nozzle locations, the pressurizer surge and spray safe end to attached piping welds. This technique incorporates the nondimensional form of through-wall stress distribution found in NUREG-0313 (Ref. 10) for axial stress, described by the fourth order polynomial:

$$\sigma/\sigma_i = \sum_{j=0}^{4} \sigma_j \xi^j,$$

where:

$\sigma_0 = 1.0$

$\sigma_1 = -6.910$

$\sigma_2 = 8.687$

$\sigma_3 = -0.480$

$\sigma_4 = -2.027$

$\xi = x/t$

$\sigma_i =$ stress magnitude at $\xi = 0$ (inner surface)

The material yield strength at operating temperature serves as a good estimate of the inner surface residual stress. Although operating stresses would add directly to residual stresses in a purely linear analysis, the total is limited by elastic-plastric material behavior. To account for some strain hardening, but still control the magnitude of the total stress, through-wall stresses are limited to 125% of the operating temperature yield strength.

Since a maximum constant through-wall stress condition is not being used to evaluate circumferential flaws, the normal condition fracture toughness acceptance criterion no longer inherently bounds the faulted condition criterion. This requires that the faulted condition fracture toughness acceptance criterion must now be checked at each crack depth, along with the normal condition criterion. Table A-1 presents the complete procedure used to incorporate the NUREG-0313 stress distribution in the determination of acceptable circumferential flaw sizes for the pressurizer surge and spray nozzle safe ends. The four major steps of this procedure are: (1) check normal condition fracture toughness, (2) check faulted condition fracture toughness, (3) check for net section collapse (limit load), and (4) calculate incremental crack growth.

The first five substeps of Step 1 are executed in Table A-2 for three configurations: the pressurizer surge nozzle safe end at 640 °F, and pressurizer spray nozzle safe end at 540 °F and 640 °F. This portion of the procedure computes stress coefficients used with the third order polynomial stress intensity factor solution of Section 4.2. A graphical representation of the generation of this third order curve is shown in Figures A-1 through A-3 for the three nozzle configurations. The remaining portion of the evaluation procedure outlined in Table A-1 has been programmed in the FORTRAN code CINL.F, listed in Appendix D of Reference 15. Program CINL.F is verified in Appendix B. Input data is contained in Appendix C.

Table A-1. Flaw Evaluation Procedure for Use with the NUREG-0313 Residual Stress Distribution

Step 1 - Check normal condition fracture toughness

1. Calculate a constant through-wall primary plus secondary operating stress using Equation (10) from Section NB-3653 of the ASME Boiler and Pressure Vessel Code (Ref. 12). This equation includes contributions from internal pressure, external piping moments and thermal discontinuity between the Alloy 600 safe end and stainless steel piping. The resultant external piping moment is derived from deadweight and thermal loads.

2. Calculate through-wall axial residual stresses using NUREG-0313's nondimensional fourth order form with the inside surface stress set equal to the material yield strength at operating temperature.

3. Calculate the sum of the fourth order residual stress and the constant through-wall operating stress.

4. Limit this total stress to 125% of the operating temperature yield strength.

5. Fit a third order polynomial curve to the data points corresponding to the "cutoff" total stress at operating temperature.

6. Calculate a normal condition stress intensity factor using the solution described in Section 4.2 for a semi-elliptical circumferential flaw.

7. Evaluate the IWB-3612 normal condition fracture toughness criterion (Ref. 4):

$$K_I(a) < K_{Ic} / \sqrt{10}$$

Step 2 - Check faulted condition fracture toughness

1. Calculate a constant through-wall axial stress for faulted conditions using ASME Code Equation (10) considering design pressure, deadweight plus thermal plus safe shutdown earthquake (SSE) seismic loads, and thermal discontinuity.

2. Calculate a faulted condition stress intensity factor and evaluate the IWB-3612 faulted condition fracture toughness criterion (Ref. 4):

$$K_I(a) < K_{Ic} / \sqrt{2}$$

Step 3 - Check for net section collapse (limit load)

1. Calculate an equivalent axial pipe load from the constant through-wall axial stress computed in Step 2.1 for faulted conditions:

$$P = \sigma_{(\text{faulted condition})} \pi (R_o^2 - R_i^2)$$

2. Calculate the limit load using the solution in Section 4.4 for semi-elliptical circumferential flaws.

3. Check that the axial pipe load from Step 3.1 is less than the limit load.

Step 4 - Calculate incremental crack growth

1. Using stresses calculated in Step 1, calculate fatigue crack growth for up to 500 heatup and cooldown cycles and stress corrosion crack growth for an equivalent, incremental time span.

Table A-2. Derivation of Nonlinear Stress Distributions

Stresses from Piping Equation No. 10

$S = C1*(p\ Do)/(2\ t) + C2*Do/(2\ I)*M + C3*E_ab*|alpha_a - alpha_b|*delta_T$

C1 =	1.0	Material "a" =	A600 safe end
C2 =	1.0	Material "b" =	316 SS pipe
C3 =	0.6		

	Pzr Surge @ 640F	Pzr Spray @ 540F	Pzr Spray @ 640F		
Do	12.750	4.500	4.500	in	
Di	10.740	3.692	3.692	in	
t	1.005	0.404	0.404	in	
I	644.27	11.01	11.01	in^4	
alpha_a	7.87E-06	7.75E-06	7.87E-06	/F	A600
alpha_b	9.66E-06	9.49E-06	9.66E-06	/F	SS
E_a	3.08E+07	3.08E+07	3.08E+07	psi	A600 @ RT per ASME Code
E_b	2.81E+07	2.81E+07	2.81E+07	psi	SS @ RT per ASME Code
E_ab	2.95E+07	2.95E+07	2.95E+07	psi	Avg. RT value
Normal Conditions					
delta_T	570	470	570	F	(T - 70F)
p	2205	2205	2205	psi	
M	832.74	43.10	43.10	in-kip	(DW + Thermal) (*)
S	40286	35562	39147	psi	
Faulted Conditions					
delta_T	570	470	570	F	(T - 70F)
p	2500	2500	2500	psi	
M	1500.80	138.46	138.46	in-kip	(DW + Thermal + SSE) (*)
S	48768	56691	60275	psi	

Note * References for applied piping moments are:
Pzr Surge Nozzle - Ref. 13
Pzr Spray Nozzle - Ref. 14

Table A-2. Derivation of Nonlinear Stress Distributions (Cont'd)

Axial Residual Stresses from NUREG-0313

S = Si * SUM(Sj * XI^j), j=0,1,2,3,4

where: S0 = 1.000 and XI = x/t
S1 = -6.910 Si = stress at XI=0 (inner surface)
S2 = 8.687
S3 = -0.480 Let Si = Oper. Temp. Yield Strength
S4 = -2.027

	Pzr Surge @ 640F	Pzr Spray @ 540F	Pzr Spray @ 640F
Si, psi =	40200	62900	60900

XI	S, psi		
0.00	40200	62900	60900
0.05	27181.02	42529.51	41177.22
0.10	15886.53	24857.28	24066.91
0.15	6283.716	9831.983	9519.36
0.20	-1672.45	-2616.84	-2533.63
0.25	-8039.21	-12578.8	-12178.8
0.30	-12886.1	-20162.5	-19521.4
0.35	-16294.7	-25495.9	-24685.2
0.40	-18359	-28725.9	-27812.5
0.45	-19185.1	-30018.5	-29064
0.50	-18891.5	-29559.1	-28619.2
0.55	-17608.6	-27551.8	-26675.8
0.60	-15479.4	-24220.2	-23450.1
0.65	-12658.8	-19806.9	-19177.1
0.70	-9314.05	-14573.5	-14110.1
0.75	-5624.7	-8800.84	-8521
0.80	-1782.44	-2788.94	-2700.26
0.85	2008.827	3143.165	3043.224
0.90	5532.939	8657.26	8381.99
0.95	8561.528	13396.02	12970.08
1.00	10854	16983	16443

Residual Stress Plus Normal Operating Stress, psi

Pzr Surge @ 640F	Pzr Spray @ 540F	Pzr Spray @ 640F
80486.2	98462.27	100046.5
67467.23	78091.78	80323.74
56172.73	60419.55	63213.43
46569.92	45394.25	48665.88
38613.75	32945.43	36612.89
32246.99	22983.5	26967.71
27400.15	15399.76	19625.1
23991.53	10066.37	14461.3
21927.22	6836.394	11334.03
21101.07	5543.738	10082.47
21394.72	6003.202	10527.33
22677.57	8010.456	12470.76
24806.82	11342.05	15696.42
27627.44	15755.4	19969.44
30972.16	20988.8	25036.44
34661.5	26761.43	30625.52
38503.77	32773.33	36446.26
42295.03	38705.44	42189.74
45819.14	44219.53	47528.51
48847.73	48958.29	52116.6
51140.2	52545.27	55589.52

Table A-2. Derivation of Nonlinear Stress Distributions (Cont'd)

Residual Stress Plus Normal Operating Stress with Cutoff at 125% Operating Temperature Yield Strength

	125% Oper. Temp. Yield, psi		
	Pzr Surge	Pzr Spray	Pzr Spray
	50250	78625	76125

	Res + Opr Stress, psi		
XI	Pzr Surge @ 640F	Pzr Spray @ 540F	Pzr Spray @ 640F
0.00	80486.2	98462.27	100046.5
0.10	56172.73	60419.55	63213.43
0.20	38613.75	32945.43	36612.89
0.30	27400.15	15399.76	19625.1
0.40	21927.22	6836.394	11334.03
0.50	21394.72	6003.202	10527.33
0.60	24806.82	11342.05	15696.42
0.70	30972.16	20988.8	25036.44
0.80	38503.77	32773.33	36446.26
0.90	45819.14	44219.53	47528.51
1.00	51140.2	52545.27	55589.52

	Res + Opr Stress w/ Cutoff, psi		
XI	Pzr Surge @ 640F	Pzr Spray @ 540F	Pzr Spray @ 640F
0.00	50250	78625	76125
0.10	50250	60419.55	63213.43
0.20	38613.75	32945.43	36612.89
0.30	27400.15	15399.76	19625.1
0.40	21927.22	6836.394	11334.03
0.50	21394.72	6003.202	10527.33
0.60	24806.82	11342.05	15696.42
0.70	30972.16	20988.8	25036.44
0.80	38503.77	32773.33	36446.26
0.90	45819.14	44219.53	47528.51
1.00	50250	52545.27	55589.52

Using the Third Order Curve Fit:

$S = SUM(Ci * XI^i), \quad i=0,1,2,3$

C0	55266.6	83704.7	82032.4
C1	-130231	-356694	-319250
C2	146351	497708	432426
C3	-18157.2	-169591	-136723

XI	Res + Opr Stress w/ Cutoff, psi		
0.00	55266.6	83704.7	82032.4
0.05	49118.66	67093.07	67133.87
0.10	43688.85	52842.79	54294.94
0.15	38963.57	40826.66	43413.04
0.20	34929.18	30917.49	34385.66
0.25	31572.08	22988.09	27110.23
0.30	28878.65	16911.26	21484.22
0.35	26835.26	12559.82	17405.09
0.40	25428.3	9806.556	14770.29
0.45	24644.15	8524.29	13477.28
0.50	24469.2	8585.825	13423.53
0.55	24889.82	9863.967	14506.48
0.60	25892.4	12231.52	16623.59
0.65	27463.33	15561.3	19672.33
0.70	29588.97	19726.11	23550.15
0.75	32255.72	24598.75	28154.51
0.80	35449.95	30052.03	33382.86
0.85	39158.06	35958.76	39132.67
0.90	43366.41	42191.74	45301.39
0.95	48061.4	48623.79	51786.48
1.00	53229.4	55127.7	58485.4

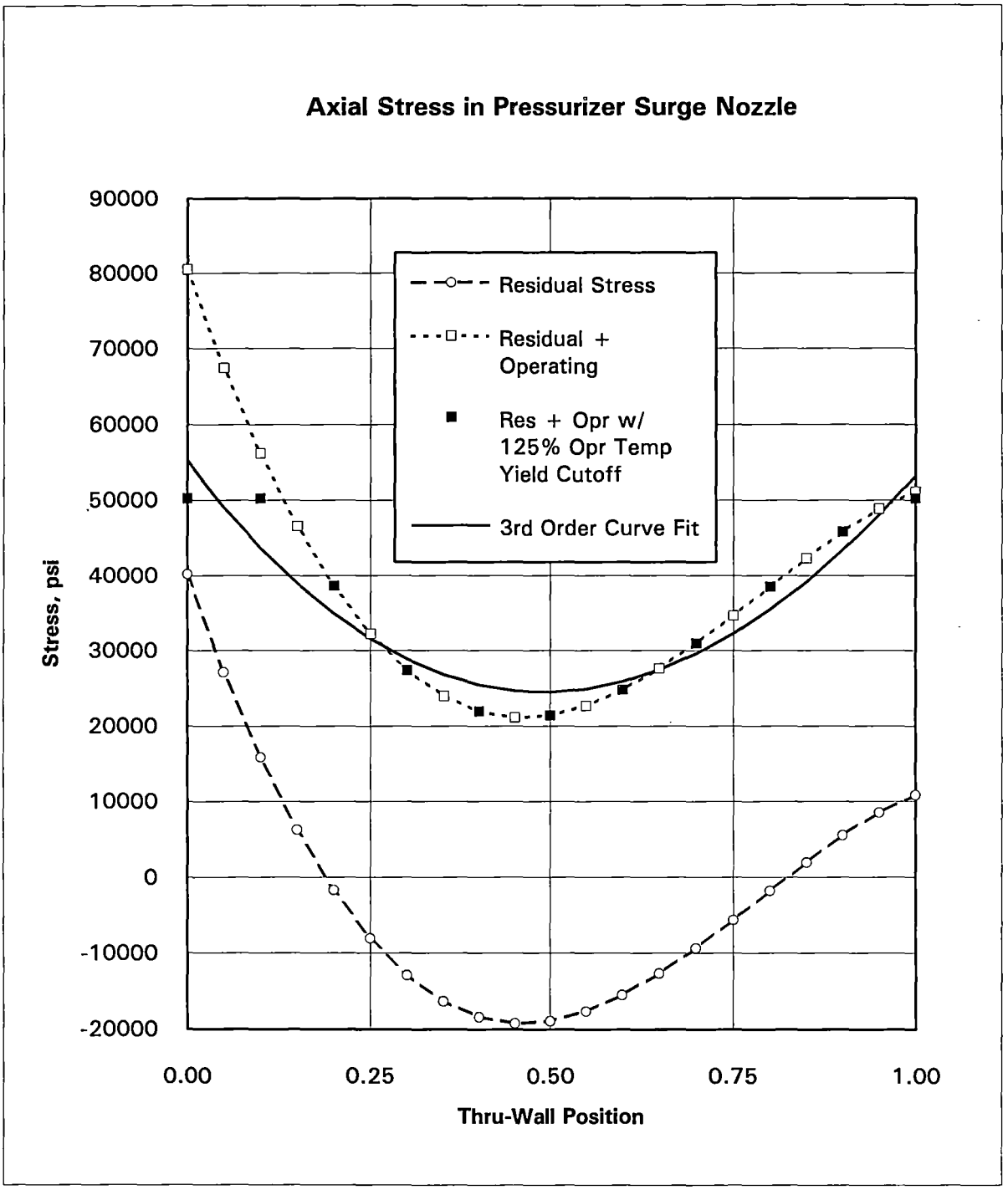

Figure A-1. Nonlinear Stress Distributions for the Pressurizer Surge Nozzle Safe End

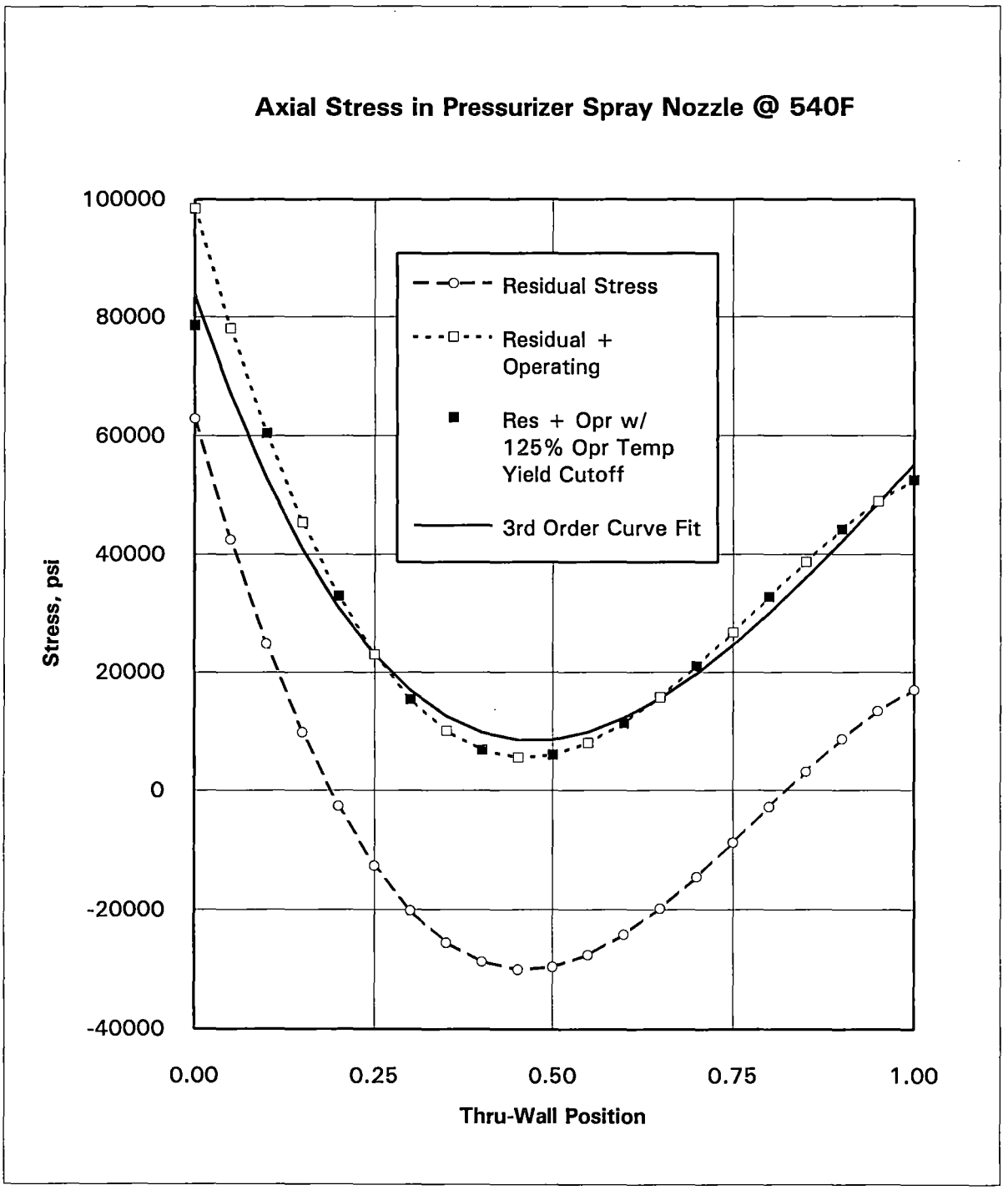

Figure A-2. Nonlinear Stress Distributions for the Pressurizer Spray Nozzle Safe End at 540F

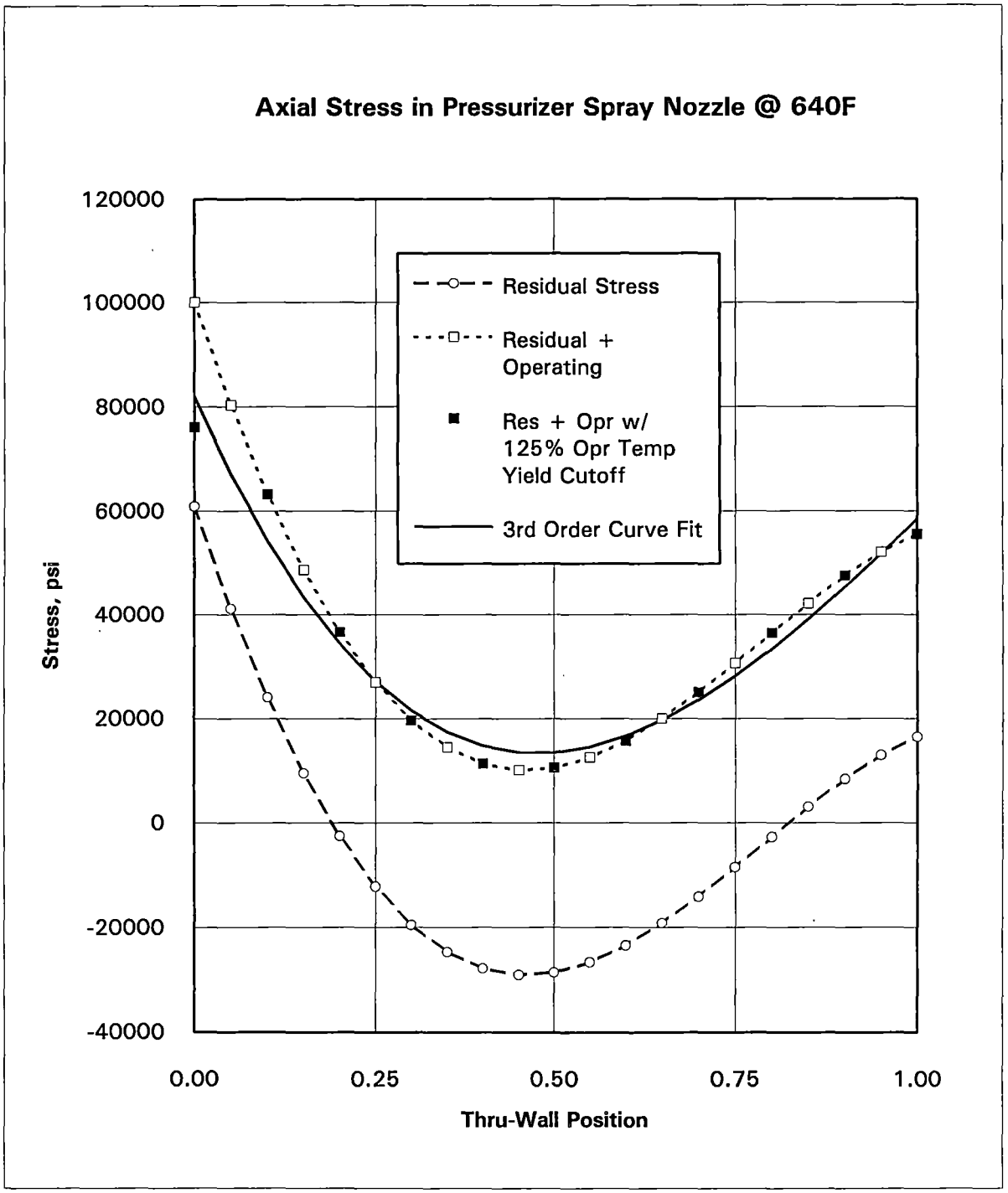

Figure A-3. Nonlinear Stress Distributions for the Pressurizer Spray Nozzle Safe End at 640F

A.2 Results and Conclusions

Table A-3 shows the estimated remaining service life of pressurizer surge and spray nozzle safe ends with circumferential flaws. These results are graphically depicted in Figures A-4 through A-6. Table A-4 contains the allowable flaw depths that can be justified for one fuel cycle (18 months) of continued operation.

Use of the NUREG-0313 nonlinear residual axial stress distribution significantly increased the remaining life of the re-evaluated components at 640 °F, especially the pressure spray nozzle safe end. This is readily apparent through a comparison of allowable 6:1 flaw depths for one fuel cycle from Tables 7 and A-4 , as shown below.

Comparison of Allowable 6:1 Circumferential Flaw Depths for Different Assumed Stress Profiles			
Component	Temperature	Constant Through-Wall Stress	Nonlinear Stress Distribution
Pzr Surge Nozzle Safe End	640 °F	.085 in.	.320 in.
Pzr Spray Nozzle Safe End	540 °F	.205 in.	.360 in.
Pzr Spray Nozzle Safe End	640 °F	.015 in.	.130 in.

Table A-3. Summary of Time to Failure for Circumferential Flaws with an Initial Depth of 0.010"

Note: Using NUREG-0313 nonlinear residual through-wall stress distribution plus constant through-wall operating stress.

ID	Component	Thick. (in.)	Circumferential Flaw Time to Failure (years) l/a=2	l/a=4	l/a=6
2	Pzr Surge SE	1.005	40.00	40.00	40.00
3	Pzr Spray SE @540°F	0.404	40.00	40.00	40.00
4	@640°F	0.404	40.00	10.64	5.36

Table A-4. Summary of Allowable Circumferential Flaws for One Fuel Cycle (18 months)

Note: Using NUREG-0313 nonlinear residual through-wall stress distribution plus constant through-wall operating stress.

ID	Component	Thick. (in.)	Circumferential Flaw Allowable Flaw Depth (in.) l/a=2	l/a=4	l/a=6
2	Pzr Surge SE	1.005	0.550	0.415	0.320
3	Pzr Spray SE @540°F	0.404	0.360	0.360	0.360
4	@640°F	0.404	0.240	0.180	0.130

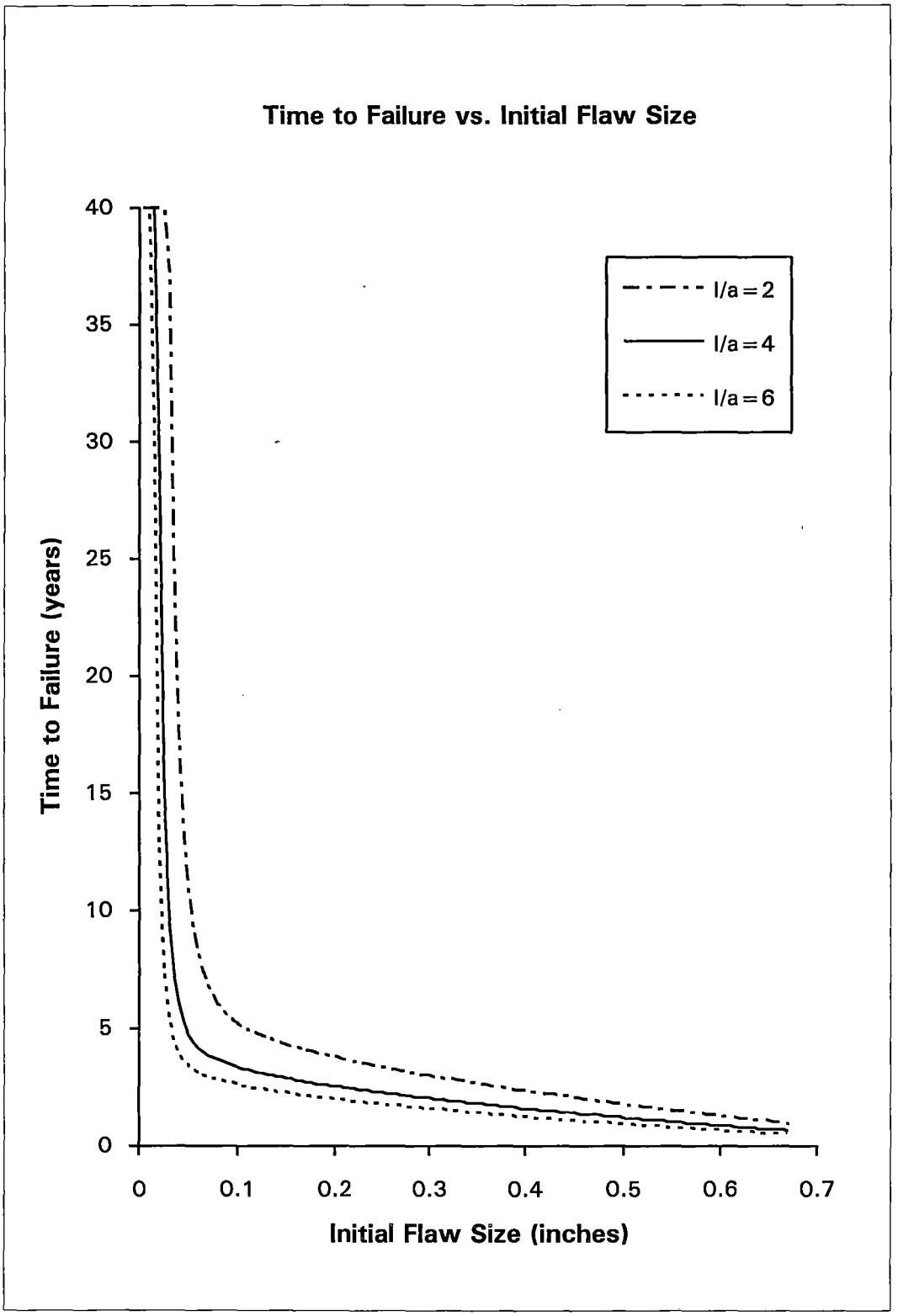

Figure A-4. Time to Failure for Pressurizer Surge Nozzle Safe End: Circumferential Semi-Elliptical Inside Surface Flaws with NUREG-0313 Nonlinear Through-Wall Stress Distribution

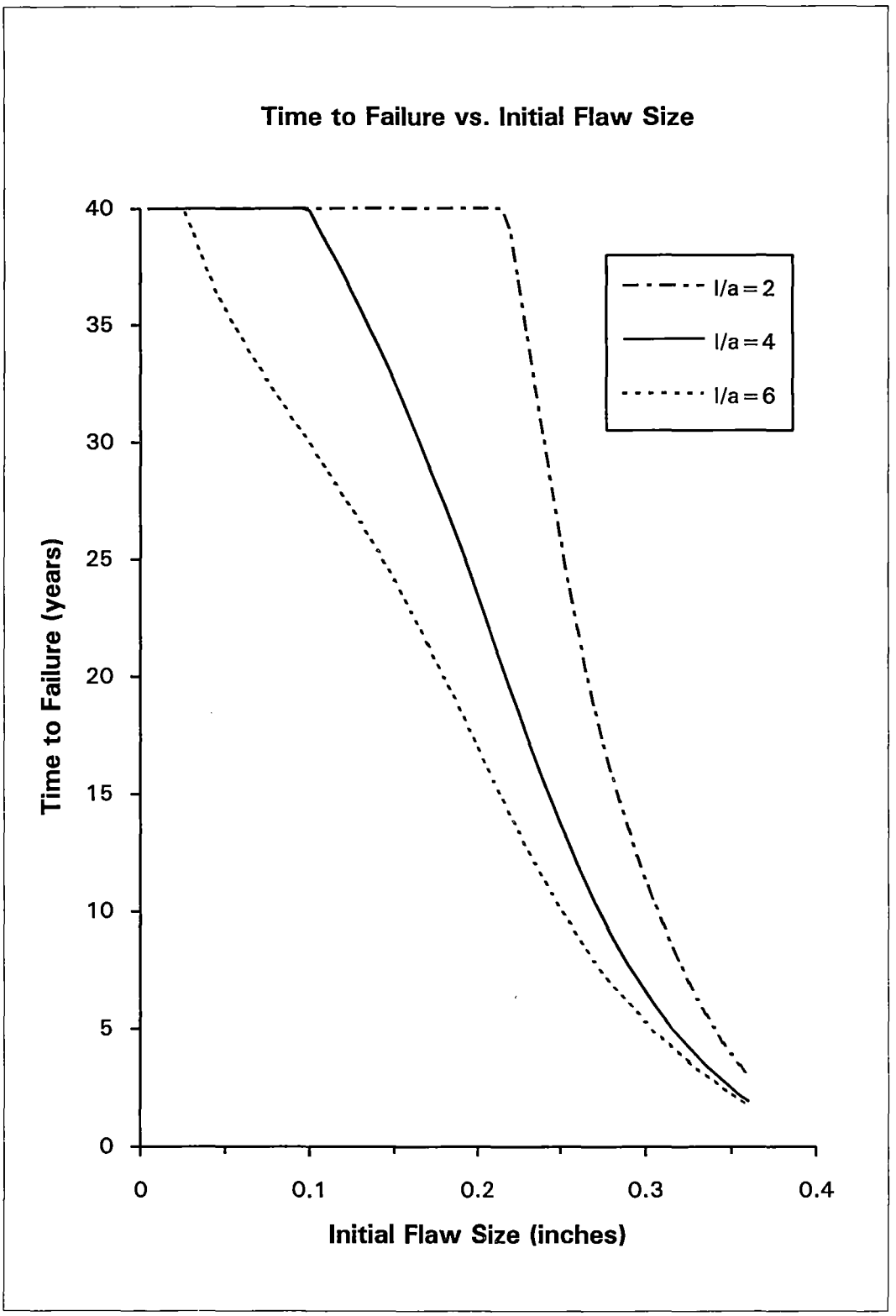

Figure A-5. Time to Failure for Pressurizer Spray Nozzle Safe End at 540F: Circumferential Semi-Elliptical Inside Surface Flaws with NUREG-0313 Nonlinear Through-Wall Stress Distribution

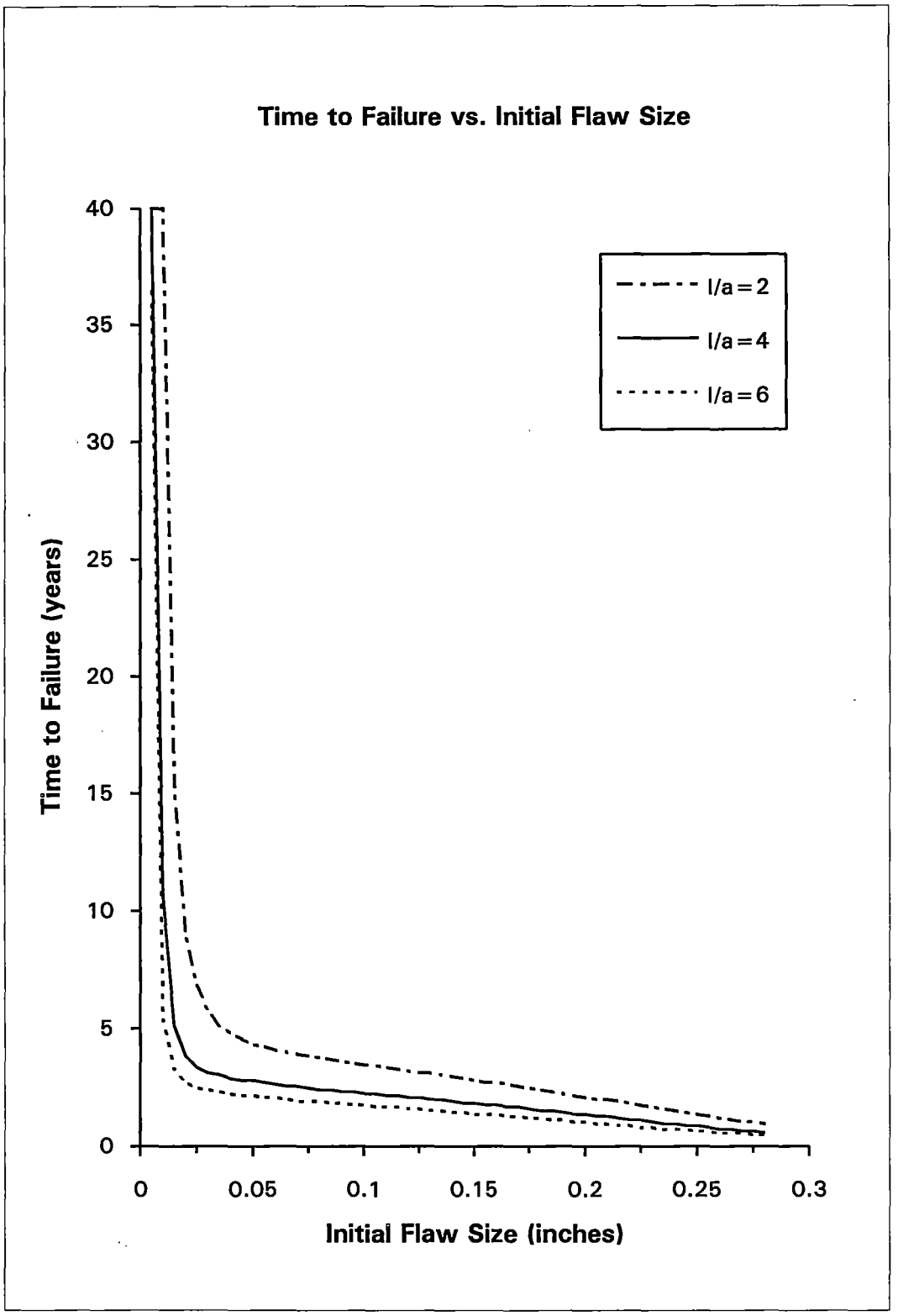

Figure A-6. Time to Failure for Pressurizer Spray Nozzle Safe End at 640F: Circumferential Semi-Elliptical Inside Surface Flaws with NUREG-0313 Nonlinear Through-Wall Stress Distribution

Appendix B Verification of FORTRAN Programs

This appendix contains calculations used to verify FORTRAN programs AX.F, CIRC.F and CINL.F. As a typical example, results will be verified for the Pressurizer Spray Nozzle Safe End at 640F.

Referenced output files (see Computer Output Microfiche):

(1) 4y_ax.out
(2) 4y_circ.out
(3) 4n_circ.out

Geometry Data:

Do =	4.500	in.
Di =	3.692	in.
Ro =	2.250	in.
Ri =	1.846	in.
t =	0.404	in.
R =	2.048	in.
Ri/t =	4.56931	
R/t =	5.06931	
a =	0.010	in.
c =	0.030	in. (l/a = 6)

Material Data:

Sy =	77.5	ksi (room temperature yield strength)
So =	60.9	ksi (operating temperature yield strength)
Sf =	95.75	ksi (room temperature flow stress)
n =	8.9	

Applied Loads:

Design pressure, pd =	2.500	ksi
Equivalent axial yield load, Py = So pi (Ro^2-Ri^2) =	316.598	kip
Faulted condition constant thru-wall stress, Sfc =	60.275	ksi
Equivalent axial faulted condition load, Pfc = Sfc pi (Ro^2-Ri^2) =	313.349	kip

3rd Order Polynomial Through-Wall Stress Fits (ksi)

	Sy	Nonlinear Operating	Sfc
S0	77.5	82.0324	60.275
S1	0	-319.250	0
S2	0	432.426	0
S3	0	-136.723	0

E.1 Axial, Semi-Elliptical Inside Surface Flaw with Constant Through-Wall Stress Field (AX.F)

E.1.1 Limit Load

				Spread-sheet	Program Output(1)	
M	=	[1 + (1.61c^2)/(R t)]^0.5	=	1.00088		
x	=	a/t	=	0.02475		
po	=	Sf (t/Ro) [1-x]/[1-(x/M)]	=	17.192	17.192	ksi
po/pd			=	6.88	6.88	

E.1.2 Stress Intensity Factor Solutions

i	A1	A2	A3	A4	A5	A6	A7	m	r
0	1.77670	-2.59750	2.75200	-1.32370	0.23630	1.06	0.28	0.58	0.41
1	0.10450	0.41890	0.00000	0.00000	0.00000	0.25	0.20	0.22	0.26
2	0.02038	-0.00397	0.42126	0.00000	0.00000	0.07	0.16	0.10	0.06
3	0.07283	-0.36006	0.66883	0.00000	0.00000	0.085	0.02	0.05	0.00

Stress Intensity Factor at Deepest Point

KI = (pi*t)^.5 * SUM(Si * Gi), i=0,1,2,3
Gi = A0 + (A1*alpha_i + A2*alpha_i^2 + A3*alpha_i^3 + A4*alpha_i^4 + A5*alpha_i^5) / F
alpha_i = (a/t)/(a/c)^m

A0 = 0

F = [0.102(Ri/t) - 0.02]^0.05 = 0.96044

ry = 1/(6 pi)*(n-1)/(n+1)*(KI(a)/Sy)^2
phi = 1/[1+(p/po)^2]
ae = a + phi*ry

ry = 0.000352
phi = 0.979292

a = 0.010 in.
c = 0.030 in.

ae = 0.010345 in.
c = 0.030 in.

i	alpha(a)	G(a)	KI(a) - ksi*in^.5 Spread-sheet	alpha(ae)	G(ae)	KI(ae) - ksi*in^.5 Spread-sheet	Program Output(1)
0	0.046811	0.080956		0.047482	0.082039		
1	0.03152	0.003863		0.032365	0.003978		
2	0.027627	0.000592		0.028483	0.000611		
3	0.02615	0.001739		0.027006	0.001788		
			7.07			7.16	7.16

Stress Intensity Factor at Surface Point

KI = (pi*t)^.5 * SUM(Si * Gsi), i=0,1,2,3
Gsi = Gi * [A6 + A7(a/t)^2] * (a/c)^r

i	Gs(a)	KI(a) - ksi*in^.5 Spread-sheet	Gs(ae)	KI(ae) - ksi*in^.5 Spread-sheet	Program Output(1)
0	0.054702		0.056211		
1	0.000726		0.000754		
2	3.89E-05		4.02E-05		
3	0.000148		0.000152		
		4.78		4.91	4.91

E.1.3 Crack Growth for One Design Cycle

Let:	ai	=	0.0800	in. (initial crack depth)
	Kmax	=	39.57	ksi*in^.5
	Kmin	=	0.00	ksi*in^.5

Fatigue Crack Growth for One Design Cycle

da/dN = C*(dK)^n in/cycle

where	C	=	4.09E-10	
	n	=	3.349	
and	dN	=	1	cycle
	dK	=	39.57	ksi*in^.5
Then:	da/dN	=	0.0001	in/cycle
	da_fatigue	=	0.0001	in.

Stress Corrosion Crack Growth for One Equivalent Design Cycle (1/12.5 years)

da/dt = D0*[C1*(Kmax)^C2]^x in/sec

with x = max{ 1.3539*(Kmax)^-0.11 , 1.0 }

where	D0	=	55.895	
	C1	=	3.386E-13	
	C2	=	1.678	
and	dt	=	(1/12.5 yr) * (365 days/yr) * (24 hr/day) * (3600 sec/hr)	
		=	2522880	sec.
Then:	x	=	1.00000	
	da/dt	=	9.07E-09	in/sec
	da_SCC	=	0.0229	in.

Total Crack Growth

da = da_fatigue + da_SCC = 0.0230 in.

	Spread-sheet	Program Output(1)	
New crack depth = ai + da =	0.1030	0.1030	in.

E.2 Circumferential, Semi-Elliptical Inside Surface Flaw with Constant Through-Wall Stress Field (CIRC.F)

E.2.1 Limit Load

			Spread-sheet	Program Output(2)	
z =	t / Ro	=	0.179556		
theta =	(pi c) / (4 Ri)	=	0.012764		
x =	a / t	=	0.024752		
A1 =	x [(1-z)(2-2z+xz)+(1-z+xz)^2]/{2[1+(2-z)(1-z)]}	=	0.010077		
alpha =	arc cos [A1*sin(theta)]	=	1.570668		
Po =	2 pi R t Sf [2*alpha/pi - (x*theta/pi)(2-2z+xz)/(2-z)]	=	497.69	497.69	kip
Po/Py =		=	1.57	1.57	

E.2.2 Stress Intensity Factor at Deepest Point

KI = (pi*t)^.5 * SUM(Si * (a/t)^i * Gi), i=0,1,2,3

Gi = A1*alpha_i + A2*alpha_i^2 + A3*alpha_i^3 + A4*alpha_i^4 + A5*alpha_i^5 + A6*alpha_i*(R/t-5)

alpha_i = (a/t)/(a/c)^m

i	A1	A2	A3	A4	A5	A6	m
0	1.8143	-1.9881	1.4382	-0.4680	0.056696	0.0067	0.50
1	1.0959	-0.9874	0.5399	-0.09303	0.0	0.0	0.38
2	1.1836	-2.3347	2.9756	-1.7652	0.39483	0.0	0.30
3	1.0029	-2.0160	2.5627	-1.4951	0.32759	0.0	0.25

ry = 1/(6 pi)*(n-1)/(n+1)*(KI(a)/Sy)^2
phi = 1/[1+(Py/Po)^2]
ae = a + phi*ry

a =	0.010	in.	ry =	0.000296	
c =	0.030	in.	phi =	0.711908	
a / t =	0.024752		ae =	0.010211	in.
			c =	0.030	in.
			ae / t =	0.025275	

			KI(a) - ksi*in^.5 Spread-sheet			KI(ae) - ksi*in^.5 Spread-sheet	Program Output(2)
i	alpha(a)	G(a)		alpha(ae)	G(ae)		
0	0.042873	0.074261		0.043322	0.075004		
1	0.037577	0.039815		0.038067	0.040316		
2	0.034416	0.038088		0.034922	0.038611		
3	0.032576	0.030618		0.03309	0.03107		
			6.48			6.55	6.55

E.2.3 Crack Growth for One Design Cycle

Let:	ai	=	0.0700	in. (initial crack depth)
	Kmax	=	36.06	ksi*in^.5
	Kmin	=	0.00	ksi*in^.5

Fatigue Crack Growth for One Design Cycle

da/dN = C*(dK)^n in/cycle

where	C	=	4.09E-10	
	n	=	3.349	
and	dN	=	1	cycle
	dK	=	36.06	ksi*in^.5
Then:	da/dN	=	0.0001	in/cycle
	da_fatigue	=	0.0001	in.

Stress Corrosion Crack Growth for One Equivalent Design Cycle (1/12.5 years)

da/dt = D0*[C1*(Kmax)^C2]^x in/sec

with x = max{ 1.3539*(Kmax)^-0.11 , 1.0 }

where	D0	=	55.895	
	C1	=	3.386E-13	
	C2	=	1.678	
and	dt	=	(1/12.5 yr) * (365 days/yr) * (24 hr/day) * (3600 sec/hr)	
		=	2522880	sec.
Then:	x	=	1.00000	
	da/dt	=	7.76E-09	in/sec
	da_SCC	=	0.0196	in.

Total Crack Growth

da = da_fatigue + da_SCC = 0.0196 in.

	Spread-sheet	Program Output(2)	
New crack depth = ai + da =	0.0896	0.0896	in.

E.3 Circumferential, Semi-Elliptical Inside Surface Flaw with Nonlinear Thru-Wall Oper. Stresses (CINL.F)

E.3.1 Limit Load

			Spread-sheet	Program Output(3)	
z =	t / Ro	=	0.179556		
theta =	(pi c) / (4 Ri)	=	0.012764		
x =	a / t	=	0.024752		
A1 =	x [(1-z)(2-2z+xz)+(1-z+xz)^2]/{2[1+(2-z)(1-z)]}	=	0.010077		
alpha =	arc cos [A1*sin(theta)]	=	1.570668		
Po =	2 pi R t Sf [2*alpha/pi - (x*theta/pi)(2-2z+xz)/(2-z)]	=	497.69	497.69	kip
Po/Pfc =		=	1.59	1.59	

E.3.2 Stress Intensity Factor at Deepest Point for Nonlinear Through-Wall Operating Stress Distribution

KI = (pi*t)^.5 * SUM(Si * (a/t)^i * Gi), i=0,1,2,3

Gi = A1*alpha_i + A2*alpha_i^2 + A3*alpha_i^3 + A4*alpha_i^4 + A5*alpha_i^5 + A6*alpha_i*(R/t-5)

alpha_i = (a/t)/(a/c)^m

i	A1	A2	A3	A4	A5	A6	m
0	1.8143	-1.9881	1.4382	-0.4680	0.056696	0.0067	0.50
1	1.0959	-0.9874	0.5399	-0.09303	0.0	0.0	0.38
2	1.1836	-2.3347	2.9756	-1.7652	0.39483	0.0	0.30
3	1.0029	-2.0160	2.5627	-1.4951	0.32759	0.0	0.25

ry = 1/(6 pi)*(n-1)/(n+1)*(KI(a)/Sy)^2
phi = 1/[1+(Pfc/Po)^2]
ae = a + phi*ry

			ry =	0.0003	
			phi =	0.716121	
a =	0.010	in.	ae =	0.010215	in.
c =	0.030	in.	c =	0.030	in.
a / t =	0.024752		ae / t =	0.025284	

			KI(a) - ksi*in^.5 Spread-sheet			KI(ae) - ksi*in^.5 Spread-sheet	Program Output(3)
i	alpha(a)	G(a)		alpha(ae)	G(ae)		
0	0.042873	0.074261		0.04333	0.075017		
1	0.037577	0.039815		0.038075	0.040325		
2	0.034416	0.038088		0.034931	0.03862		
3	0.032576	0.030618		0.033099	0.031077		
			6.52			6.58	6.58

E.3.3 Stress Intensity Factor at Deepest Point for Constant Through-Wall Faulted Condition Stress

KI = (pi*t)^.5 * SUM(Si * (a/t)^i * Gi), i=0,1,2,3

Gi = A1*alpha_i + A2*alpha_i^2 + A3*alpha_i^3 + A4*alpha_i^4 + A5*alpha_i^5
+ A6*alpha_i*(R/t-5)

alpha_i = (a/t)/(a/c)^m

i	A1	A2	A3	A4	A5	A6	m
0	1.8143	-1.9881	1.4382	-0.4680	0.056696	0.0067	0.50
1	1.0959	-0.9874	0.5399	-0.09303	0.0	0.0	0.38
2	1.1836	-2.3347	2.9756	-1.7652	0.39483	0.0	0.30
3	1.0029	-2.0160	2.5627	-1.4951	0.32759	0.0	0.25

ry = 1/(6 pi)*(n-1)/(n+1)*(KI(a)/Sy)^2
phi = 1/[1+(Pfc/Po)^2]
ae = a + phi*ry

			ry =	0.000179	
			phi =	0.716121	
a =	0.010	in.	ae =	0.010128	in.
c =	0.030	in.	c =	0.030	in.
a / t =	0.024752		ae / t =	0.02507	

			KI(a) - ksi*in^.5			KI(ae) - ksi*in^.5	
			Spread-			Spread-	Program
i	alpha(a)	G(a)	sheet	alpha(ae)	G(ae)	sheet	Output(3)
0	0.042873	0.074261		0.043147	0.074714		
1	0.037577	0.039815		0.037876	0.04012		
2	0.034416	0.038088		0.034724	0.038406		
3	0.032576	0.030618		0.032889	0.030893		
			5.04			5.07	5.07

E.3.3 Crack Growth for One Design Cycle

Let:	ai	=	0.2800	in. (initial crack depth)
	Kmax	=	31.96	ksi*in^.5
	Kmin	=	0.00	ksi*in^.5

Fatigue Crack Growth for One Design Cycle

da/dN = C*(dK)^n in/cycle

where	C	=	4.09E-10	
	n	=	3.349	
and	dN	=	1	cycle
	dK	=	31.96	ksi*in^.5
Then:	da/dN	=	0.00004	in/cycle
	da_fatigue	=	0.00004	in.

Stress Corrosion Crack Growth for One Equivalent Design Cycle (1/12.5 years)

da/dt = D0*[C1*(Kmax)^C2]^x in/sec

with x = max{ 1.3539*(Kmax)^-0.11 , 1.0 }

where	D0	=	55.895	
	C1	=	3.386E-13	
	C2	=	1.678	
and	dt	=	(1/12.5 yr) * (365 days/yr) * (24 hr/day) * (3600 sec/hr)	
		=	2522880	sec.
Then:	x	=	1.00000	
	da/dt	=	6.34E-09	in/sec
	da_SCC	=	0.0160	in.

Total Crack Growth

da = da_fatigue + da_SCC = 0.0160 in.

	Spread-sheet	Program Output(3)	
New crack depth = ai + da =	0.2960	0.2960	in.

Appendix C Computer Input Files

File	Description
geometry.inp	Outside and inside diameters for each nozzle.
ax_cof.inp	Influence coefficients for an axial flaw.
circ_cof.inp	Influence coefficients for a circumferential flaw.
#y.inp	Miscellaneous input for nozzle ID "#" for use with programs AX.F and CIRC.F for constant through-wall stresses (#=1,2,3,...,14).
#n.inp	Miscellaneous input for nozzle ID "#" for use with program CINL.F for NUREG-0313 nonlinear through-wall stress distributions (#=2,3,4).

File geometry.inp

#	OD	ID
1	1.315	0.815
2	12.750	10.740
3	4.500	3.692
4	4.500	3.692
5	13.000	10.741
6	12.750	10.741
7	2.375	1.689
8	1.250	0.625
9	1.250	0.377
10	13.000	10.741
11	3.500	2.693
12	2.375	1.689
13	1.250	0.625
14	1.250	0.377

File ax_cof.inp

A_0	A_1	A_2	A_3	A_4	A_5	A_6	A_7	m	r
0.0	1.7767	-2.5975	2.7520	-1.3237	0.2363	1.06	0.28	0.58	0.41
0.0	0.1045	0.4189	0.0	0.0	0.0	0.25	0.20	0.22	0.26
0.0	0.02038	-0.00397	0.42126	0.0	0.0	0.07	0.16	0.10	0.06
0.0	0.07283	-0.36006	0.66883	0.0	0.0	0.085	0.02	0.05	0.0

File circ_cof.inp

A_1	A_2	A_3	A_4	A_5	A_6	m
1.8143	-1.9881	1.4382	-0.4680	0.056696	0.0067	0.50
1.0959	-0.9874	0.5399	-0.09303	0.0	0.0	0.38
1.1836	-2.3347	2.9756	-1.7652	0.39483	0.0	0.30
1.0029	-2.0160	2.5627	-1.4951	0.32759	0.0	0.25

File 1y.inp

```
4.09E-10                        ! Paris Law scaling constant
3.349                           ! Paris Law slope constant
310.18                          ! Kic
46.2 36.3                       ! RT & oper temp yield stress
72.2                            ! RT flow stress
8.9                             ! strain hardening coefficient
1                               ! number of fatigue groups
1 500                           ! fatigue group no. & cycles
0.0 0.25 0.50 0.75 1.00         ! z/t locations
46.2 46.2 46.2 46.2 46.2        ! operating stresses
46.2 46.2 46.2 46.2 46.2        ! SCC stresses
55.895                          ! SCC coefficient at 640F
```

File 2y.inp

```
4.09E-10                        ! Paris Law scaling constant
3.349                           ! Paris Law slope constant
310.18                          ! Kic
51.2 40.2                       ! RT & oper temp yield stress
75.75                           ! RT flow stress
8.9                             ! strain hardening coefficient
1                               ! number of fatigue groups
1 500                           ! fatigue group no. & cycles
0.0 0.25 0.50 0.75 1.00         ! z/t locations
51.2 51.2 51.2 51.2 51.2        ! operating stresses
51.2 51.2 51.2 51.2 51.2        ! SCC stresses
55.895                          ! SCC coefficient at 640F
```

File 3y.inp

```
4.09E-10                        ! Paris Law scaling constant
3.349                           ! Paris Law slope constant
310.18                          ! Kic
77.5 62.9                       ! RT & oper temp yield stress
95.75                           ! RT flow stress
8.9                             ! strain hardening coefficient
1                               ! number of fatigue groups
1 500                           ! fatigue group no. & cycles
0.0 0.25 0.50 0.75 1.00         ! z/t locations
77.5 77.5 77.5 77.5 77.5        ! operating stresses
77.5 77.5 77.5 77.5 77.5        ! SCC stresses
3.687                           ! SCC coefficient at 540F
```

File 4y.inp

```
4.09E-10                        ! Paris Law scaling constant
3.349                           ! Paris Law slope constant
310.18                          ! Kic
77.5 60.9                       ! RT & oper temp yield stress
95.75                           ! RT flow stress
8.9                             ! strain hardening coefficient
1                               ! number of fatigue groups
1 500                           ! fatigue group no. & cycles
0.0 0.25 0.50 0.75 1.00         ! z/t locations
77.5 77.5 77.5 77.5 77.5        ! operating stresses
77.5 77.5 77.5 77.5 77.5        ! SCC stresses
55.895                          ! SCC coefficient at 640F
```

File 5y.inp

```
4.09E-10                        ! Paris Law scaling constant
3.349                           ! Paris Law slope constant
306.28                          ! Kic
51.2 41.0                       ! RT & oper temp yield stress
75.75                           ! RT flow stress
8.9                             ! strain hardening coefficient
1                               ! number of fatigue groups
1 500                           ! fatigue group no. & cycles
0.0 0.25 0.50 0.75 1.00         ! z/t locations
51.2 51.2 51.2 51.2 51.2        ! operating stresses
51.2 51.2 51.2 51.2 51.2        ! SCC stresses
15.316                          ! SCC coefficient at 590F
```

File 6y.inp

```
4.09E-10                        ! Paris Law scaling constant
3.349                           ! Paris Law slope constant
306.28                          ! Kic
51.2 41.0                       ! RT & oper temp yield stress
75.75                           ! RT flow stress
8.9                             ! strain hardening coefficient
1                               ! number of fatigue groups
1 500                           ! fatigue group no. & cycles
0.0 0.25 0.50 0.75 1.00         ! z/t locations
51.2 51.2 51.2 51.2 51.2        ! operating stresses
51.2 51.2 51.2 51.2 51.2        ! SCC stresses
15.316                          ! SCC coefficient at 590F
```

File 7y.inp

```
4.09E-10                        ! Paris Law scaling constant
3.349                           ! Paris Law slope constant
306.28                          ! Kic
37.1 29.7                       ! RT & oper temp yield stress
65.15                           ! RT flow stress
8.9                             ! strain hardening coefficient
1                               ! number of fatigue groups
1 500                           ! fatigue group no. & cycles
0.0 0.25 0.50 0.75 1.00         ! z/t locations
37.1 37.1 37.1 37.1 37.1        ! operating stresses
37.1 37.1 37.1 37.1 37.1        ! SCC stresses
15.316                          ! SCC coefficient at 590F
```

File 8y.inp

```
4.09E-10                        ! Paris Law scaling constant
3.349                           ! Paris Law slope constant
306.28                          ! Kic
39.8 31.8                       ! RT & oper temp yield stress
67.25                           ! RT flow stress
8.9                             ! strain hardening coefficient
1                               ! number of fatigue groups
1 500                           ! fatigue group no. & cycles
0.0 0.25 0.50 0.75 1.00         ! z/t locations
39.8 39.8 39.8 39.8 39.8        ! operating stresses
39.8 39.8 39.8 39.8 39.8        ! SCC stresses
15.316                          ! SCC coefficient at 590F
```

File 9y.inp

```
4.09E-10                        ! Paris Law scaling constant
3.349                           ! Paris Law slope constant
306.28                          ! Kic
48.0 38.4                       ! RT & oper temp yield stress
73.5                            ! RT flow stress
8.9                             ! strain hardening coefficient
1                               ! number of fatigue groups
1 500                           ! fatigue group no. & cycles
0.0 0.25 0.50 0.75 1.00         ! z/t locations
48.0 48.0 48.0 48.0 48.0        ! operating stresses
48.0 48.0 48.0 48.0 48.0        ! SCC stresses
15.316                          ! SCC coefficient at 590F
```

File 10y.inp

```
4.09E-10                        ! Paris Law scaling constant
3.349                           ! Paris Law slope constant
306.28                          ! Kic
51.2 41.5                       ! RT & oper temp yield stress
75.75                           ! RT flow stress
8.9                             ! strain hardening coefficient
1                               ! number of fatigue groups
1 500                           ! fatigue group no. & cycles
0.0 0.25 0.50 0.75 1.00         ! z/t locations
51.2 51.2 51.2 51.2 51.2        ! operating stresses
51.2 51.2 51.2 51.2 51.2        ! SCC stresses
3.687                           ! SCC coefficient at 540F
```

File 11y.inp

```
4.09E-10                        ! Paris Law scaling constant
3.349                           ! Paris Law slope constant
302.33                          ! Kic
37.1 30.1                       ! RT & oper temp yield stress
65.15                           ! RT flow stress
8.9                             ! strain hardening coefficient
1                               ! number of fatigue groups
1 500                           ! fatigue group no. & cycles
0.0 0.25 0.50 0.75 1.00         ! z/t locations
37.1 37.1 37.1 37.1 37.1        ! operating stresses
37.1 37.1 37.1 37.1 37.1        ! SCC stresses
3.687                           ! SCC coefficient at 540F
```

File 12y.inp

```
4.09E-10                        ! Paris Law scaling constant
3.349                           ! Paris Law slope constant
302.33                          ! Kic
37.1 30.1                       ! RT & oper temp yield stress
65.15                           ! RT flow stress
8.9                             ! strain hardening coefficient
1                               ! number of fatigue groups
1 500                           ! fatigue group no. & cycles
0.0 0.25 0.50 0.75 1.00         ! z/t locations
37.1 37.1 37.1 37.1 37.1        ! operating stresses
37.1 37.1 37.1 37.1 37.1        ! SCC stresses
3.687                           ! SCC coefficient at 540F
```

File 13y.inp

```
4.09E-10                    ! Paris Law scaling constant
3.349                       ! Paris Law slope constant
303.33                      ! Kic
39.8 32.3                   ! RT & oper temp yield stress
67.25                       ! RT flow stress
8.9                         ! strain hardening coefficient
1                           ! number of fatigue groups
1 500                       ! fatigue group no. & cycles
0.0 0.25 0.50 0.75 1.00     ! z/t locations
39.8 39.8 39.8 39.8 39.8    ! operating stresses
39.8 39.8 39.8 39.8 39.8    ! SCC stresses
3.687                       ! SCC coefficient at 540F
```

File 14y.inp

```
4.09E-10                    ! Paris Law scaling constant
3.349                       ! Paris Law slope constant
302.33                      ! Kic
48.0 38.9                   ! RT & oper temp yield stress
73.5                        ! RT flow stress
8.9                         ! strain hardening coefficient
1                           ! number of fatigue groups
1 500                       ! fatigue group no. & cycles
0.0 0.25 0.50 0.75 1.00     ! z/t locations
48.0 48.0 48.0 48.0 48.0    ! operating stresses
48.0 48.0 48.0 48.0 48.0    ! SCC stresses
3.687                       ! SCC coefficient at 540F
```

File 2n.inp

```
12.750 10.740               ! OD & ID
4.09E-10 3.349              ! da/dN constants: C & n
310.18                      ! Kic
51.2 40.2                   ! RT & oper temp yield stress
75.75                       ! RT flow stress
8.9                         ! strain hardening coefficient
55.895                      ! SCC coefficient at 640F
1                           ! number of fatigue loads
1 500                       ! fatigue load no. & cycles
48.768                      ! faulted condition stress
0.00,  50250.               ! x/t position
0.10,  50250.               !    vs.
0.20,  38613.75             ! residual + operating stress
0.30,  27400.15
0.40,  21927.22
0.50,  21394.72
0.60,  24806.82
0.70,  30972.16
0.80,  38503.77
0.90,  45819.14
1.00,  50250.
```

File 3n.inp

```
4.500 3.692                    ! OD & ID
4.09E-10 3.349                 ! da/dN constants: C & n
310.18                         ! Kic
77.5 62.9                      ! RT & oper temp yield stress
95.75                          ! RT flow stress
8.9                            ! strain hardening coefficient
3.687                          ! SCC coefficient at 540F
1                              ! number of fatigue loads
1 500                          ! fatigue load no. & cycles
56.691                         ! faulted condition stress
0.00,  78625.                  ! x/t position
0.10,  60419.55                !    vs.
0.20,  32945.43                ! residual + operating stress
0.30,  15399.76
0.40,  6836.394
0.50,  6003.202
0.60,  11342.05
0.70,  20988.8
0.80,  32773.33
0.90,  44219.53
1.00,  52545.27
```

File 4n.inp

```
4.500 3.692                    ! OD & ID
4.09E-10 3.349                 ! da/dN constants: C & n
310.18                         ! Kic
77.5 60.9                      ! RT & oper temp yield stress
95.75                          ! RT flow stress
8.9                            ! strain hardening coefficient
55.895                         ! SCC coefficient at 640F
1                              ! number of fatigue loads
1 500                          ! fatigue load no. & cycles
60.275                         ! faulted condition stress
0.00,  76125.                  ! x/t position
0.10,  63213.43                !    vs.
0.20,  36612.89                ! residual + operating stress
0.30,  19625.1
0.40,  11334.03
0.50,  10527.33
0.60,  15696.42
0.70,  25036.44
0.80,  36446.26
0.90,  47528.51
1.00,  55589.52
```

Appendix D List of Computer Output Microfiche

The computer output microfiche listed below are contained in Reference 15.

File	Description	Date
fail_ax.out	Output file with time to failure data from program AX.F for all nozzles.	3/22/95
fail_circ.out	Output file with time to failure data from program CIRC.F for all nozzles.	3/23/95
fail_cinl.out	Output file with time to failure data from program CINL.F for nozzle ID #'s 2,3 and 4.	3/23/95
sum_ax.out	Output file with summary of crack growth results from program AX.F for all nozzles.	3/22/95
sum_circ.out	Output file with summary of crack growth results from program CIRC.F for all nozzles.	3/23/95
sum_cinl.out	Output file with summary of crack growth results from program CINL.F for nozzle ID #'s 2,3 and 4.	3/23/95
#y_ax.out	Output files with detailed crack growth results from program AX.F for nozzle ID "#" (#=1,2,3,...,14).	3/22/95
#y_circ.out	Output files with detailed crack growth results from program CIRC.F for nozzle ID "#" (#=1,2,3,...,14).	3/23/95
#n_circ.out	Output files with detailed crack growth results from program CINL.F for nozzle ID "#" (#=2,3,4).	3/23/95